DOCUMENT RESUME

ED 194 300 SE 031 938

AUTHOR Nash, W. A.; And Others
TITLE Development of Facilities for an Ocean Engineering Laboratory. Final Report.
INSTITUTION Massachusetts Univ., Amherst. Dept. of Civil Engineering.
SPONS AGENCY National Science Foundation, Washington, D.C.
REPORT NO UMass-1759-1
PUB DATE Jul 75
GRANT NSF-GZ-1759
NOTE 101p.: Contains occasional marginal legibility.

EDRS PRICE MF01/PC05 Plus Postage.
DESCRIPTORS College Science; *Engineering Education; Higher Education; *Laboratory Equipment; *Laboratory Manuals; *Laboratory Procedures; *Oceanography; Science Laboratories
IDENTIFIERS *Hydrostatics

ABSTRACT

A collection of seven laboratory facilities and processes dedicated to improving student understanding of the fundamental concepts associated with the structural mechanics of oceanic structures is described. Complete working drawings covering all mechanical and electrical aspects of these systems are presented so that the systems may be reproduced in any instructional laboratory. Three of the facilities are suitable for hydrostatic pressure testing of scale models of deep submergence structures. One presentation details simple and inexpensive ways to fabricate thin shells suitable for student use. Another presentation outlines experimental apparatus associated with dynamics of shells, particularly submerged ones. The last two sections present a new manner of applying dynamic radical loads to thin elastic rings and techniques for determination of wave forces acting on piles. (Author/DS)

Engineering Research Institute

UNIVERSITY OF MASSACHUSETTS

AMHERST, MASSACHUSETTS

Sponsored by the National Science Foundation

Grant GZ 1759

Final Report

DEVELOPMENT OF FACILITIES FOR AN OCEAN ENGINEERING LABORATORY

W.A. Nash
J.M. Colonell
R.B. MacPherson

Department of Civil Engineering

University of Massachusetts

Amherst, Massachusetts

July, 1975

ABSTRACT

A collection of seven laboratory facilities and processes dedicated to improving student understanding of the fundamental concepts associated with the structural mechanics of oceanic structures is described. Complete working drawings covering all mechanical and electrical aspects of these systems are presented so that the systems may be reproduced in any instructional laboratory.

TABLE OF CONTENTS

INTRODUCTION

This report details a set of laboratory facilities which will aid the student in developing an understanding of the general area of structural mechanics pertinent to a wide variety of oceanic structures. These include surface structures as well as deep submergence systems. The structures examined are subject to both static and dynamic loading. The models indicated could be fabricated in any well-equipped university machine shop and no unusual electronic instrumentation is involved.

The investigation was divided into seven phases, each devoted to development of a laboratory facility or process selected to illustrate certain characteristics of structural behavior of oceanic structures. A detailed outline of each of these facilities is presented. Complete working drawings covering all mechanical and electrical aspects of each system are given so that these systems may be reproduced as desired.

The first three facilities (I, II, and III) are suitable for hydrostatic pressure testing of scale models of deep submergence structures. Such static pressure tests give the student an insight into the mechanism of collapse of cylindrical, conical, or spherical shells under hydrostatic loading. Further, they aid him in developing an understanding of contemporary and new analytical approaches to prediction of collapse loads. The first facility (I) is a transparent tank suitable for low hydrostatic pressures so that the student can actually view the progressive collapse mechanism.

The fourth presentation in this report details simple and inexpensive ways to fabricate thin shells suitable for student laboratory use. The

fifth section outlines experimental apparatus associated with dynamics of shells, particularly submerged ones. The sixth section presents a new and unique manner of applying dynamic radial loads to thin elastic rings. The seventh and last section presents techniques for determination of wave forces acting on piles.

I. 50 psi, 1.2 ft^3 Acrylic Pressure Tank

The first of the three pressure tanks has a working pressure range of 0 to 50 psi. Detailed plans of this tank are shown in Figures 1-5. The design concept is that of a cylinder with flat end plates, and it is a relatively easy item to fabricate in any modestly equipped machine shop. The cylinder is a 19-1/2-inch length of 12-inch O.D. x 3/8-inch wall cast acrylic tubing which allows visual observation of models while they are undergoing a test. 6061-T6 Aluminum Alloy is specified for the end plates, and a standard size "O-Ring" is used to seal the cylinder to the plates. The tie rods are threaded on each end where they pass through the end plates and two nuts are provided on each end. This is done to allow the end plates to be positioned about 1/16-inch from the end of the cylinder, thereby preventing the tie rods from transmitting longitudinal stress into the cylinder wall.

The piping and hydraulic diagram for the 50 psi acrylic tank is shown in Figure 6. Water is the working fluid, and compressed air is used for the high pressure source. Except for the air line, all piping for this system is 3/8-inch x 0.035 wall type L copper tubing, and all joints are made with mechanically swaged fittings. A 1/4-inch NPT pipe plug in the top end plate is used for an air bleed. For the safety of the observers it is absolutely necessary that all air be evacuated from the tank before pressurizing. CAUTION: Do not exceed 50 psi.

II. 400 psi, 6.7 ft^3 Steel Pressure Tank

The second pressure tank is a 400 psi, 6.7 ft^3 steel vessel. Again, the basic design concept is that of an unstiffened cylinder with flat end plates and connecting tie rods. This tank is considerably larger than the 50 psi tank.

Detailed plans of this pressure tank are shown in Figures 7-12. The cylinder is a 42-inch length of 20" O.D. x 1/2" wall grade B seamless steel tube, ASTM-A53, and the end plates are of 2024-T351 aluminum. A standard size "O-Ring" is used with a plug type seal, and again as in the 50 psi tank, the end plates are set about 1/16-inch off the cylinder ends by adjusting the tie rod nuts.

The piping and hydraulic diagram for this pressure tank is shown in Figure 13. Hydraulic oil is used for the working fluid in the system, and the high pressure is developed with a manually operated hydraulic pump. Filling and emptying of the tank is accomplished with a small electric pump rated at 4 G.P.M. Most of the pipe fittings are mechanically swaged and type L copper tubing is used everywhere except on the hydraulic pump line.

Both the 50 gallon pressure tank and the 55 gallon oil reservoir are mounted on a frame with casters to allow the unit to be easily moved about. Figures 14 and 15 are photographs of the completed facility.

III. 3,000 psi - 16 ft^3 Steel Pressure Tank

The third pressure tank is a 3,000 psi - 16 ft^3 capacity vessel. The design concept is that of an unstiffened cylinder capped on one end with an elliptical dished head and on the other end by a removable flat plate which mates to a bolting flange.

The detailed plans of this vessel are shown in Figures 16-20. A considerable amount of welding is required in the fabrication of this tank. The cylinder is HY-80 steel which has been rolled and welded with full penetration welds, and both the elliptical head and bolting flange are welded to the cylinder. The flat end closure is a double thickness of a 4-inch HY-80 steel plate bolted to the flange with 16, 2/12-inch diameter bolts. These bolts must be torqued evenly before pressurizing the tank. The seal between the flange and flat plate is made with a series 6900-type F Gasko-Seal.

Due to the pressure involved most of the hydraulics for the high pressure system were purchased from manufacturers. An air operated hydraulic pumping unit is powered by compressed air from the laboratory air system, and the required 3,000 psi is developed using about 75 psi air pressure. The piping system for filling and emptying the vessel is a separate unit mounted on casters which is wheeled into position when needed. Hyraulic oil is used for the working fluid to avoid short circuiting any instrumentation which might be inside the tank.

IV. Techniques for Fabricating Shells

A. Vacuum Forming of Various Shell Geometries from Thin Sheet Plastic

As part of the program to develop techniques for easily fabricating shell models, the authors have investigated vacuum forming of thin sheet plastics. If the required vacuum forming machine is on hand, the additional apparatus required to form the shells can be easily fabricated and the models produced by this process are found to be of good quality.

Basically, the technique involves the heating of a thin plastic sheet to make it flexible, then drawing it to shape by means of a vacuum. A mold is of course necessary. Excellent models of spherical, ellipsoidal and torispherical shells can be quickly fabricated using this procedure. Also, initial imperfections can be easily introduced into the shells by appropriately altering the mold. A photo of the basic apparatus is shown in Figure 21. Any commercially available vacuum forming machine should be suitable.

It was found that the best technique for fabricating molds was to make them of laminated hard wood with an outer coating of hard epoxy glue. The glue used to laminate the wood as well as the outer epoxy covering must be heat resistant to avoid delamination and blistering of the mold during the forming process. Temperatures as high as 200°F can be experienced by the mold. Although any hard wood is suitable for this application it was found that birch produced good quality molds and was easy to obtain and shape.

After trying several methods of shaping the molds, it was found

that lathe turning and polishing produced the best results. This technique of course, yields symmetrical shapes. If irregularities and out-of-roundness are desired they can be introduced by unevenly adding epoxy filler to the surface of the mold. Finally the entire surface of the mold should be coated with a thin, uniform coating of epoxy and sanded smooth.

It was found that no vacuum draw holes should be bored through the mold, but rather the suction should act only at the base of the mold. This is accomplished by simply placing the mold over the vacuum hole in the platen of the forming machine.

After forming, the plastic will look like a hat with a wide brim around it. The "brim" is cut to the required size and shape and is used to clamp the shell to the pressure test apparatus, see Figure 22. Shells may be subjected to external pressure by placing them inside a pressure tank or to internal pressure by placing them atop a pressure tank as shown in Figure 23. This last configuration may be employed to illustrate buckling of certain geometry torospherical shells subject to internal pressure. Consistent with accepted vacuum forming methods, some release agent should be used on the mold's surface. If not, it is nearly impossible to remove the formed plastic shell from the mold without damaging it.

It was found after many trials that the junction of the shell and "brim" could be made a smooth curve by assuring that the bottom of the mold was flush on the platen with the vacuum hole at its center. If the mold was not flush on the platen but rather was slightly above the platen surface it was found that a sharp corner was formed at the junction of the shell and its brim which is undesirable for model testing.

Figures 24 and 25 show a torisopherical shell mold and clamping ring. Excellent models were made of polystyrene otherwise known as PVC (polyvinyl chloride), as well as with polymethyl methacrylate (Lucite or Plexiglass) in gages ranging from 0.015 to 0.125 inch. These are both thermoplastics and are well suited for vacuum forming. Thermosetting plastics should not be used for this application.

B. Cylindrical Shells

A family of cylindrical shells has been developed for instructional use in the pressure tanks. Most of these are intended for the 50 psi acrylic pressure tank since in that case the shell can be observed visually during the test.

For both the stiffened and the unstiffened cylindrical models, the major design problem is the method of attaching and sealing the end closures. It is important that no stress concentrations be induced in the shell at the junction with the end closure. One possible scheme for avoiding this problem is to allow the cylinder walls to gradually thicken at the ends where the end closure will mate. This, however, is difficult and costly to fabricate. A better solution to this design problem was developed and is illustrated in Figures 26-28. The concept is very simple and involves making a slightly rounded, shallow plug for each end plate. As the shell deforms under pressure it does not encounter a sharp boundary or edge at the end closure seal and consequently does not suffer any serious stress concentrations. Also, this end plate is reusable since it can be detached and fitted to another cylinder after the first has been tested.

The unstiffened cylinder shown in Figure 26 is 7.50 inches long with a wall thickness of 0.125 inches. This will collapse at approximately 31 psi. Other suggested designs are 11.00 inches long with a wall thickness of 0.156 inches (collapse at about 48 psi), and 9.500 inches long with a wall thickness of 0.094 inches (collapse at about 17 psi).

A suggested design for a ring stiffened cylinder is shown in Figure 29. Again this is an acrylic shell so the cylinder can be purchased as seamless plexiglass tube. The ring stiffeners are to be cut from a smaller acrylic tube and then glued inside the shell according to the diagram. For an overall cylinder length of up to 36 inches the shell will fail by elastic instability at 35 psi or less; however, for length in excess of 36 inches the shell will fail by elastic general instability. The design of this ring stiffened cylinder was accomplished using the theory of Pulos and Salerno [1] for the case of elastic collapse and that of Kendrick [2] to determine general instability.

V. Impact Testing of Hull Penetration Reinforcements

Two special instruments have been developed by the authors for testing pressure hull penetrations under abrupt impact loadings. Both devices are inexpensive and can be fabricated in a modestly equipped machine shop.

One of the testing instruments utilizes a sliding weight to impart an impact loading to a spherical model at the base of a vertical guide rod. An assembly drawing of this fixture is shown in Figure 30. The hollow vertical rod is welded into a disc, Figure 31, which bolts onto the 1-inch thick base plate shown in Figure 32. A test sphere has a large hole in the bottom and a smaller reinforced hole at the top through which a 15 ft stainless steel verticale rod passes to act as a guide for a sliding weight which may be dropped from any height on the shaft. Impact velocities of up to about 30 ft/sec can be achieved by the sliding weight which is shown in Figure 33.

Figure 34 shows a cross section of a typical test sphere with a welded coaming insert. The sphere is purchased as a spun steel shape, 8-1/4-inch dia. with 0.032-inch wall. Similar spun spheres can be obtained quite inexpensively from most metal spinning shops.

The velocity of the falling weight is measured by a photoelectric technique. A 1/16-inch diameter hole is bored into the hollow shaft about 2-inches above the level of the coaming in the sphere. Then a small flashlight-type light bulb is placed inside the hollow rod so that its light shines directly out of the 1/16-inch hole toward a photocell. When the falling slide weight passes the pin hole it interrupts the light signal to the photocell and the duration of this interruption is

measured on a "holding oscilloscope". Since the dimensions of the sliding weight are known, its velocity just prior to impact can be calculated by knowing the exact blackout time measured by the photocell. Figure 35 is a schematic view of the photocell apparatus and Figures 37 and 37 show the detail of the components in the photocell aiming mechanism. Figure 38 shows the electronic circuit for the photocell, light bulb and "holding oscilloscope".

The second impact testing instrument was developed for testing models under deep submergence pressure conditions and is intended for use inside a pressure tank such as the types described elsewhere in this report. This impact testing device operates with a spring actuated slide weight that is remotely triggered with an electromagnet. Figure 39 shows the entire device and Figures 40-43 are detailed drawings of the components. The concept for mounting the sphere and coaming are shown in Figures 44-46. Since the sphere must be pressure proof all welding must be done carefully to avoid leaks.

The velocity of the sliding weight is determined with the same photoelectric technique as for the previously discussed impact testing device.

VI. Apparatus for Dynamic Radial Loading of Rings

Ring stiffeners are employed to increase the strength characteristics of cylindrical, conical, and spherical shells used for deep submergence systems. A comprehensive analysis and design of any ring-stiffened shell involves knowledge of the response of the ring alone to static or dynamic applied loads. Although the case of a statically applied radial load on a thin circular ring is a classical buckling problem whose solution has been known for many years, there is little information (particularly experimental) available for the corresponding problem of a dynamically loaded ring [3]. This essentially stems from the difficulty of applying to the ring a radial load having specified pressure-time characteristics. Consideration of the difficulties involved in developing a mechanical system capable of applying the desired dynamic radial load led the authors to develop an electromagnetic system which is described below.

The concept which was selected makes use of a fundamental rule of electromagnetics:

$$\overline{dF} = I(\overline{d\ell} \times \overline{B}) \qquad \text{VI-1}$$

Stated in words, this expression relates the force $\overline{dF}$ on an elemental length of current-carrying wire in a magnetic field to the product of the current magnitude I times the vector cross product of the elemental length $d\ell$ and magnetic flux density $\overline{B}$. In the event that $d\ell$ is an element of a closed circuit assumed to be a ring whose circumferential path is C, then the total force F_T on the circuit is found by vector integration:

$$\overline{F}_T = I \oint_C (\overline{d\ell} \times \overline{B}) \qquad \text{VI-2}$$

If the rationalized M.K.S. system of units is used, F is in Newtons, ℓ in meters along the circumference, I in amperes and B in Webers/m^2. Thus, in the case of a circular path (the ring) the total force is found by integration to be:

$$F_T = (I)\ (\pi D)\ (B)\ \text{Sin}\ \theta \qquad \text{VI-3}$$

D is the outside diameter of the ring

θ is the angle between the plane of the ring and the direction of B.

Clearly F_T is a maximum for $\theta = 90°$: i.e. $F_T = (I)\ (\pi D)\ (B)$ VI-4

Expanding upon this concept, the authors designed a magnet which could establish a uniform and continuous magnetic field normal to the plane of a test ring. Then, by establishing an electric current in the ring, a force is exerted which by its electromagnetic nature satisfies the desired conditions.

The magnet is shown in Figures 47 and 48. The working field is in the 0.750 inch air gap between the two opposing pole pieces where the 14-inch diameter test rings are placed. The pole faces are ground flat and parallel to ± 0.001-inch which assures a uniform field intensity in the region covering the ring.

As shown, the pole pieces are thick walled cylinders so an annular shaped field is established which extends inward and outward from the rings circumference for about 4-inches. This allows the ring to deflect a considerable distance while remaining in a constant and uniform field. Measurements made with a sensitive gauss meter show that the field varies by less than one part in 1000 across an annular region of dimensions 17.0 inch outside diameter by 11.0 inch inside diameter and 0.750 inch thick.

The magnet is energized by wire wrapped about the four symmetrically spaced winding posts as indicated in Figure 49. Each post has 480 turns of #8 square enameled copper wire and the total resistance of all four is 1.7 ohms. The windings are in a series circuit with a 25 amp x 40 volt d.c. power supply. The inductance of the windings and power supply are carefully matched.

All components of the magnet are made of low carbon steel, grade 1020. This was selected to reduce magnetic hysteresis effects. Careful measurements indicate that the field intensity in this magnet is 4.59 x 10^3 gauss = 0.459 webers/m^2.

Rings are tested in the magnet by wrapping a layer of very thin, flexible copper foil about the outside circumference of the plastic rings. The foil is connected to a variable d.c. power supply and then the ring is placed in the air gap of the magnet. Next, the magnet is energized and allowed a few seconds to stabilize. Static loadings on the ring are developed by slowly increasing the current to the ring. Dynamic loadings are developed by instantaneously switching on the ring current which has been preset to some desired valve.

The power supply used to energize the magnet was purchased as a stock item from an electrical components manufacturer. The variable power supply for the ring was designed and built especially for this application. A schematic of it is shown in Figure 50. It is powered by a 12V battery which is a simple way to achieve the direct current which is essential for this concept to function properly. The current supply is capable of close, continuous current regulation from 0 to about 60 amperes.

The use of copper foil may at first seem objectionable; however, it has some distinct advantages. If the rings are made of some conductor then the tape is not required since the current can be induced in the ring itself, but in the case of testing rings made of non-conducting materials the tape is essential. Also, using the tape allows multiple electrical turns to be established about the ring by winding the tape more than once around. Then by Equation VI-4 it may be seen that a considerably greater force is exerted on the ring.

In actual tests the magnet has been successful in developing both static and dynamic pressures of up to 1.1 psi on thin plexiglass rings. The rise time of the pressure for the dynamic tests is less than 0.002 seconds. Also, in both static and dynamic tests, failure modes greater than the primary two lobe pattern have been observed which is indication of the excellent uniformity of the pressure. Figure 51 plots some of the results of these tests and is evidence of the success of the ring magnet.

It is proposed that this concept could be expanded for building much larger and more powerful magnets. Also, it is proposed that the apparatus could be easily modified to test cylinders by allowing a wider air gap between the pole faces.

VII. Wave Forces Acting on Piles

Wave Force Theory

The forces on a pile due to water wave passage can be represented by the Morison equation [4]. This equation is based on the assumption that the total horizontal force on a pile is the sum of two forces; an inertia force proportional to the water particle accelration, and a drag force proportional to the square of the water particle velocity. This equation appears in many forms. One of them considers the elemental force acting on a differential length (ds) of a pile and is given by (see Figure 52).

$$dF = \left[\frac{1}{2} D\rho C_D |u|u + \frac{\rho\pi D^2}{4} C_M \frac{\partial u}{\partial t}\right] ds \qquad \text{VII-1}$$

where

D = diameter of the pile

ρ = mass density of fluid

C_D = coefficient of drag

C_M = coefficient of mass

u = water particle velocity; the notation $|u|u$ is introduced to preserve the sign of the drag term

$\frac{\partial u}{\partial t} = \dot{u}$ = water particle acceleration

The first term is the drag force which is the usual representation of the force on a cylindrical body in a flowing fluid. The inertia term is the force which is experienced by a body when it is accelerated through a fluid. This force is expressed in terms of fluid mass and is called the "virtual mass" effect. This will be the force experienced by the body held in an accelerating fluid.

From linear water wave theory [5] for a small amplitude progressive wave travelling in the positive X-direction (Figure 52) in an inviscid fluid, the velocity potential ϕ is given by

$$\phi = \frac{ag}{\sigma} \frac{\cosh k(h+y) \sin \theta}{\cosh kh} \qquad \text{VII-2}$$

where

k = wave number $\frac{2\pi}{L}$

σ = frequency (radians/second) = $\frac{2\pi}{T}$

η = water surface elevation from MWL = $a \cos (kx - \sigma t)$

h = water depth (bottom to MWL)

a = wave amplitude

T = wave period

L = wave length

θ = phase angle = $(kx - \sigma t)$

t = time

γ = specific weight of water

The horizontal velocity of the water particle at any depth is given by

$$u = -\frac{\partial \phi}{\partial x} = \frac{agk}{\sigma} \frac{\cosh k(h+y) \cos \theta}{\cosh kh} \qquad \text{VII-3}$$

and the acceleration associated with this is

$$\frac{\partial u}{\partial t} = -agk \frac{\cosh k(h+y) \sin \theta}{\cosh kh} \qquad \text{VII-4}$$

Assuming that small amplitude kinematics apply, and by substituting Equations VII-3 and VII-4 intc equation VII-1 and integrating over the entire submerged length of the pile, the total force F is given by

$$F = \int_0^{h+\eta} dF = \frac{\gamma C_D D a^2}{2} \frac{kh \cos \sigma t |\cos \sigma t|}{\sinh 2kh} \left[\frac{1}{2kh} \sinh 2kh\left(1+\frac{\eta}{h}\right) + \left(1+\frac{\eta}{h}\right)\right] - \frac{\gamma C_M \pi D^2}{4} \frac{a \sin \sigma t}{\cosh kh} \left[\sinh kh\left(1+\frac{\eta}{h}\right)\right] \qquad \text{VII-5}$$

Similarly, the bending moment M about the bottom of the pile (point of fixity) is given by

$$M = \int_0^{h+\eta} s\, dF$$

$$= \frac{\gamma C_D D a^2}{4} \frac{kh^2 \cos \sigma t |\cos \sigma t|}{\sinh 2kh} \left[\frac{(1+\frac{\eta}{h})^2}{2} + \frac{(1+\frac{\eta}{h})}{2kh} \sin 2kh(1+\frac{\eta}{h})\right.$$

$$\left. + \frac{1}{2(kh)^2} (1 - \cosh 2kh(1+\frac{\eta}{h}))\right]$$

$$- \frac{\gamma C_M \pi D^2}{4} \frac{ah \sin \sigma t}{\cosh kh} \left[(1+\frac{\eta}{h}) \sinh kh(1+\frac{\eta}{h})\right.$$

$$\left. + \frac{1}{kh} (1 - \cosh kh(1+\frac{\eta}{h}))\right] \qquad \text{VII-6}$$

Laboratory Experiments and Techniques

With the recent increase in research concerning wave forces, a variety of measuring techniques have been developed. These techniques vary according to the desired data, the dimensions of the research facility, the size and type of waves, and the research objectives. In this section some of the more relevant research on this subject is described, as are various approaches to the data collection problem.

Hinge and Wire

In 1950 Morison [4] used a right circular cylindrical column hinged to the bottom of a wave tank by a leaf spring (Figure 53a). The column was secured to the sides of the tank by two tension springs and changes in loading were sensed by an induction coil. Moment and wave height data were recorded. One example of the scale of his experiment was a column of approximately one inch diameter, a water depth of 2.03 feet, wave period

of 1.68 seconds, and wave length of 12.25 feet. The tests were conducted using uniform sinusoidal waves only. Values for the coefficients C_m and C_d were determined experimentally to be 1.508 and 1.626, respectively.

Inner Strain Bar

A completely different approach appeared in Jen's work of 1968 [6]. A complex strain measuring system was used, consisting of two strain bars placed inside a 6-inch diameter hollow plexiglass cylinder. A simplified diagram appears in Figure 53b. Calibration was performed using pulleys and hanging weights. The wave facility used was 200 feet long, 8 feet wide, and 6 feet deep. Both uniform and random waves were generated by a piston-type wave generator which was controlled by a magnetic tape recorder.

Sectional Model

Another approach is to use a sectional model, as Hayashi [7] did in his research of pile breakwaters to locate the distribution of moment (Figure 54). The model pile was constructed of 22 short brass tubes of 2.36 in. diameter and 1.18 in. height. Through the center of the tubing was placed a bottom-fixed steel bar of 29.2 in. length, 1.58 in. width, and 0.236 in . thickness. Each tube was attached to the rod by a pair of set screws. Along the rod was a series of strain gages capable of sensing moment about the bottom. These strain gages were kept dry by sealing the tubing joints with vinyl tape. Calibrations were performed by pushing a ring-type compression link against the column. The wave facility was 31.5 in. wide, 27.6 in. deep, and 98 feet long.

The water depth was 15.7 in., the period of the waves was 1.7 seconds, and wave height varied between 7.53 and 7.3 in.

Two Load Cells

One of the most commonly used approaches in wave-produced moment measurements is the mounting of two sets of strain gages a distance ℓ apart. The gages sense two moments, M_1, M_2, where M_1 is nearer the fixed end. The force can either be obtained electrically by wiring the gages as in Figure 53c or indirectly by measuring two moments, Figures 54b and 54c enabling the computation of force by the following equation:

$$F = \frac{M_1 - M_2}{\ell} \qquad \text{VII-7}$$

The moment arm about point 1 is in both cases:

$$z_1 = \frac{M_1}{M_1 - M_2} \quad \ell = \frac{M_1}{F} \qquad \text{VII-8}$$

This technique has been used by several researchers, some of whose works are discussed below.

In Harleman's study [8] of 1955, the two-moment technique was used. The strain gages were wired to give moment and force directly (Figure 53c). The model was hung from the top of the tank and its diameter was varied from 0.5 to 6.0 inches. The load cells were changed to give the necessary sensitivity under different loading conditions. The natural frequency of the system varied from five to eleven cps. Uniform waves were produced by a piston-type generator with the heights varied from 0.4 to 0.84 feet and lengths from 4 to 10 feet. Calibrations were performed with suspended weights.

Nagai [9] in 1966 measured two moments and calculated the force using these moments and the distance between them. The top-mounted column was 4 inches in diameter, wave periods varied from 1.23 to 1.80 seconds, and wave height was varied between 5.1 and 7.86 inches. Wave lengths varied from 6.5 to 9.75 feet, while water depth was varied from 15.8 to 23.8 inches. The wave research facility was 81.5 feet long, 6.54 feet wide, and 3.91 feet deep.

In Sorenson's report [10] of 1969, a two-moment load cell system suspended from above the water was used. The voltage outputs were proportional to force and moment. The test was performed to consider the effects of pile roughness with a model of 3.716 inches in diameter. The column experienced a maximum deflection of less than 0.1 inch. The waves were mechanically generated and the facility was two feet wide, three feet deep, and 120 feet long. It was found that C_d varied between 1.0 and 1.2 and C_m between 1.5 and 2.0.

Other Techniques

Nath [11] in 1969 used sonic techniques to measure displacements of two and four leg plexiglass frames. The facility was 108 feet long, 8 ft. 7 in. wide, with a water depth of 3 ft. 9 in. Sonic sensors were also used to measure wave heights. In 1971 Herbich [12] studied response to wave impingement of spring-retained submerged shapes. Changes in loadings were measured with a cable mounted over a pulley and attached to a load cell.

Wind Wave Research Facility

The experiments were conducted in the Wind Wave Research Facility of

the Civil Engineering Department at the University of Massachusetts in Amherst (Figure 55). The flume is 48 feet long, 22 inches wide, 4 feet deep and has a water depth of 2 feet. The flume is covered by lucite panels which are secured to the frame. Waves are generated by drawing air over the water surface by means of a fan at the exhaust end of the flume. The wind speed can be varied from about 15 fps to 60 fps. A mechanical wave maker (bottom-hinged) can also be installed in the tank to generate periodic waves whose amplitude and period can be varied by changing the stroke and frequency of the wave maker. The walls and floor of the flume are built of plywood for five of the six panels, the remaining panel being made of transparent lucite. It was within the lucite section of the flume that the structural model was placed for the investigation described by this report; that is, at a distance (or fetch) of 35 feet from the air inlet. A detailed description of the facility and its operational characteristics has been provided by Colonell [13].

Description of the Model

The structural column (Figure 56) was fabricated from a 25-inch length of plexiglass tube with outside and inside diameters of 3.0 in. and 2.75 in., respectively. A mounting flange of the same material was cemented to the base of the column while the top was fitted with a watertight plexiglass lid. The design of the column was based on previous experimental results obtained by Clines and Colonell [14].

Strain gages were mounted on the inside surface of the column, one set at the base and the other set six inches above the base. Each set

consisted of four strain gages, two for each side, arranged as shown in Figure 57 to provide for temperature compensation and to obtain increased sensitivity to bending moment experienced by the column. The strain gages used were SR-4 Polymide-backed resistance gages, each having a resistance of 120 ohms. These gages are provided by the manufacturer with leads attached, this feature facilitating their application. The vertically oriented gages were the active gages while the horizontal ones acted as "dummy gages" (Figure 57). Each set of gages was connected by the circuit shown in Figure 57, to form the arms of a Wheatstone bridge. The gages were adhered to the plexiglass with GA-1 cement, following standard strain gage application techniques.

The wire leads from the strain gages were passed through two holes at the base of the column, on opposite sides along the neutral axis as shown in Figure 58. These leads were four-conductor Beldfoil, shielded, plastic-jacketed cables, which were passed through Tygon tubing to ensure their waterproof integrity. The cables were then guided through two L-shaped aluminum tubes which were attached to the side of the flume.

Two-Moment Principle Application

A method for estimation of the resultant force exerted on a cantilever consists of measuring the bending moments at two points near the fixed end of the cantilever (Figure 58). If M_1 and M_2 are the moments at these two points and 'y' is the distance between these points, the resultant force is given by

$$F = \frac{M_1 - M_2}{y} \quad ; \quad |M_1| > |M_2| \qquad \text{VII-9}$$

The system in this case should be such that all the forces act beyond those points where the moments are being measured. This principle was utilized in the model column experiments to measure the wave forces to which it was subjected. In the model the distance 'y' between the points of bending moment measurement was six inches. For these experiments it was assumed that all the wave forces acted above the points at which the bending moments were measured. This assumption is justified by the following explanation.

The Morison equation (VII-1) states that the total force on a pile is the sum of inertia and drag forces, the inertia force being proportional to the water particle acceleration and the drag force being proportional to the square of the velocity. The velocity potential function is given by VII-2. From this the local horizontal velocity and acceleration of the water particle can be obtained as in Equations VII-3 and VII-4. It can be shown readily that at depths greater than about one-half the wave length, the wave-induced water motion becomes negligible. This is due to the exponential decay of the velocity and acceleration components with depth, as indicated by the presence of the hyperbolic functions in Equations VII-3 and VII-4. Accordingly, it is below a depth of about one-half wavelength that the two measurements of bending moment should be made.

For the experiments reported here, the greatest wavelengths were approximately two feet and the water depth was maintained at two feet. Consequently, the wave-induced water motion at depths greater than one foot was regarded as negligible. A slow wind-induced drift current at

the bottom of the flume possibly contributed to a slight DC bias in the time histories of bending moment but the data processing procedures effectively eliminated this from the analysis.

Instrumentation

The strain gages were connected to a Sanborn 358-1100 Pre-amplifier and Chart Recorder System which supplied the excitation voltage to the bridge circuits. The output signals from the strain gages were monitored by the paper chart recorder and also recorded on magnetic tape by an Ampex SP-300, seven-channel, AM/FM Instrumentation Recorder. Two capacitive wave sensors were used during all experiments, their output signals being monitored and recorded along with the strain gage output.

The two wave sensors were placed slightly ahead (i.e. upwind) and to each side of the model column. Calibration of the wave sensors was performed with a cranking device which allowed movement of the sensor in vertical increments as small as 0.001 inch. The change in output voltage of the wave sensor, which resulted from a series of vertical displacements, then provided a measure of the sensor response as a function of its submergence. To avoid errors due to mechanical binding or slippage of this cranking device, all calibrations were performed by cranking it in one direction only, starting at the uppermost position and proceeding to the lowest. The calibration steps were recorded in increments of 0.2 inch, with several steps being used to establish the essentially linear relationship of the wave sensor to change in water surface elevation.

Calibration of the strain gages for the purpose of measuring bending moment was accomplished by the application of a series of horizontal forces

at the top of the column. The calibrating forces, which produced both tensile and compressive bending stresses in the column, were measured by means of a Hunter L-1 Force Indicator. The forces were applied essentially by the indicator itself as it was caused to push or pull on the column from its position in a screw-driven sliding bracket. To prevent excessive continuous loading of the strain gages, the indicator was returned to its zero position after each calibration step. The steps generally proceeded from maximum tensile to maximum compressive bending stress. Zero positions were measured at the beginning, middle, and end of each calibration. The maximum frictional error was determined to be 0.02 pound, the smallest division on the indicator being 0.01 pound. The calibrations were normally performed with increments of 0.1 pound. The bending moment indicated by the strain gages was determined from multiplication of the applied force by the distance to the strain gages.

Data Processing

The experiment was arranged to enable the direct measurement of bending moment at two positions and water surface elevation (i.e. wave height) at two positions upwind of the structural model. Data were recorded on magnetic tape using an Ampex SP-300 tape recorder in FM mode at a speed of 1 7/8 inch per second implying a frequency response of 0 to 312 hz. The recording represents an analog presentation of the data; however, the data were digitized to allow comprehensive analysis by a variety of digital computational programs. The complete data processing sequence is illustrated by Figure 59.

Results

This laboratory experiment allows the investigation of many facets of the wave force problem. For example, the time series analysis of water surface elevations and structural bending moment enables the construction of direct correlation between wave action and resultant force on the model pile. Utilization of various statistical measures in addition to conventional spectral analysis procedures permits evaluation of many theoretical approaches to this problem. The necessity of a stochastic approach to the analysis is an additional benefit.

References

1. Pulos, J.G., and Salerno, V.L., "Axisymmetric Elastic Deformations and Stresses in a Ring-Stiffened, Perfectly Circular Cylindrical Shell under External Hydrostatic Pressure," David Taylor Model Basin Report No. 1497, 1961.

2. Kendrick, S., "The Buckling, Under External Pressure, of Circular Cylindrical Shells with Evenly Spaced, Equal Strength, Circular Ring Frames - Part III," Naval Construction Research Establishment, Dunfermline, Scotland, Report R244, 1953.

3. Wah, T., "Dynamic Buckling of Thin Circular Rings," International Journal of Mechanical Sciences, Vol. 12, No. 2, pp. 143-155, 1970.

4. Morison, J.R., et al., "The Forces Exerted by Surface Waves on Piles," Petroleum Transactions, AIME, Vol. 189, pp. 149-154, 1950.

5. Ippen, A., Estuary and Coastline Hydrodynamics, McGraw-Hill Pub. Co., New York, 1966.

6. Jen, Yuan, "Laboratory Study of Inertia Forces on Piles," Journal of Waterways and Harbor Division, ASCE, Vol. 94, No. EM5, Proc. Paper 5806, February 1968, pp. 59-76.

7. Hayashi, Taiso, et al., "Hydraulic Research on the Closely Spaced Pile Breakwater," Proceedings, Tenth Conference on Coastal Engineering, Tokyo, Japan, ASCE, Vol. 2, pp. 873-884, 1966.

8. Harleman, D.R.F., and Shapiro, W.C., "Experimental and Analytical Studies of Waves Forces on Offshore Structures," Part 1, MIT Hydrodynamics Laboratory Report No. 19, 1955.

9. Nagai, S., "Researches on Steel Pipe Breakwaters," Proceedings Tenth Conference on Coastal Engineering, Tokyo, Japan, ASCE, Vol. 2, pp. 873-884, 1966.

10. Sorenson, Robert M. and Burton, William J., "Effects of Pile Roughness on Wave Forces on Piles," Civil Engineering in the Oceans II, ASCE, Miami Beach, Florida, pp. 441-460, 1969.

11. Nath, John N. and Harleman, D.R.F., "The Dynamics of Fixed Towers in Deep Water Random Waves," Journal of Waterways and Harbors Division ASCE, Vol. 95, No. WW4, Proc. Paper 6924, pp. 539-556, 1969.

12. Herbich, John B., and Shank, G., "Forces Due to Waves on Submerged Structures," Journal of Waterways, Harbors, and Coastal Engineering Division, ASCE, Vol. 97, No. WW1, Proc. Paper 7870, pp. 57-71, 1971.

13. Colonell, J.M., "A Wind Wave Research Facility," ONR Contract Report UM-72-2, School of Engineering, University of Massachusetts, Amherst, March 1972.

14. Clines, C.A., and Colonell, J.M., "Laboratory Modelling of Structural Response to Ocean Wave Excitation," ONR Contract Report UM-72-3, School of Engineering, University of Massachusetts, Amherst, April 1972.

Assembly Drawing of 50 PSI Acrylic Pressure Tank

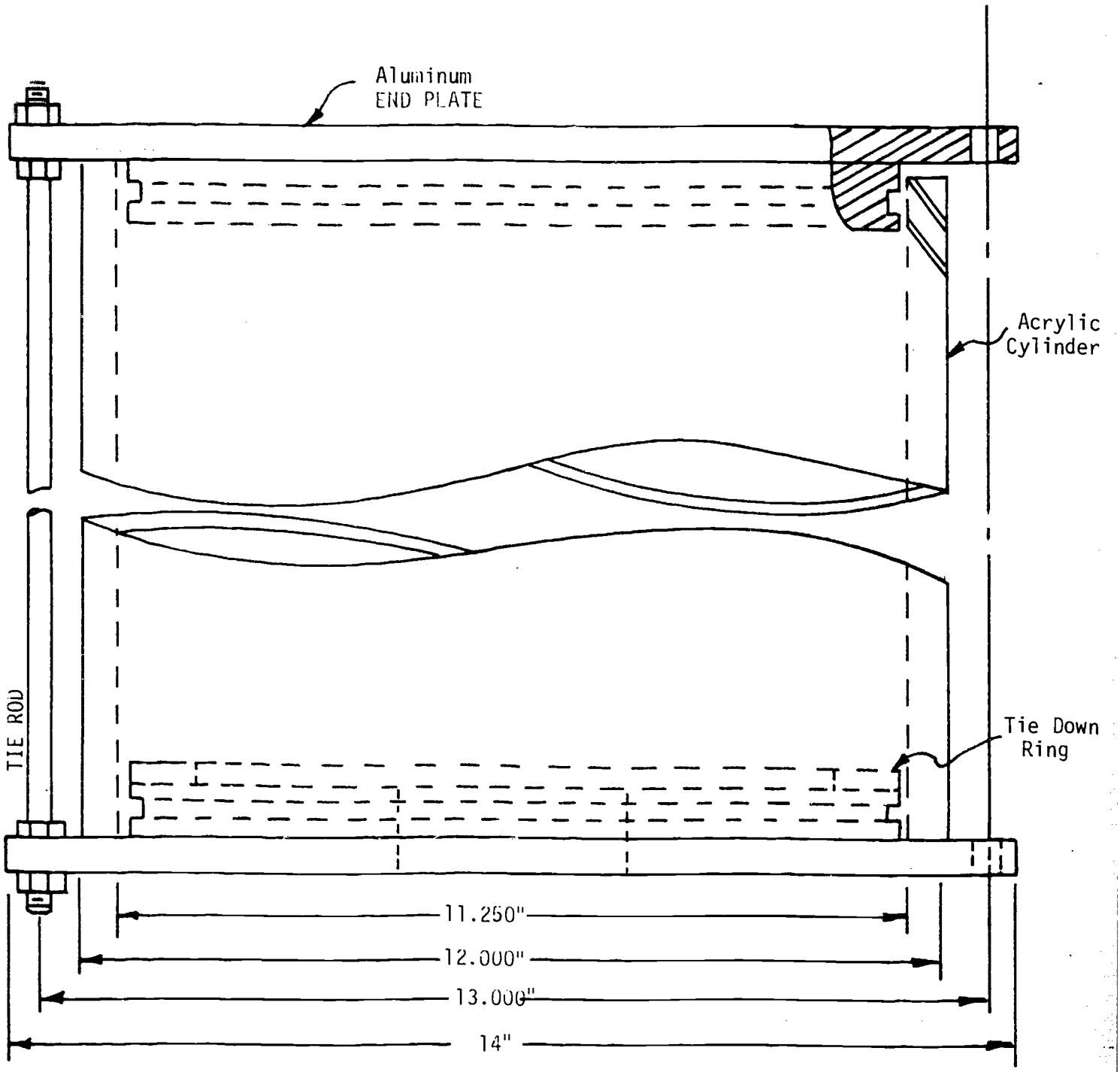

Figure 1

Material: 12" O.D x 3/8" Wall Cast Acrylic Tube

Finish Ends and Cut Chamfer

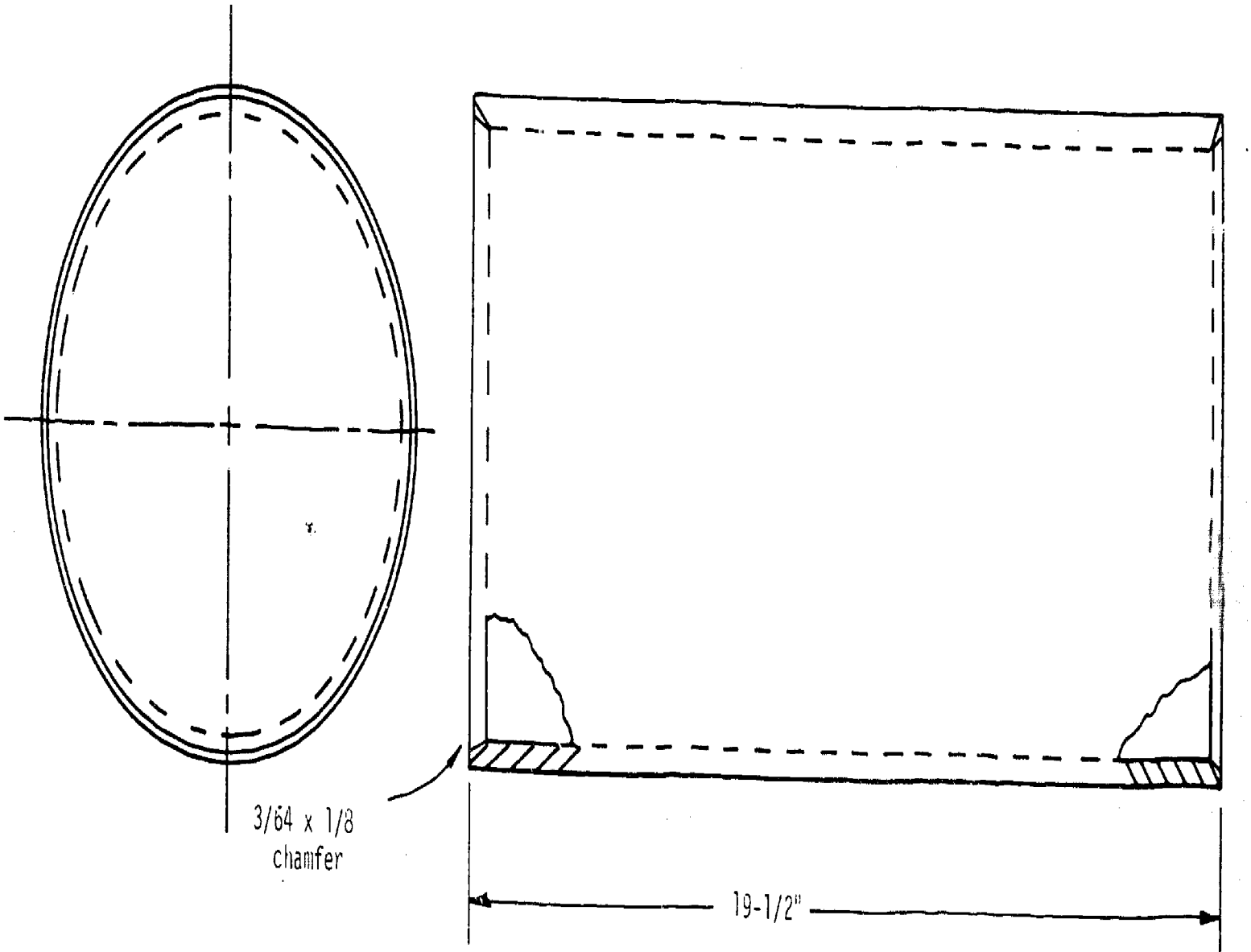

Figure 2

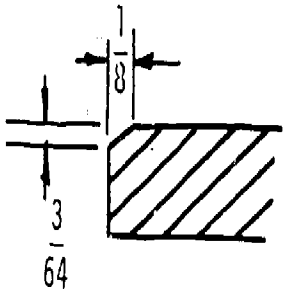

Chamfer Detail

END PLATE

Mat: 6061-T6 AL
No Reg: 2

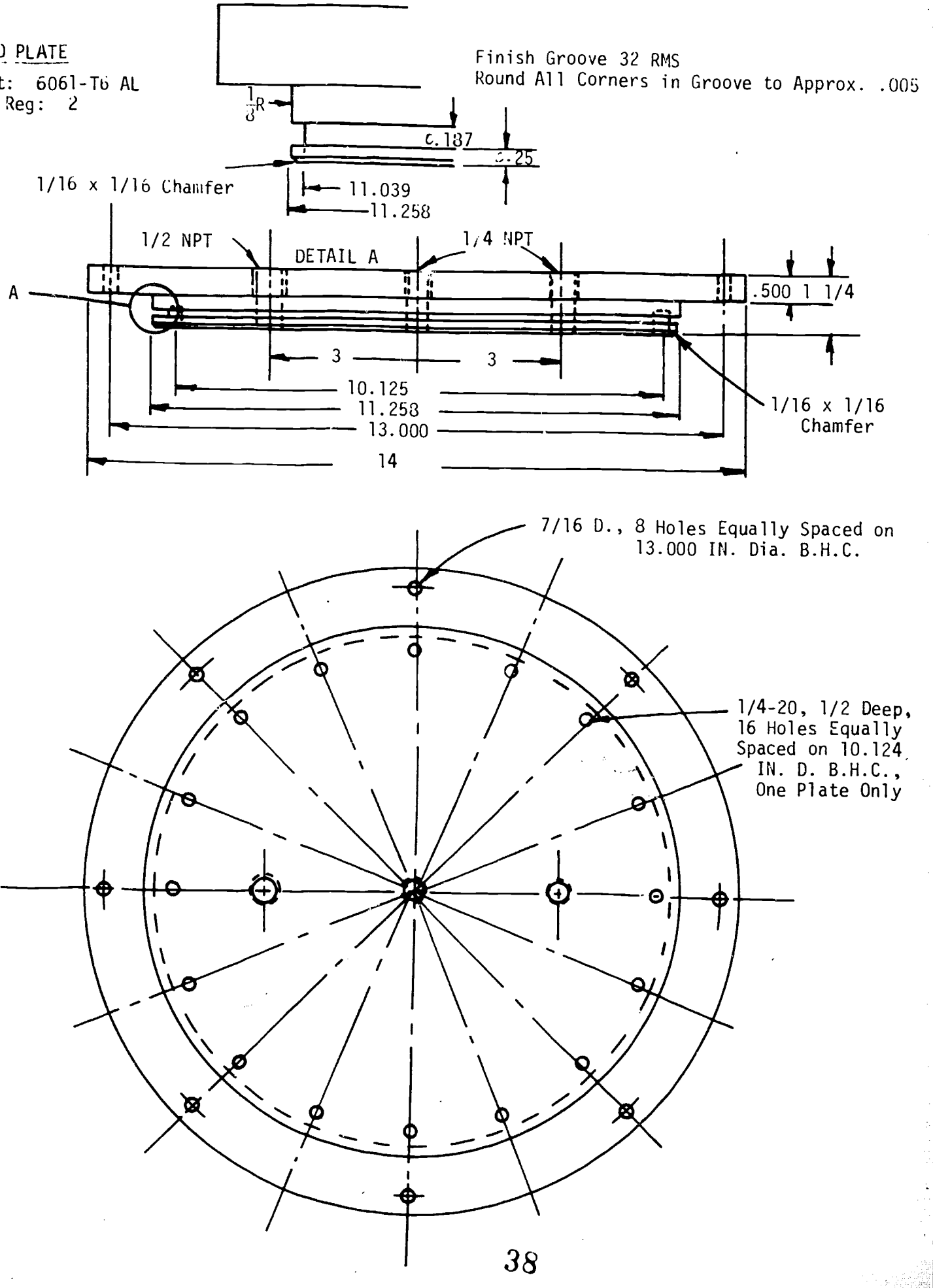

Figure 3

TIE DOWN RODS

Mat.: 3/8 Steel Rod
No. Req.: 8

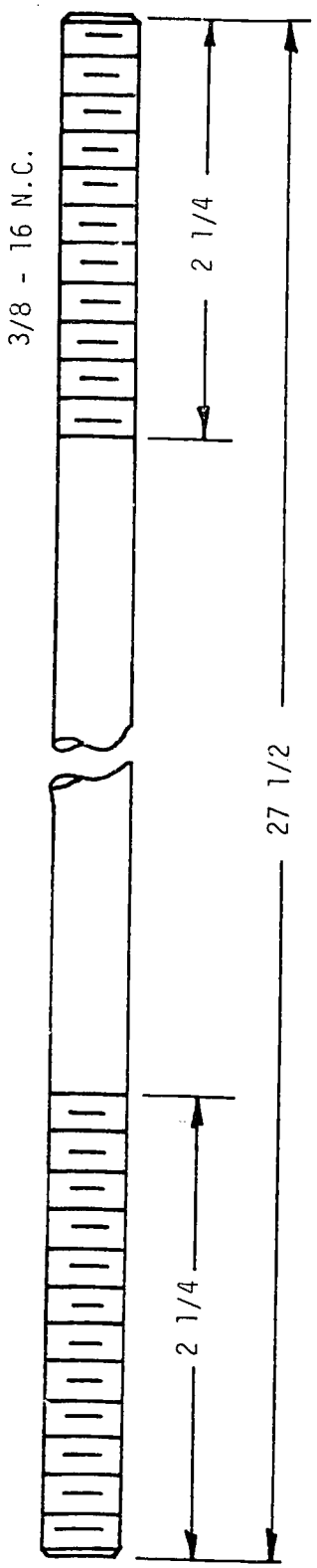

Figure 4

NOTE - THICKNESS AS GIVEN

5/16 D., 16 Holes Equally Spaced
on 10.125 D.B.H.C.

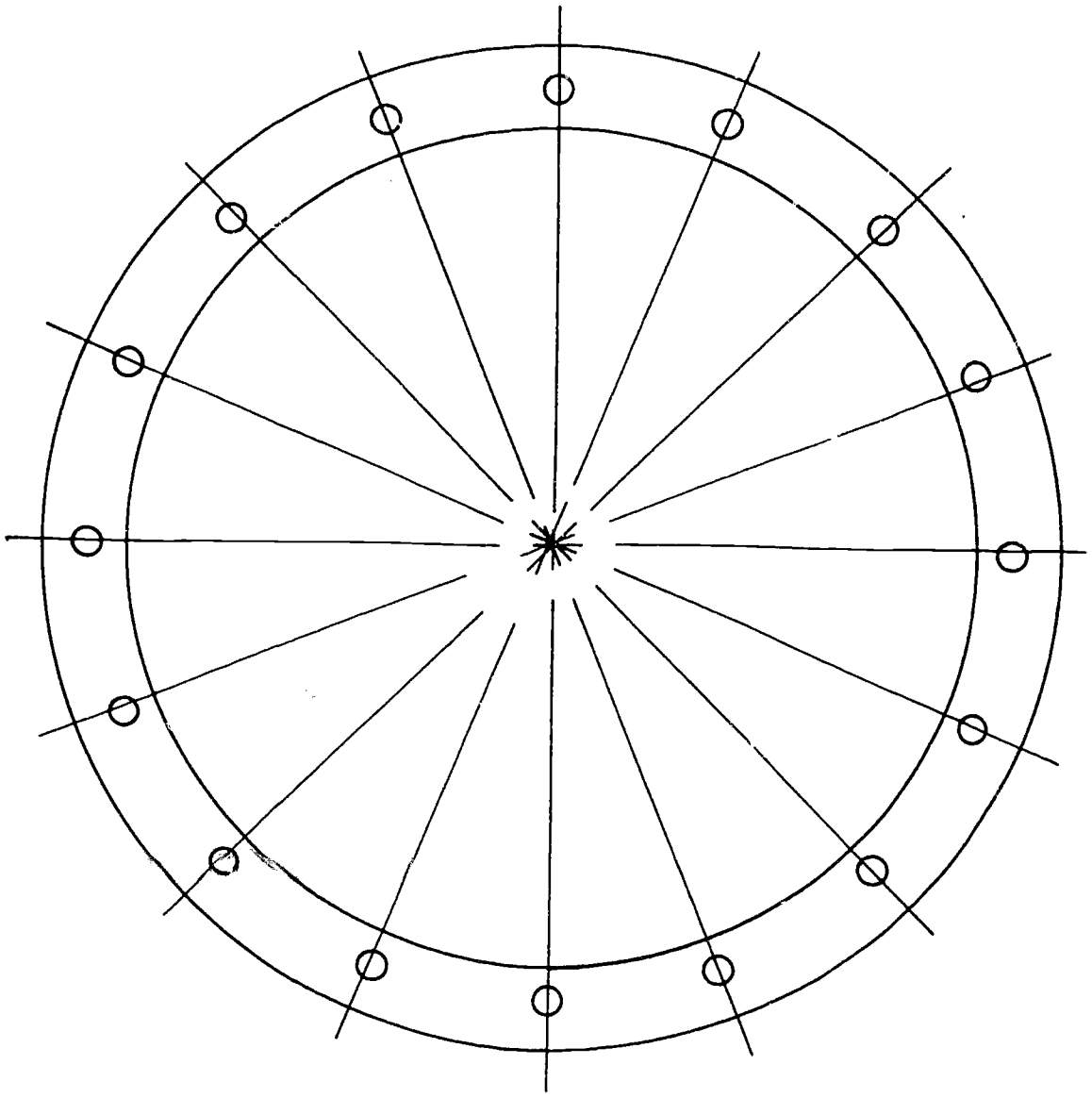

TIE DOWN RING

Mat: 6061-T6 AL
No. Req: 1

Figure 5

Piping and Hydraulics for

50 PSI Acrylic Pressure Tank

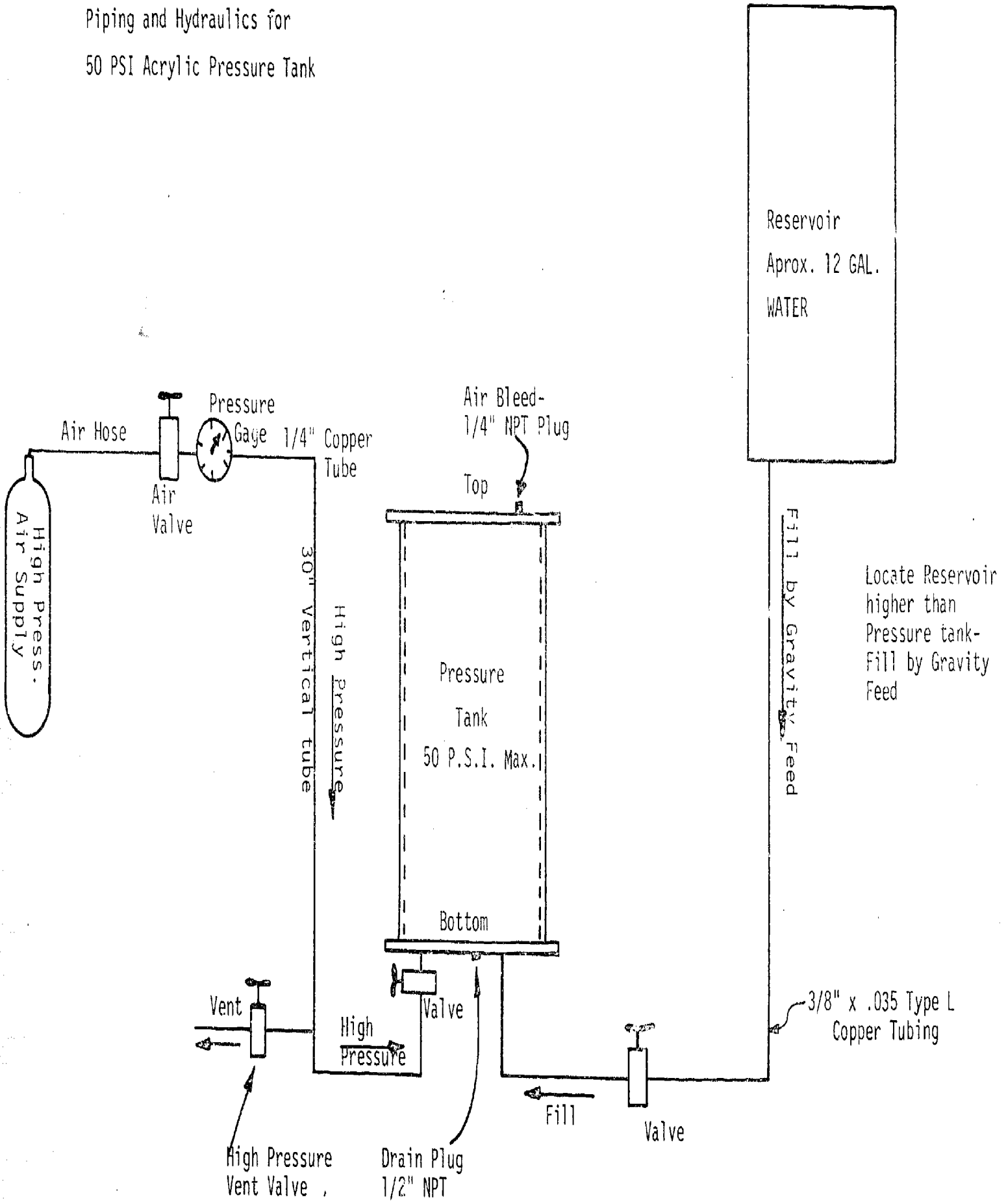

Figure 6

Assembly Drawing of 400 PSI, 6.7 ft^3 Steel Pressure Tank

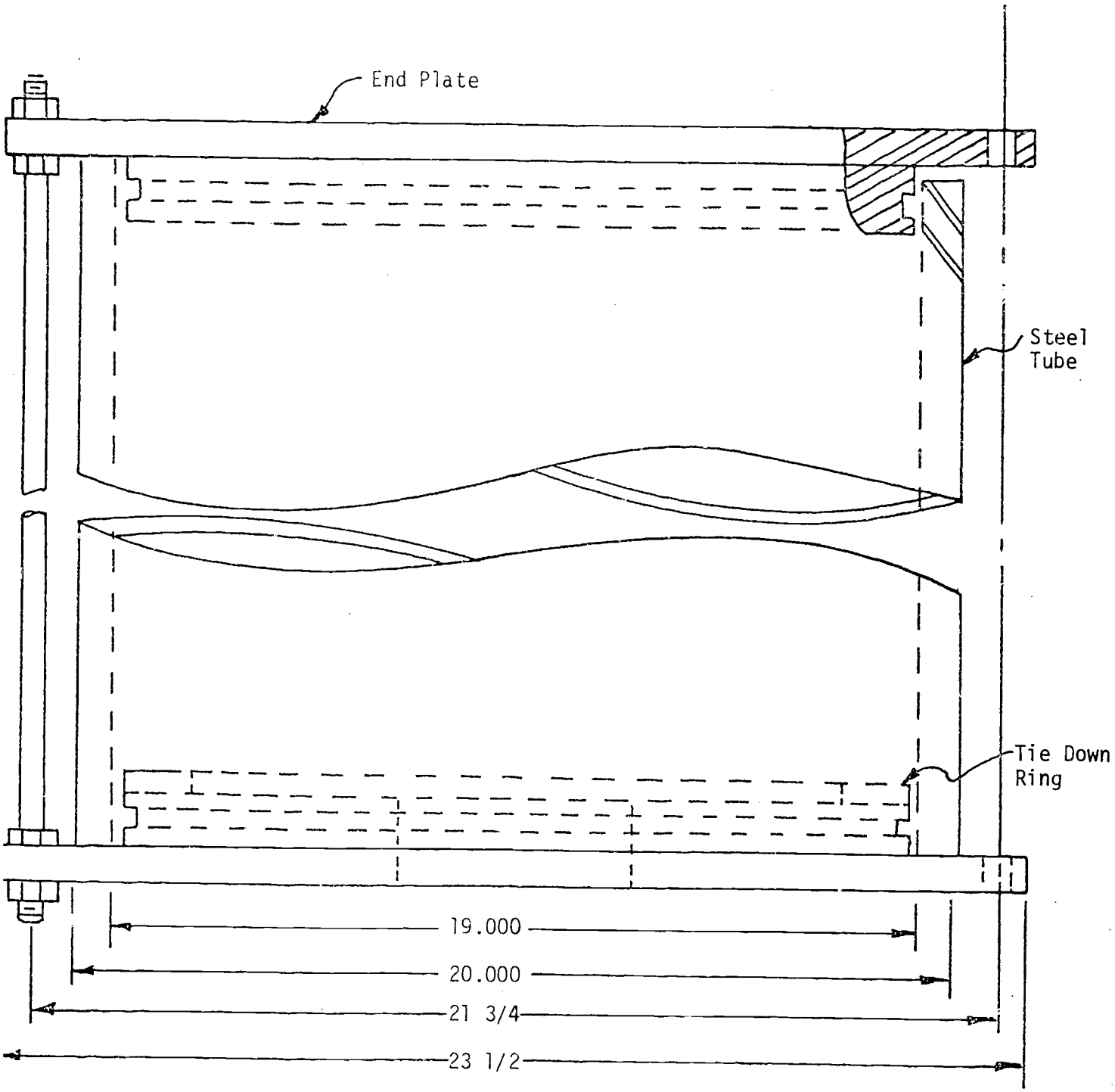

Figure 7

Material: 20" O.D. - 1/2" Wall Grade B Seamless Steel Pipe, ASTM-A53
Tensile Strength = 60 Msi Minimum

NOTE: Finish Inside of Cylinder 1" Down Both Ends

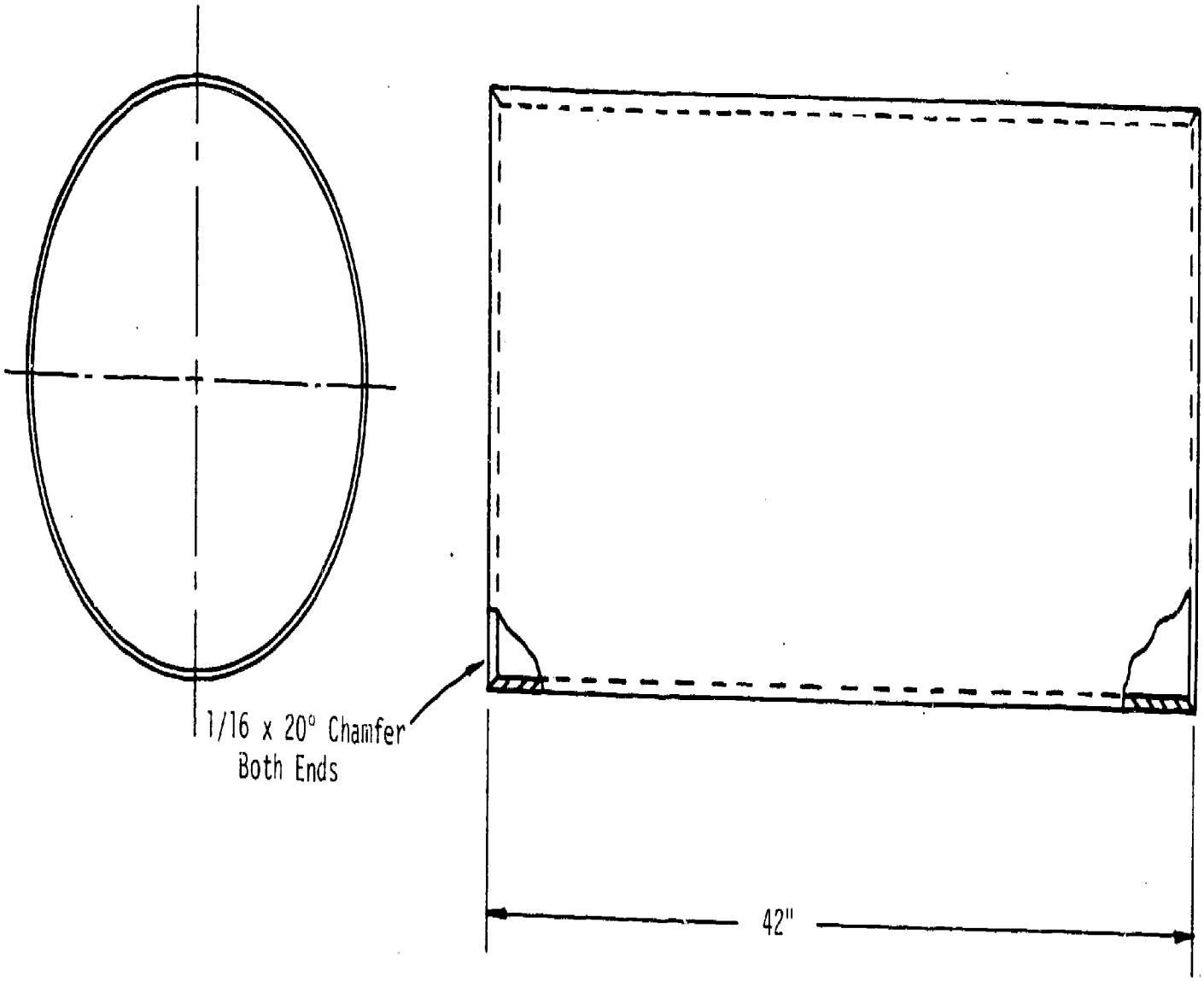

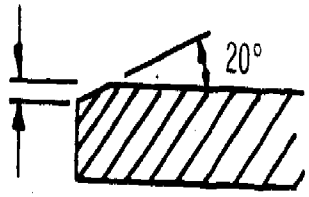

Figure 8

Top End Plate for 400 PSI Pressure Tank

Materials: 2024-T351 Aluminum Plate
No. Req: 1

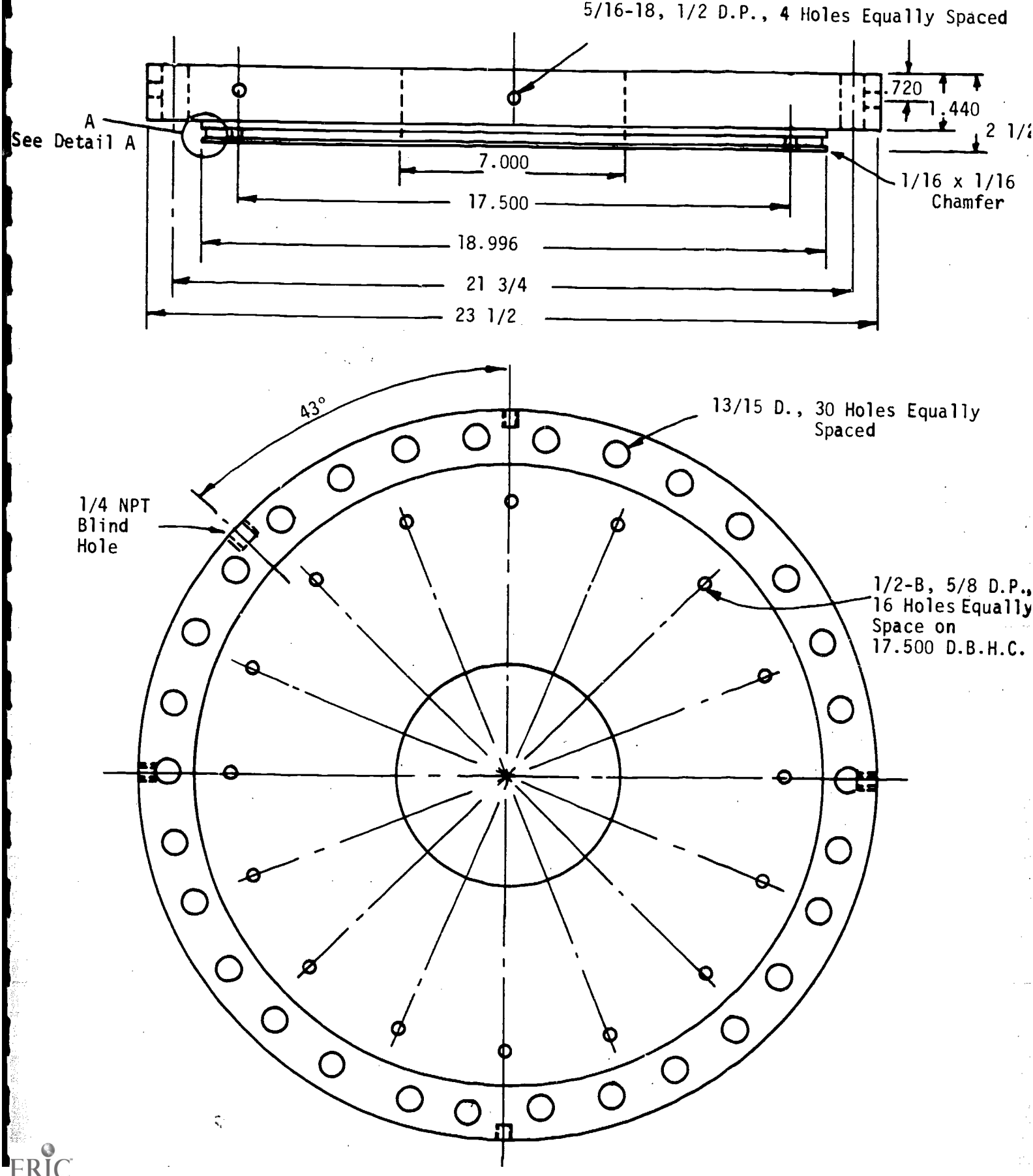

DETAIL A

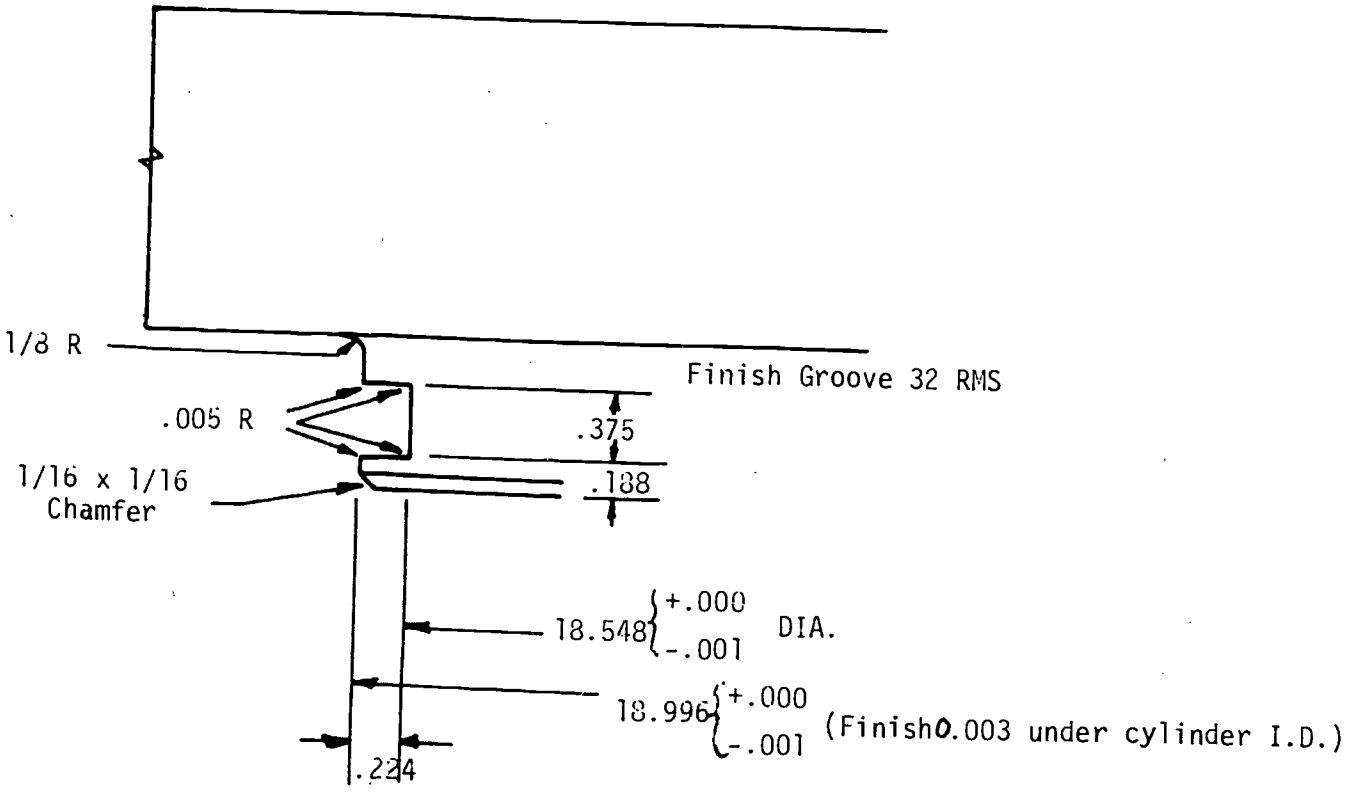

Figure 10

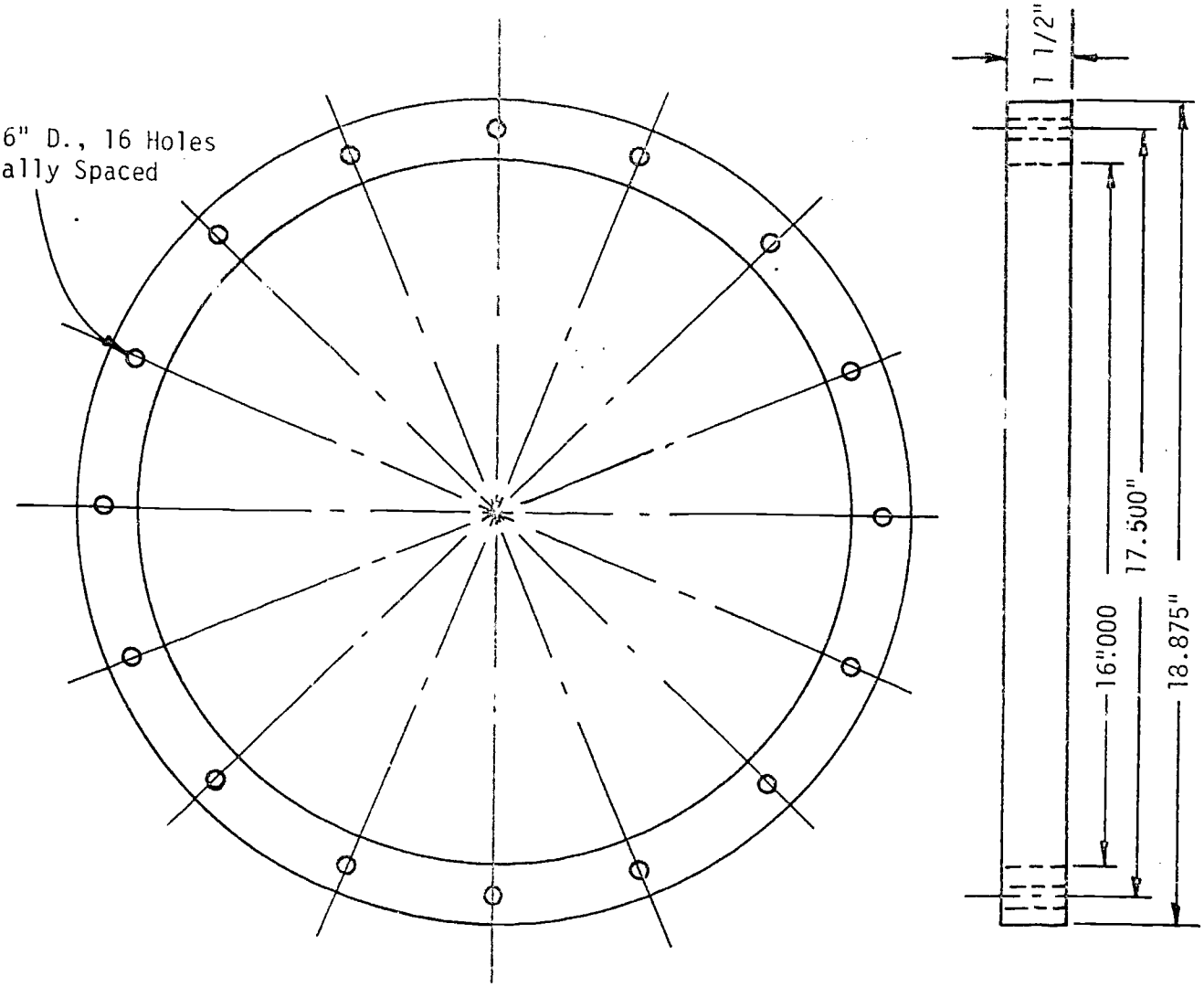

TIE DOWN RING

Mat: 6061-T6 AL
No. Req: 1

Figure 11

Tie Rod, 400 PSI Pressure Tank

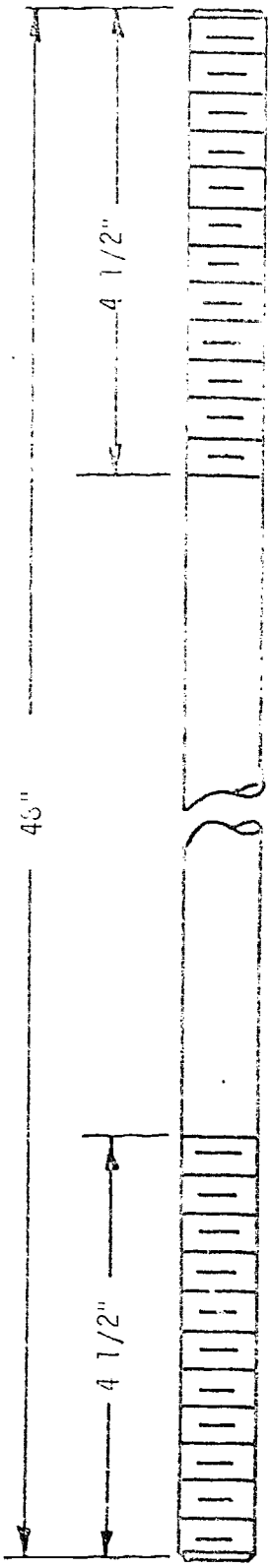

Material: 1045 Carbon Steel Rod, 3/4" Diameter

No. Required: 30

Thread: 3/4" - 16

1045 Carbon Steel Rod, 3/4" Diameter

Figure 12

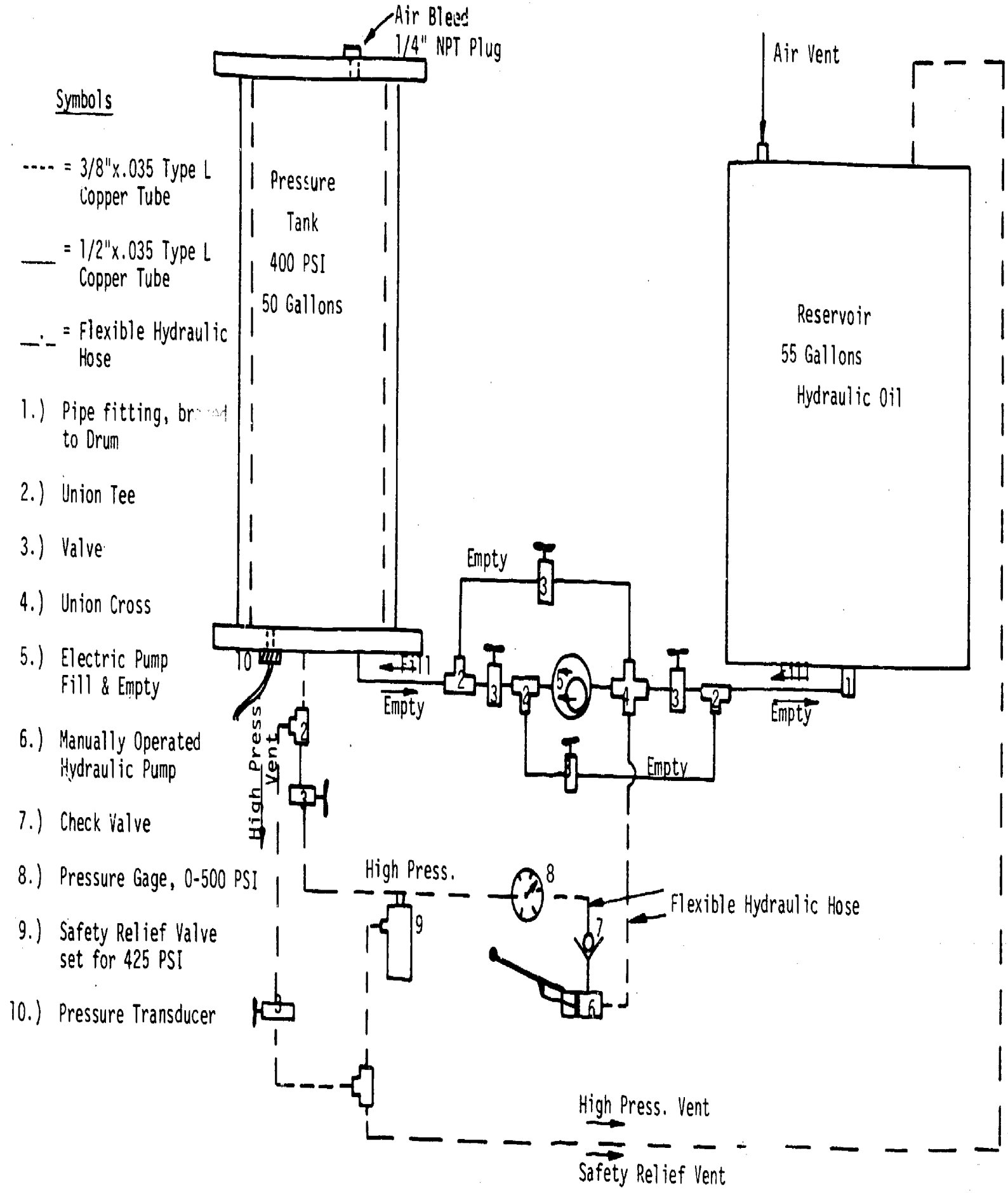

Piping and Hydraulics for 400 PSI, 6.7ft^3 Pressure Tank

Figure 13

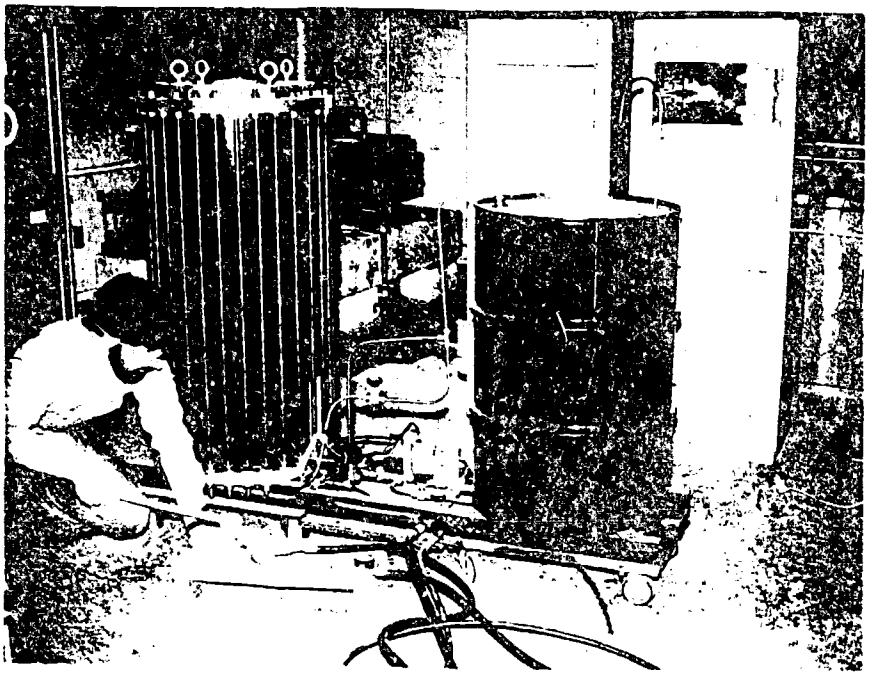

Figure 14

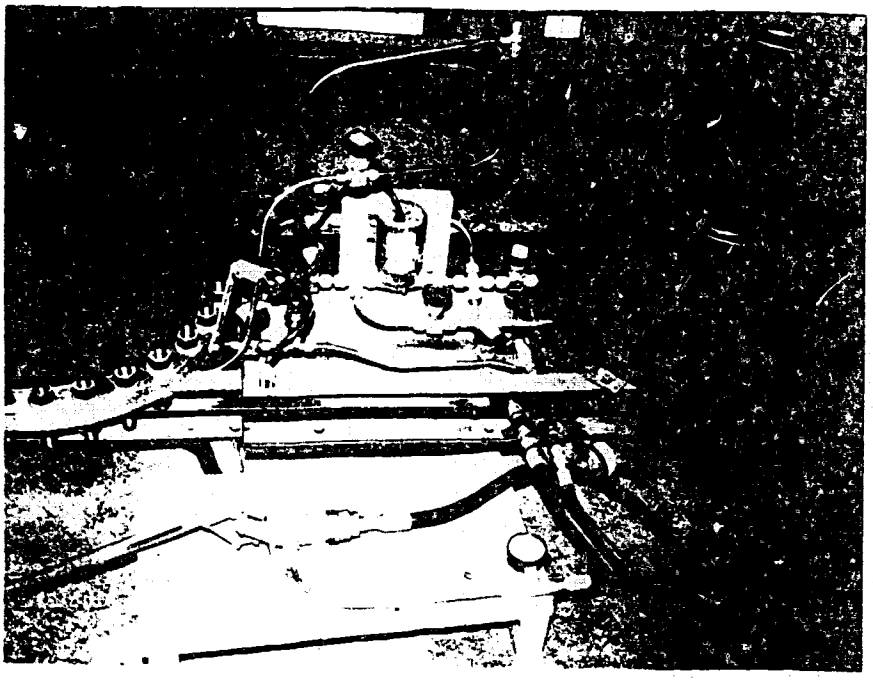

Figure 15

3000 PSI Pressure Tank

Assembly Drawing

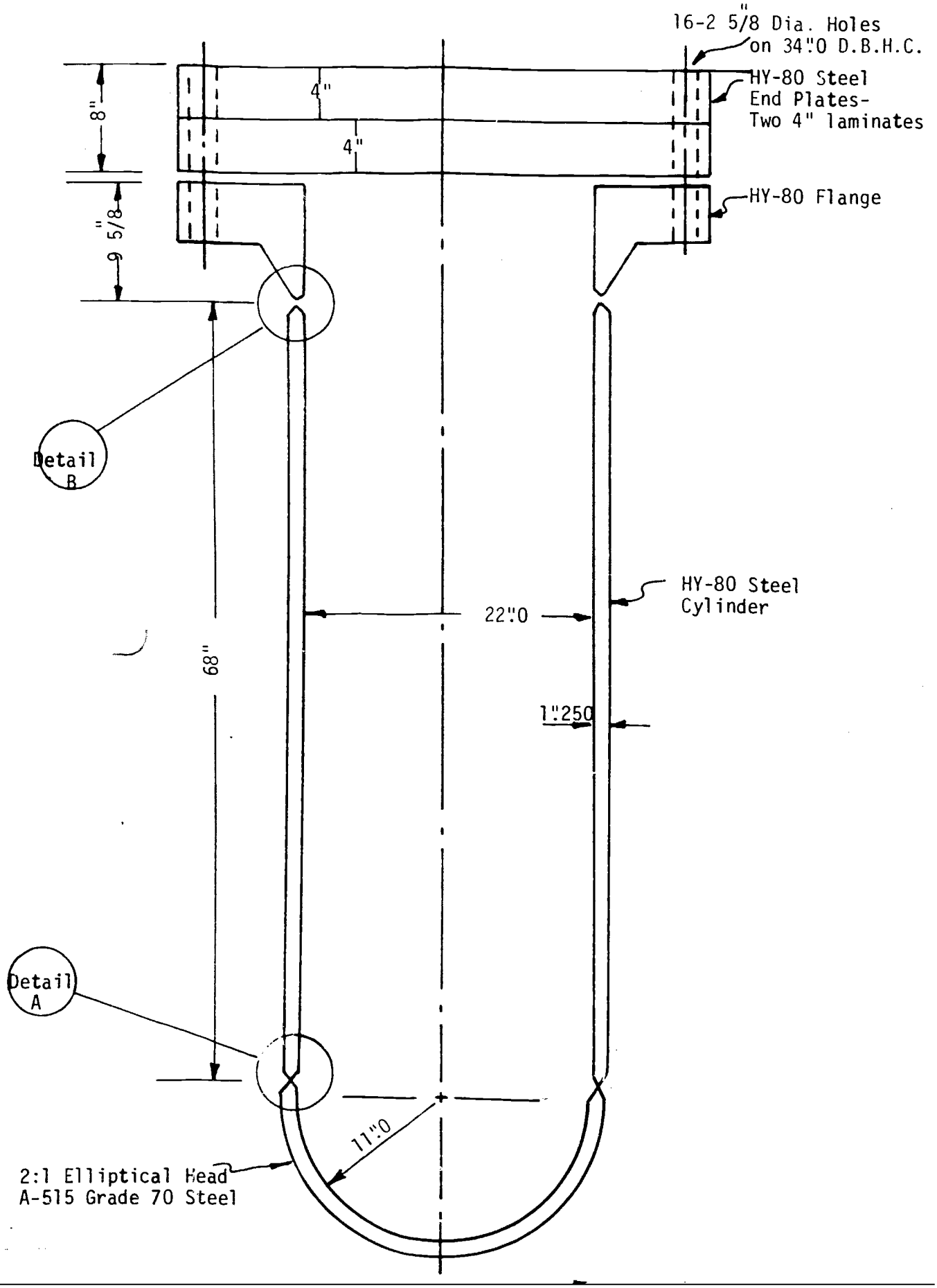

Det-il A: Elliptical Head

No. Req: one
Tolerance:

fraction	Decimal
± 1/8	± 0.125

60° included Angle
Double-V Joint
1/3 inside
2/3 outside

All welding to
meet specifications
of NAV SHIPS
0900-000-1000

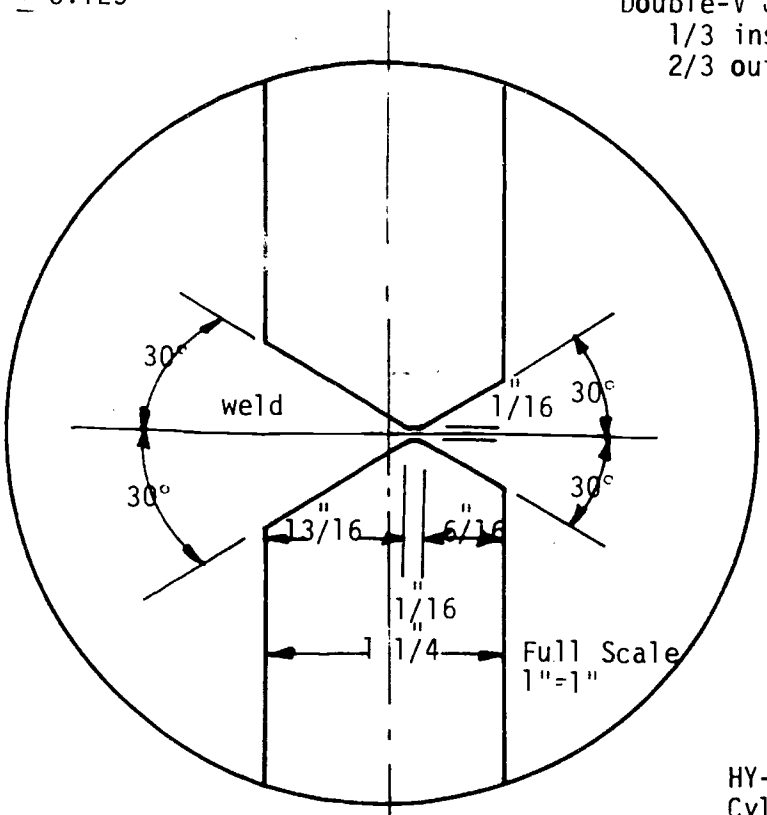

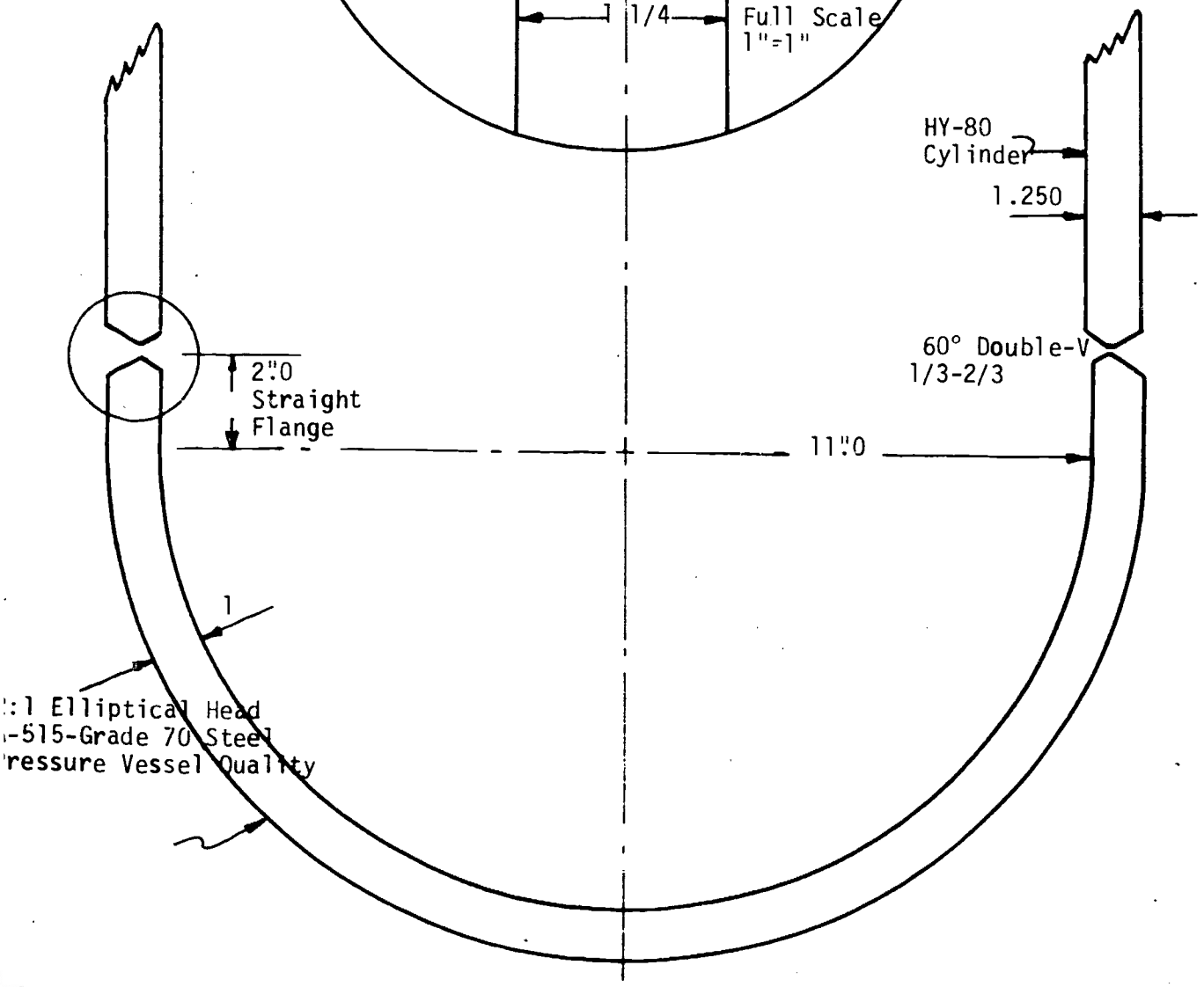

Detail B: Bolting Flange

No. Req: one
Tolerance: ± 1/16"

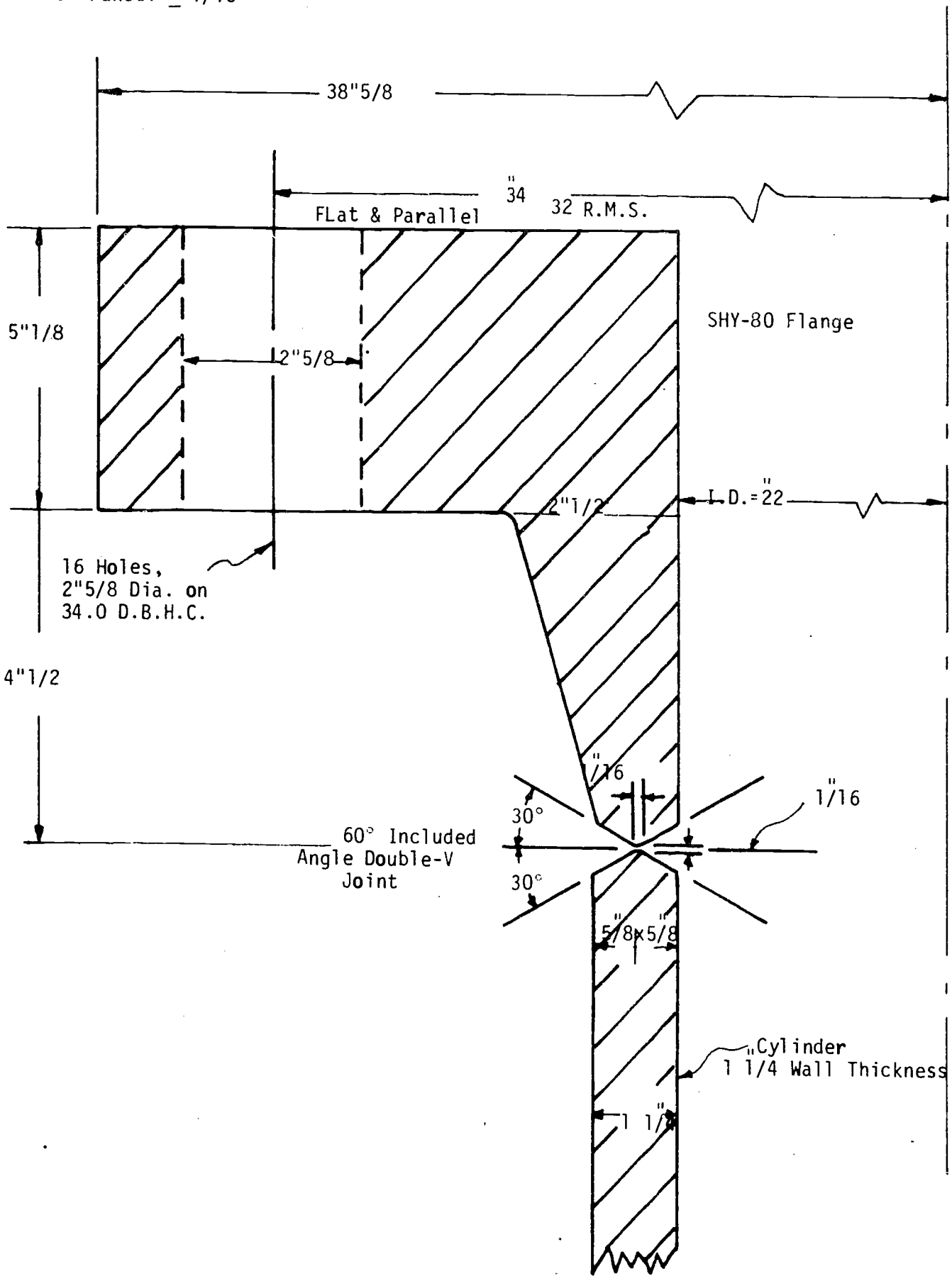

Figure 18

End Plates for 3,000 PSI Pressure Tank

Material: HY-80 Steel
No. Req.: Two

Note: 63 RMS Finish on one side only

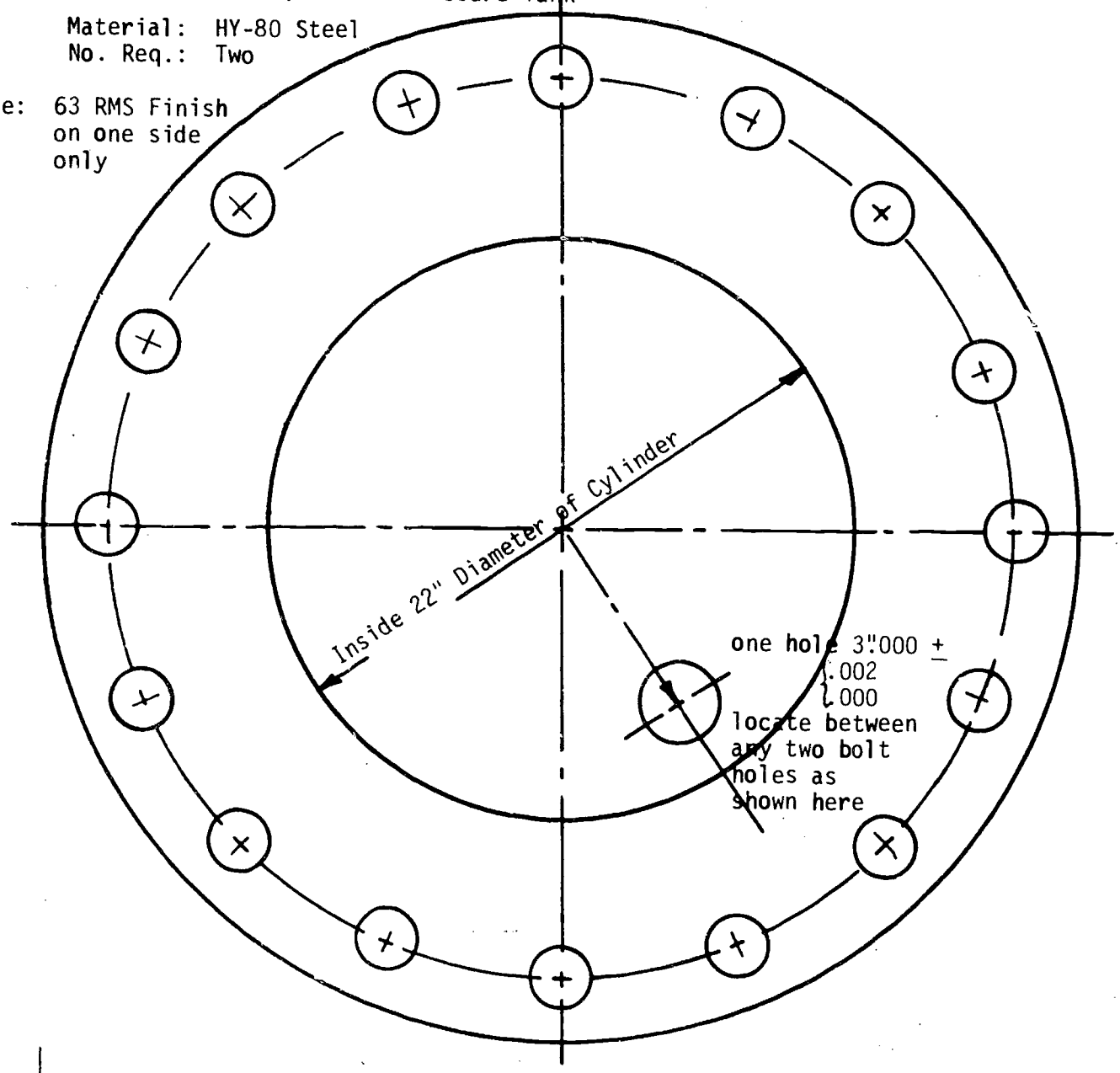

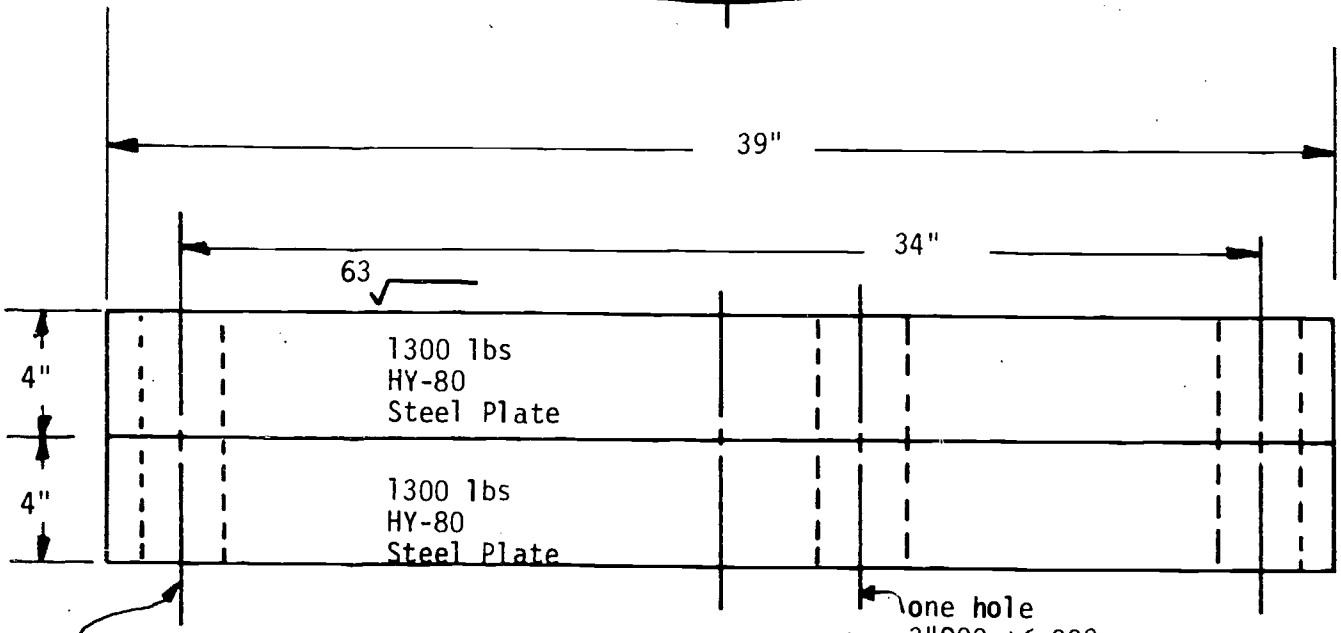

Figure 19

END PLATE BOLTS
FOR 3,000 PSI
PRESSURE TANK

Material: A-193 B7 Steel

No. Req. 16

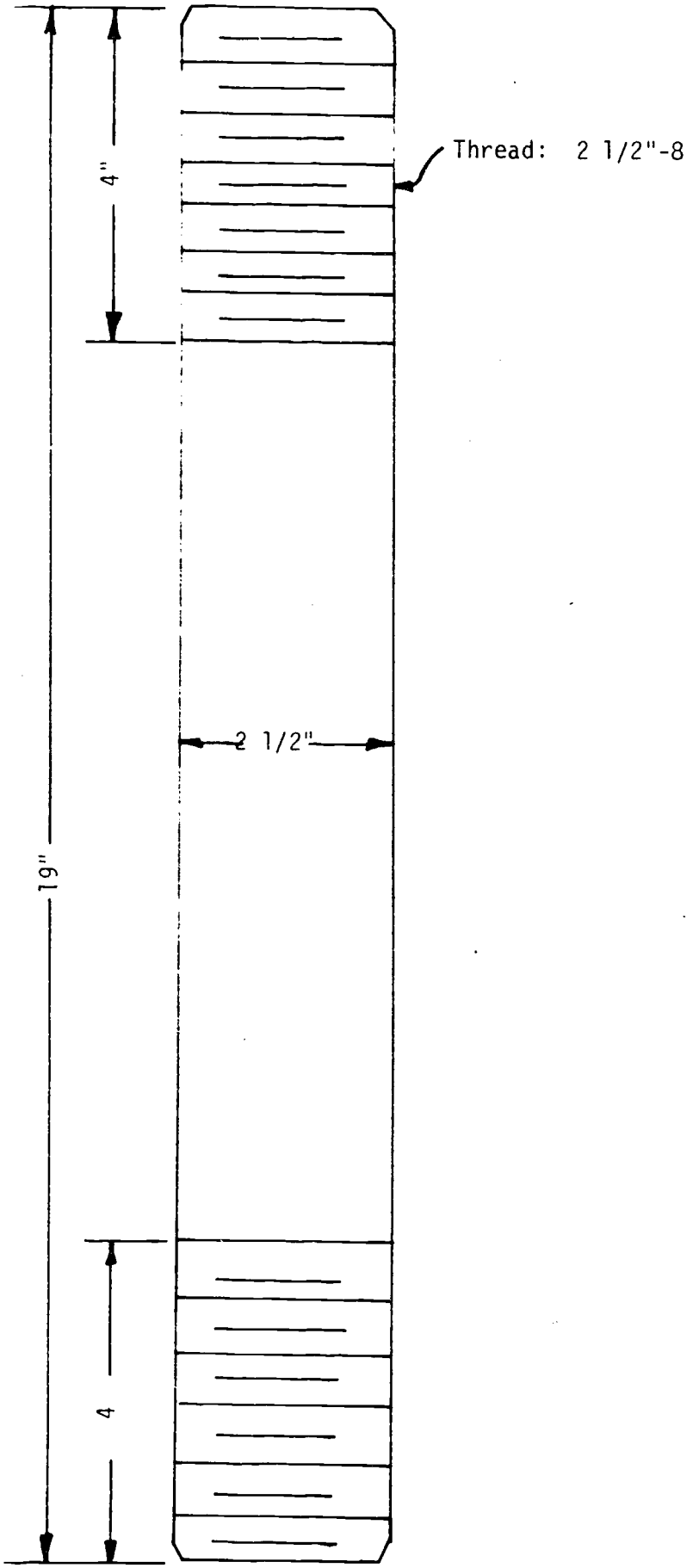

Figure 20

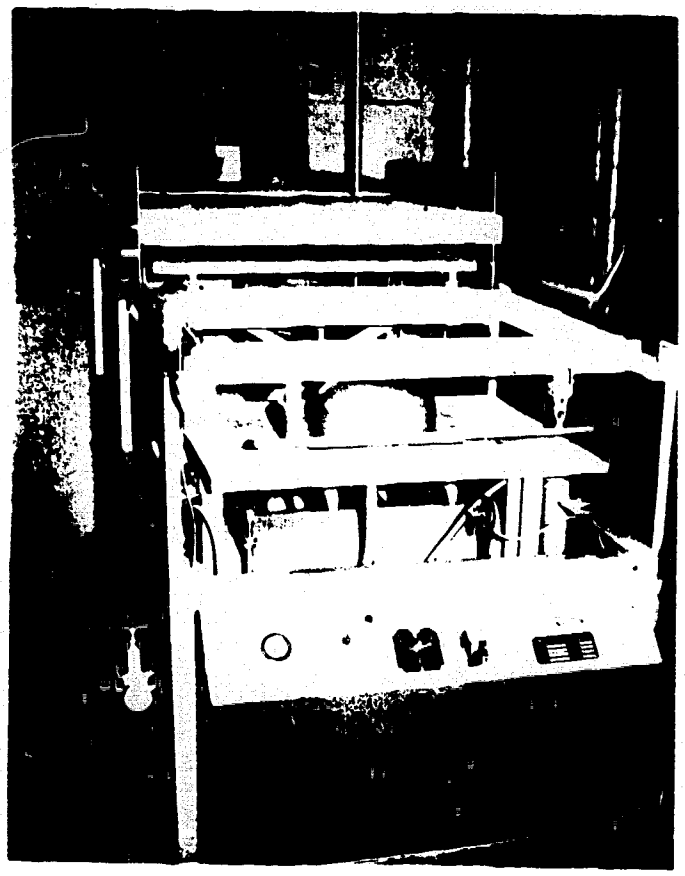

Figure 21

Figure 22

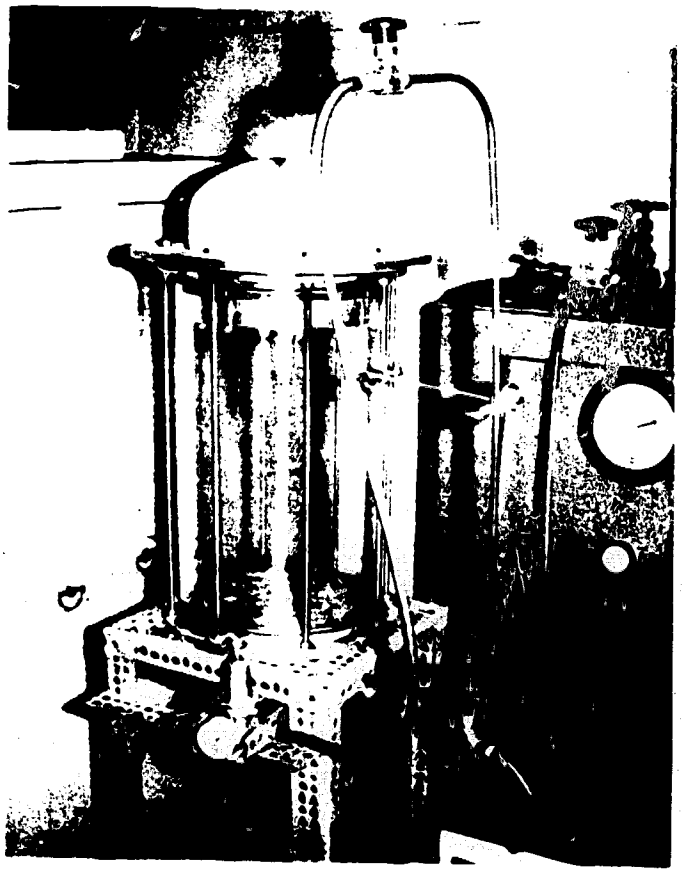

Figure 23

Side View of Mould for
Torispnerical Snell

Material: Hard Wood
No. Req: one
Tolerance: ± 1/16" closer if possible

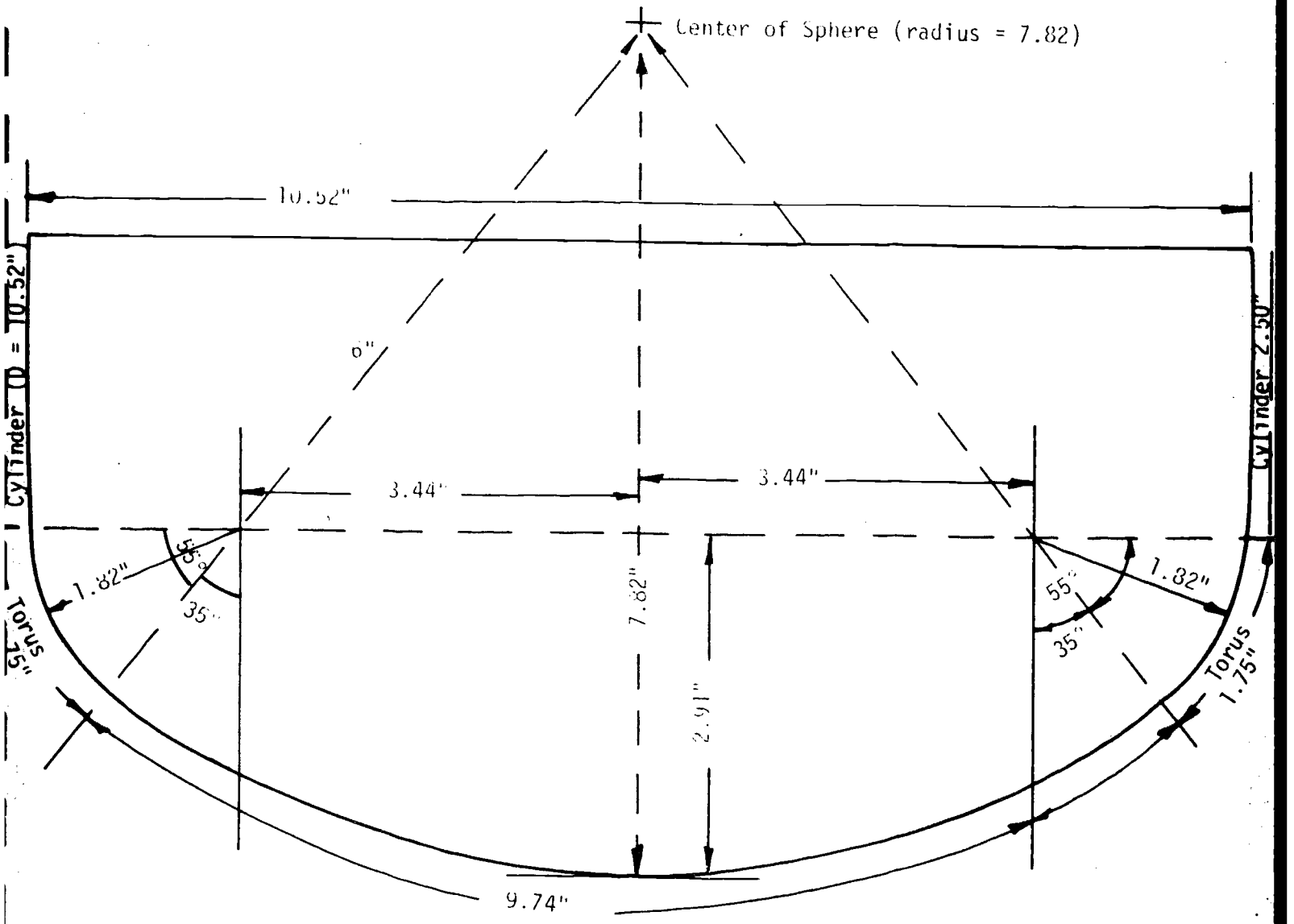

Spnerical Surface, radius = 7.82"

Figure 24

Clamping Ring for Torispherical Shells

Material: 6061-T6 Aluminum Plate, 1/2" nominal thickness

No. Req.: 1

Tolerance: ±.010 unless otherwise specified

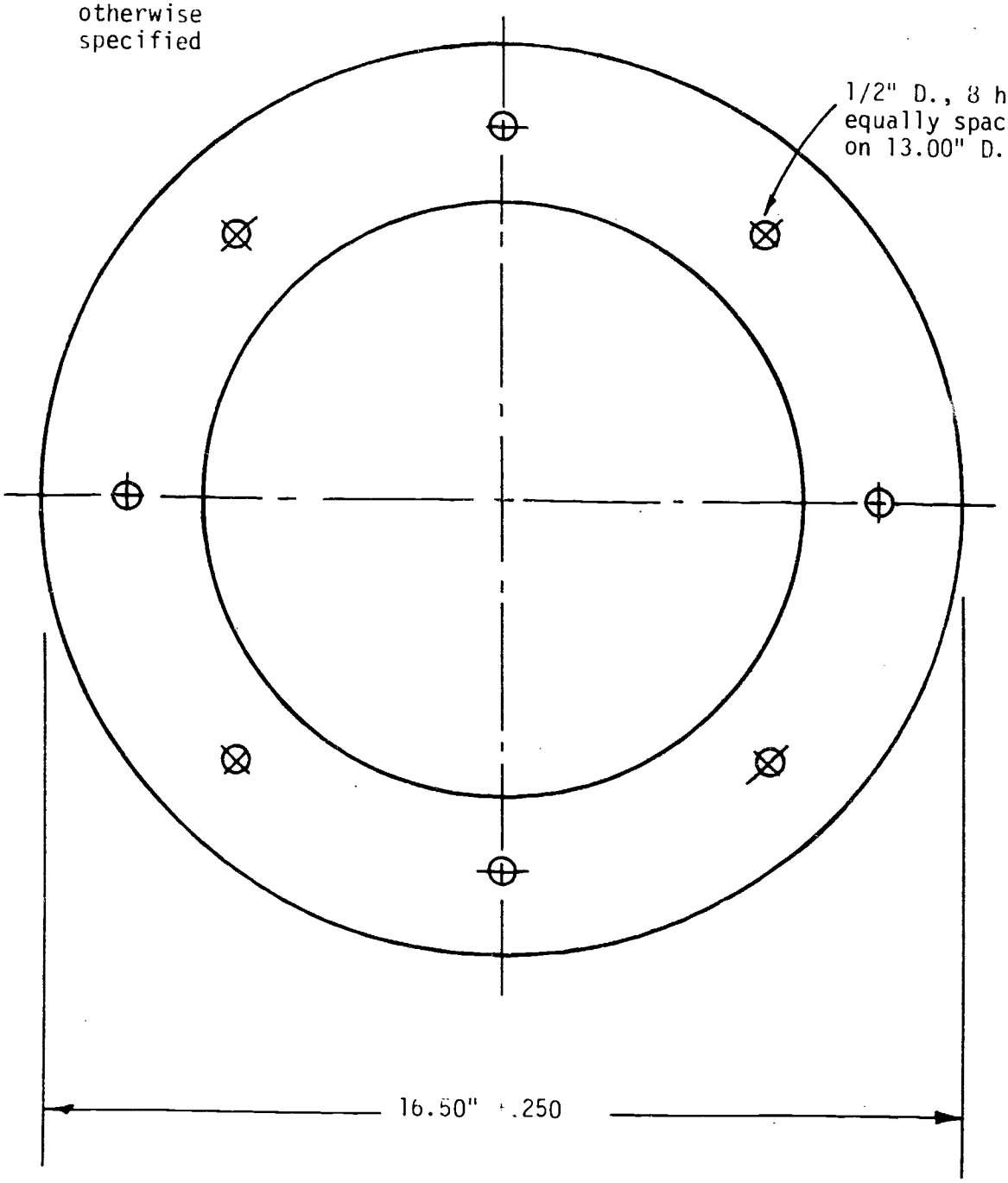

NOTE: Finish only on surfaces so marked - all others have ne required finish.

Figure 25

Material: Cylinder = plexiglass
End Plates = plexiglass

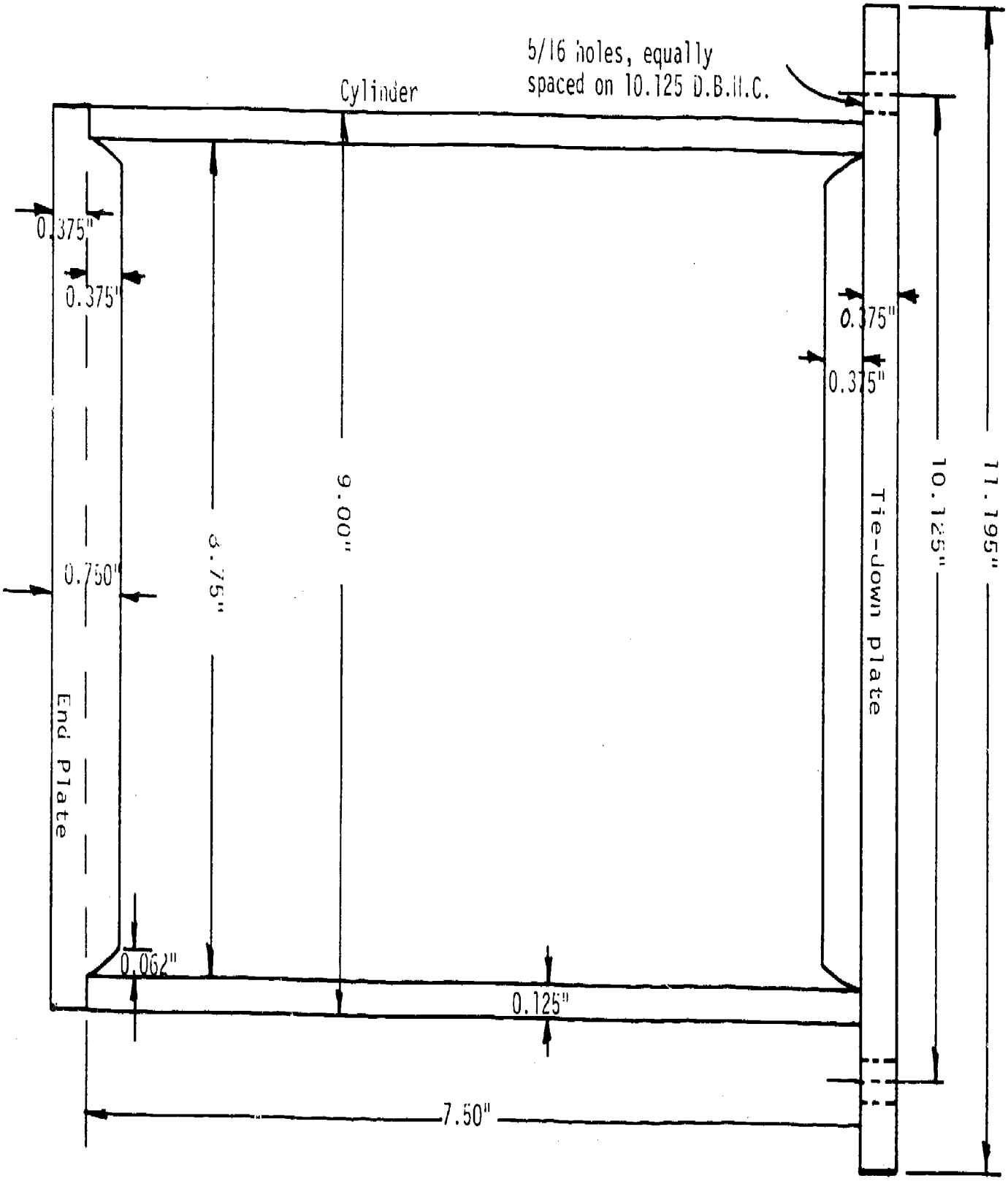

Assembly Drawing Cylindrical Test Specimen
Collapse Pressure: 31 PSI

Figure 26

Detail of Tie-down Plate
Material: Plexiglass

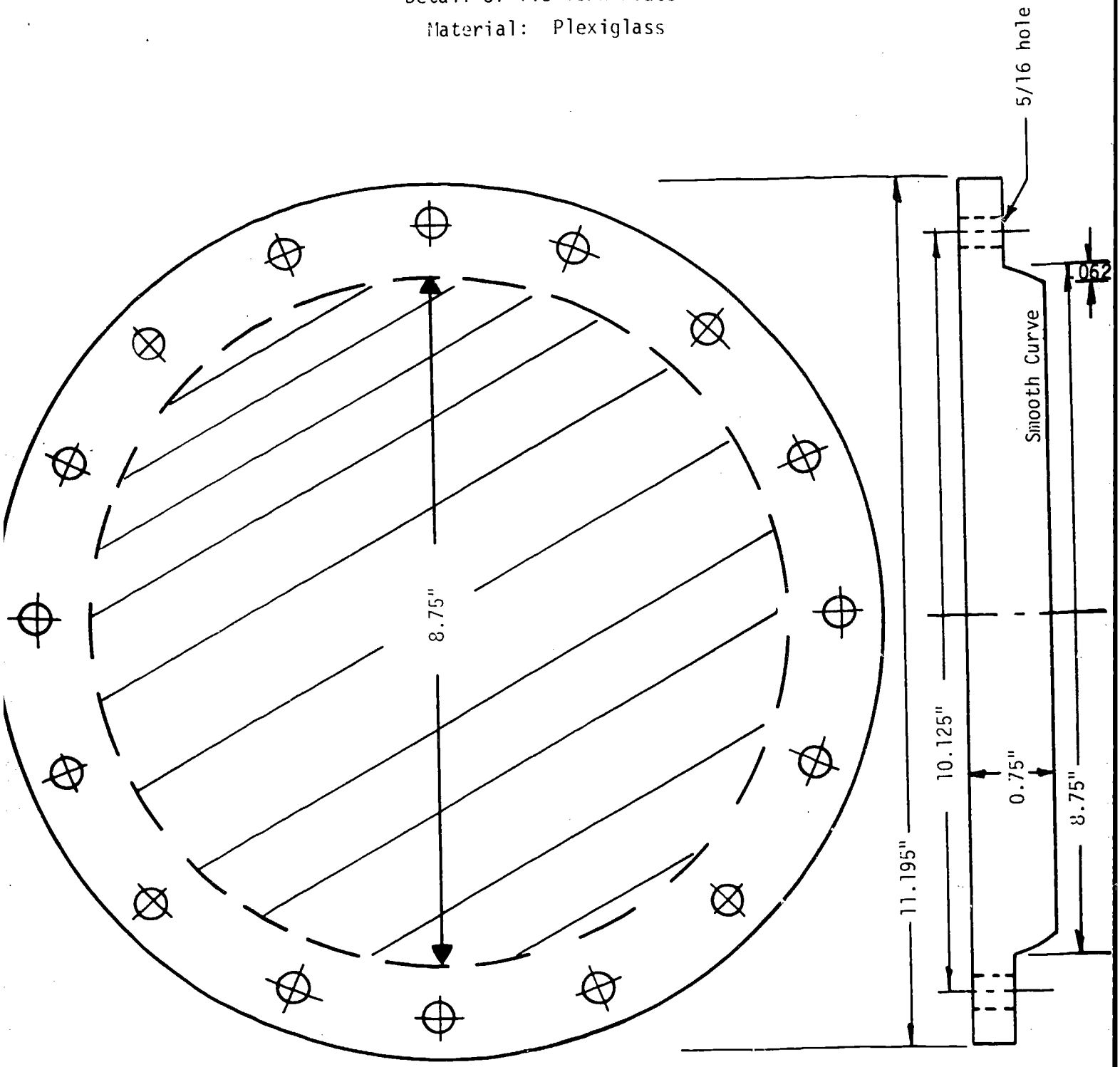

5/16 D., 16 Holes
equally spaced on
10.125 D.B.H.C.

Figure 27

Detail of End Plate
Material: Plexiglass

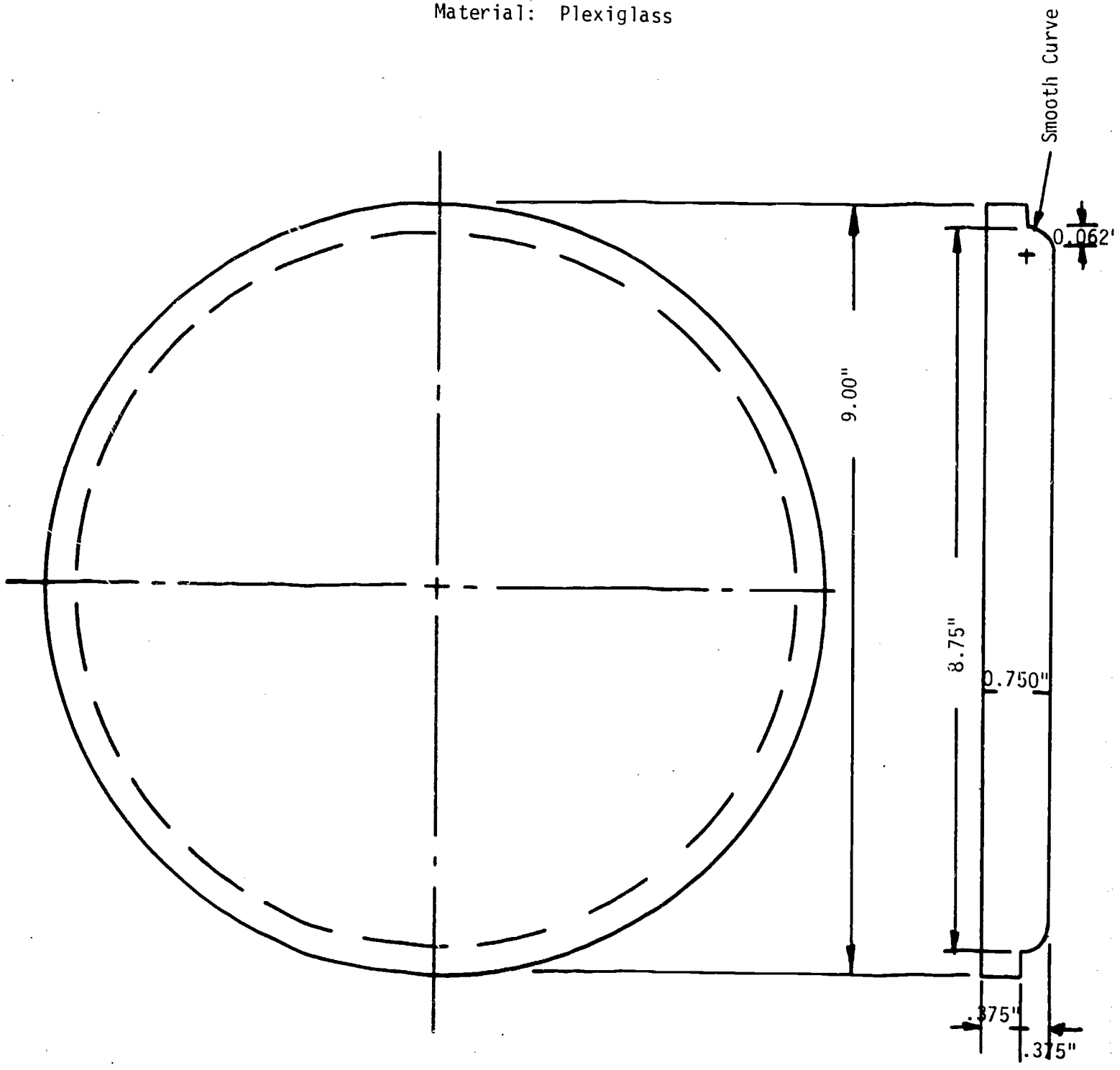

Figure 28

Ring Stiffened Cylindrical Shell

Material: Acrylic Scale: 1"=2"
Collapse Pressure: 35 PSI for L< 36-inches Failure by Elastic Instability

For L> 36-inches, Pcrit < 35 PSI and Failure is by Elastic General Instability

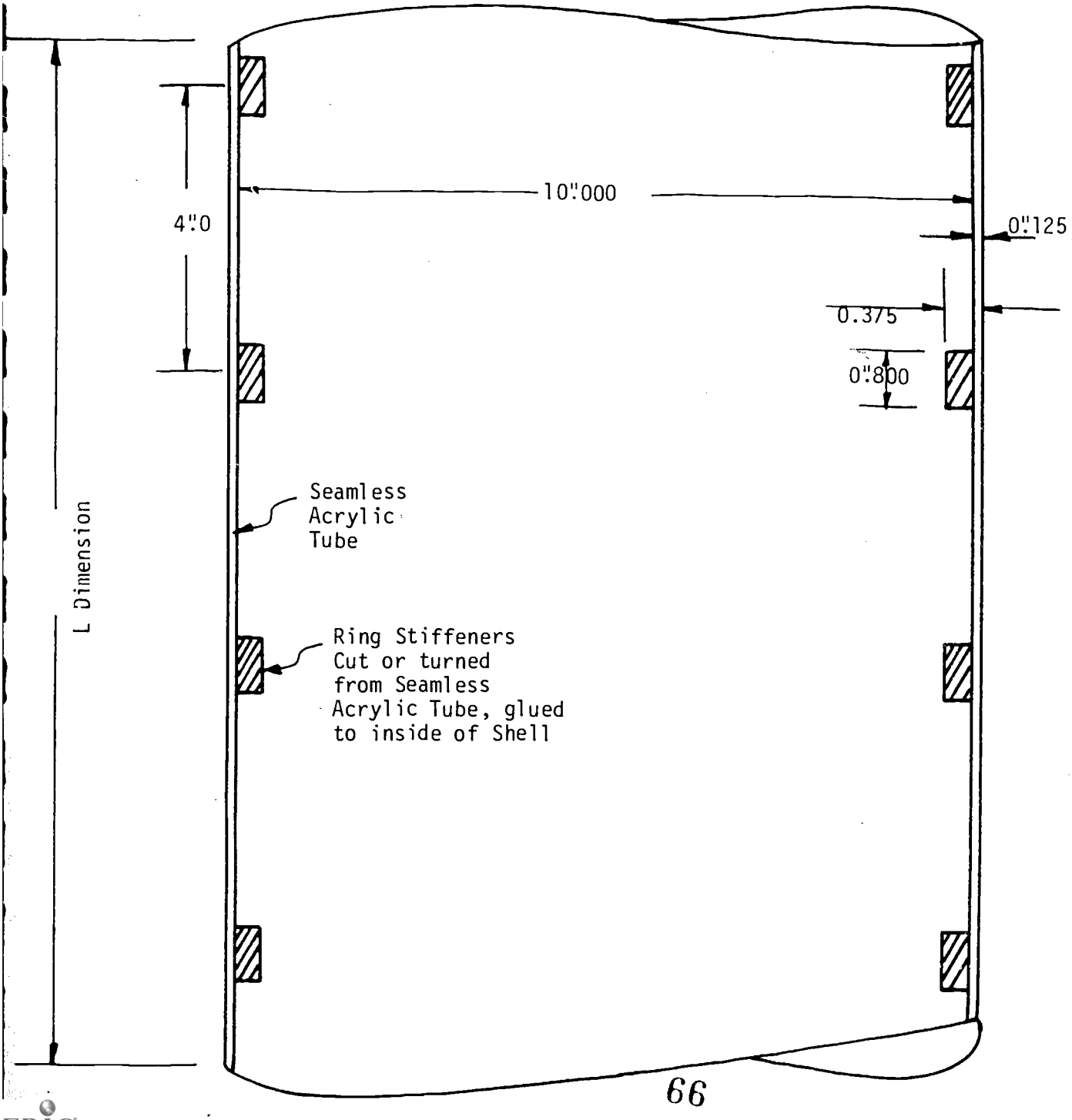

Figure 29

Assembly drawing

Fixture to apply impact landing on hatch apenings.

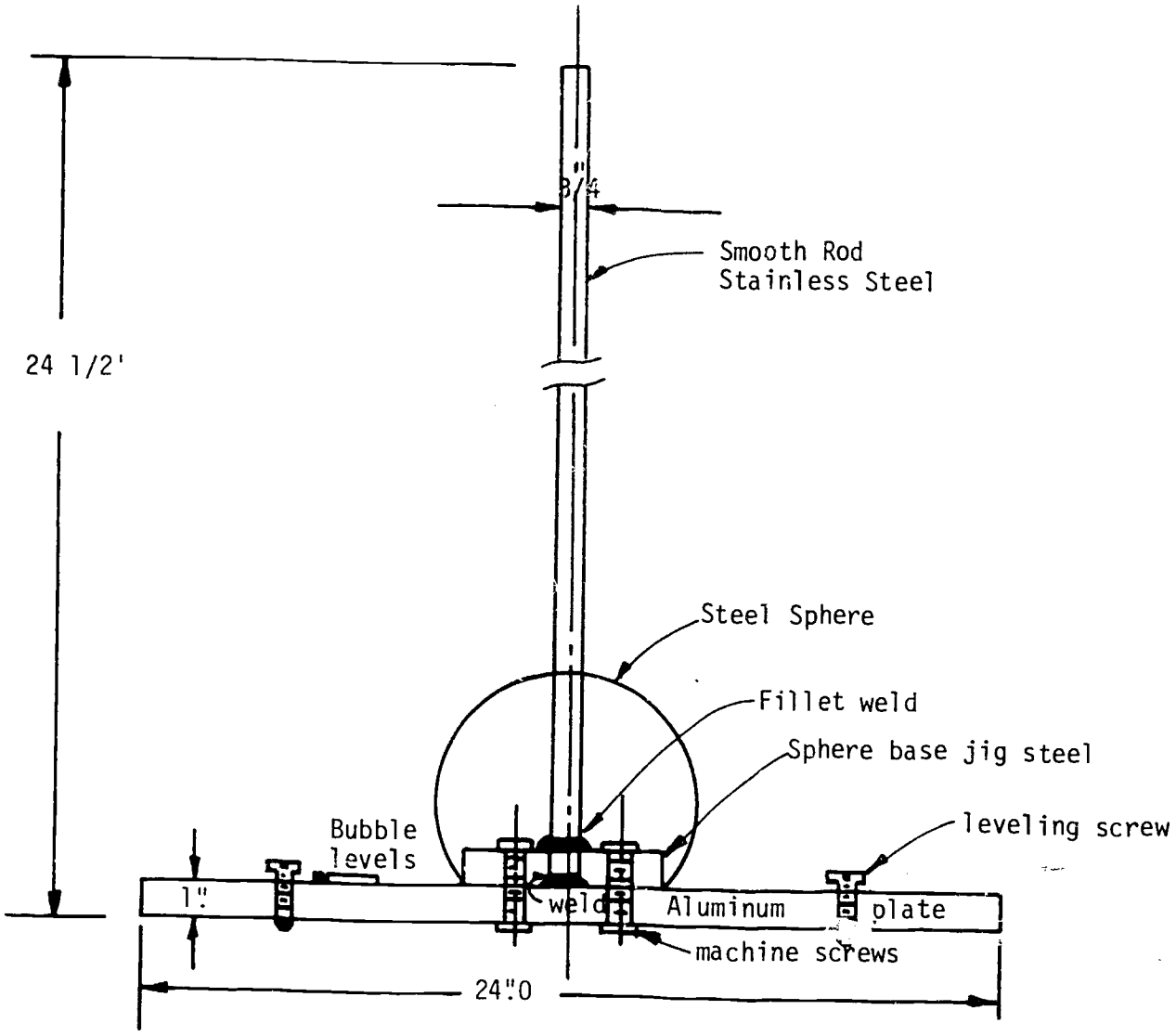

Scale: 1"=5"

Figure 30

Base Plate

Material: 24" x 24" x 1" 6061-T6 Aluminum Plate
Number req: 1

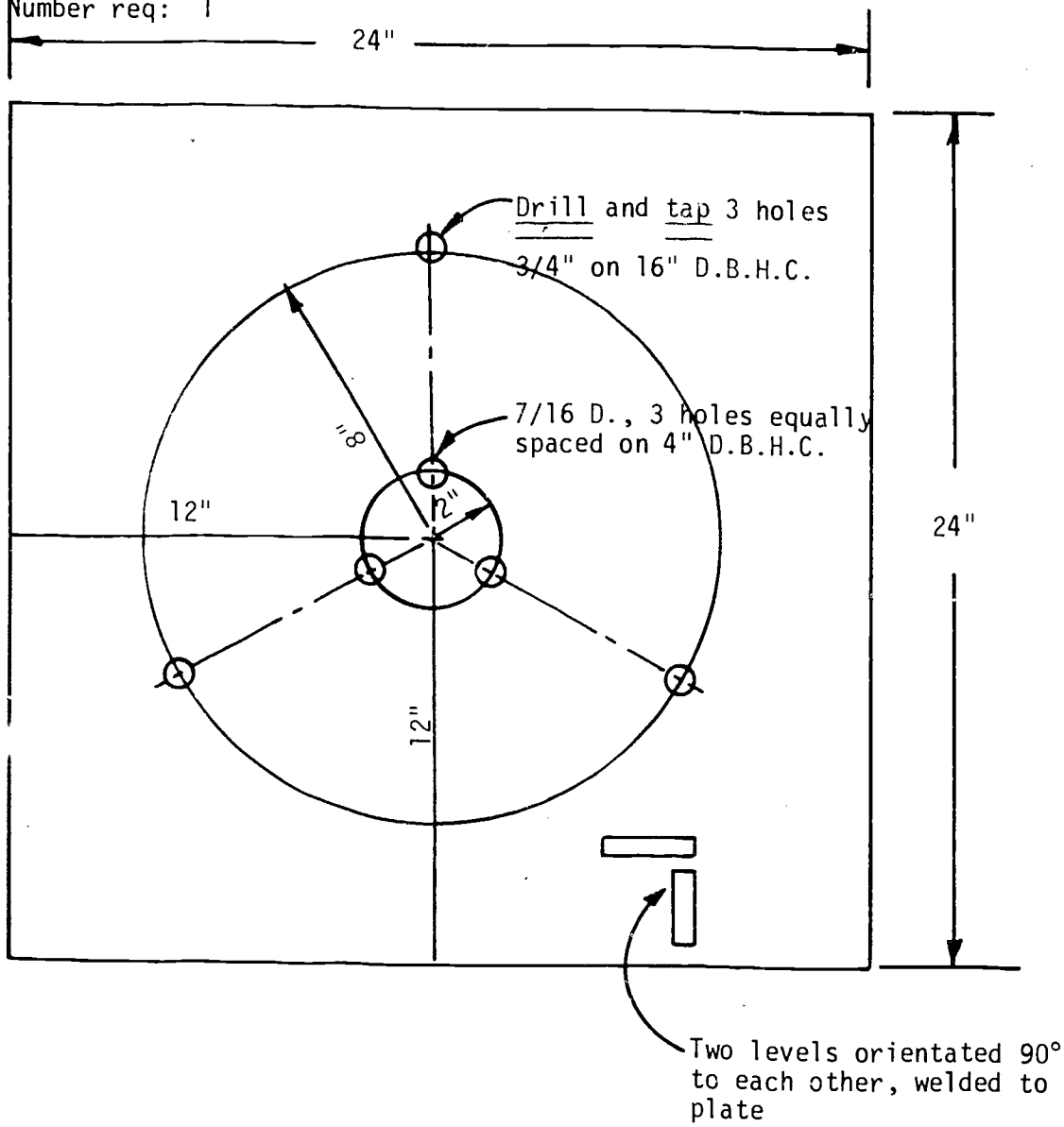

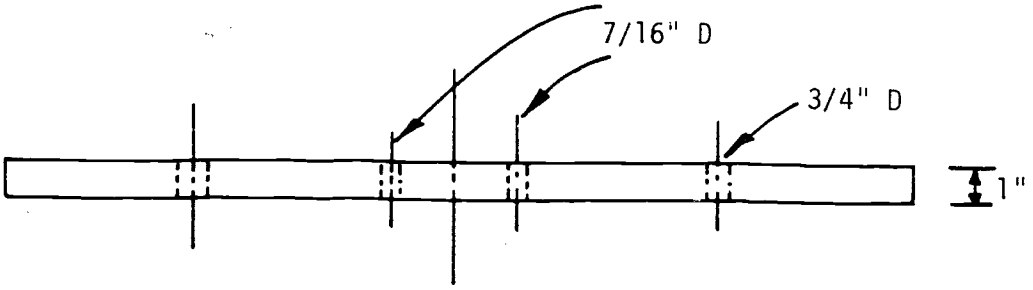

1"=5" SCALE

Figure 3

Rod and Sphere Jig

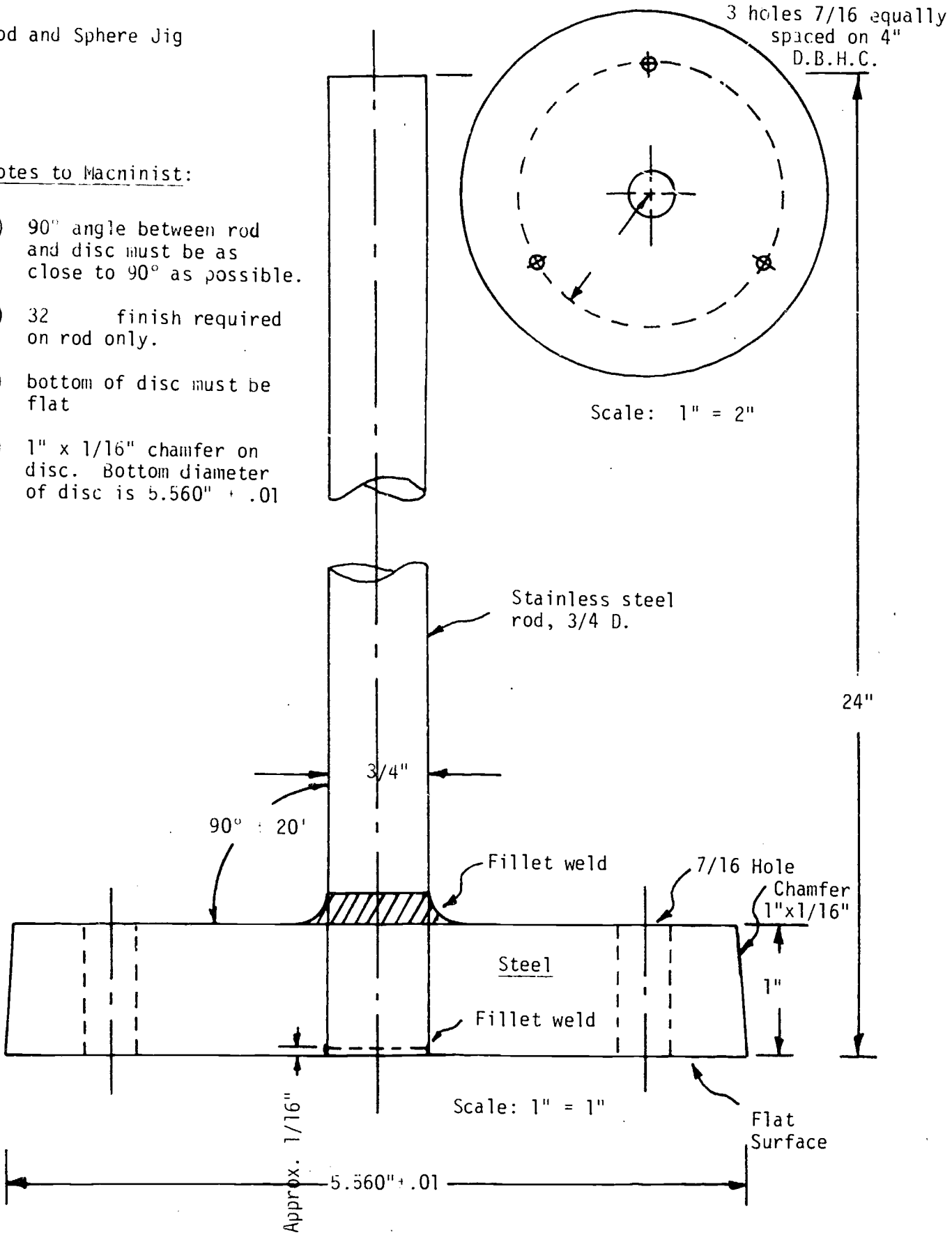

Figure 32

Slide Weight

Material - Stainless Steel Rod
No. Required = 1
Tolerance: ±1/32" unless specified

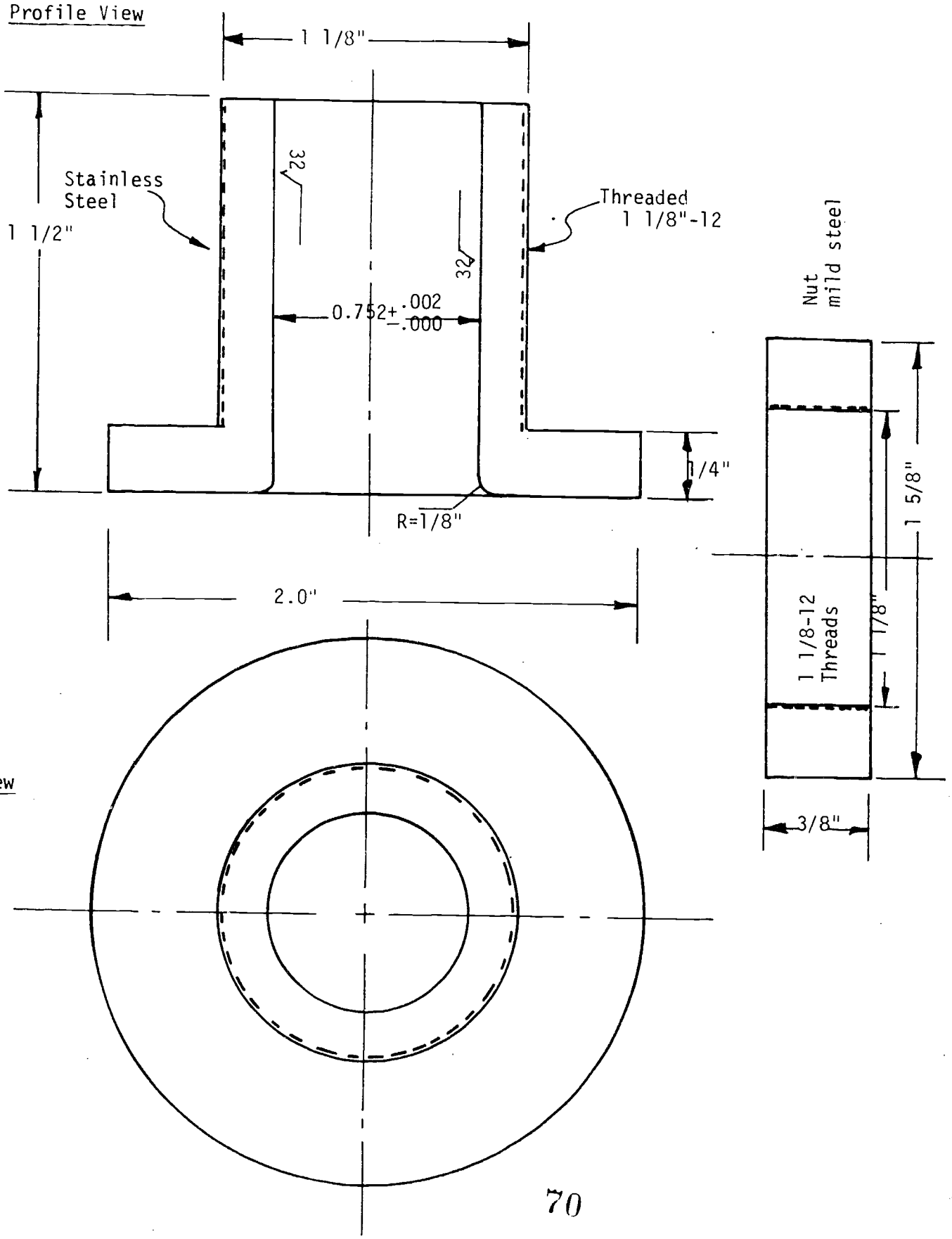

Figure 33

Hatch Coaming

Number Req'd; Two: one per Detail A
one per Detail B

Tolerance: as specified

Material: Sphere: Steel
Coaming: Steel

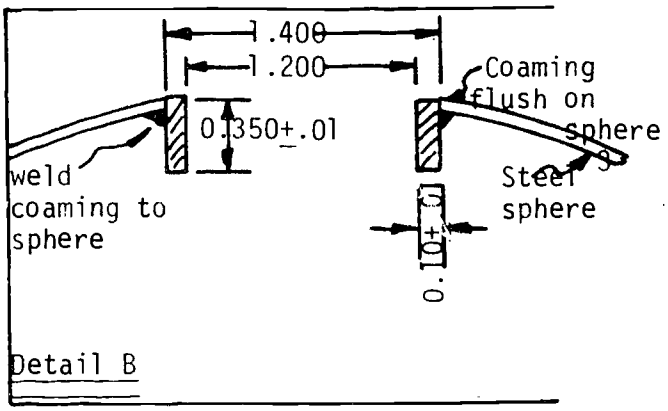

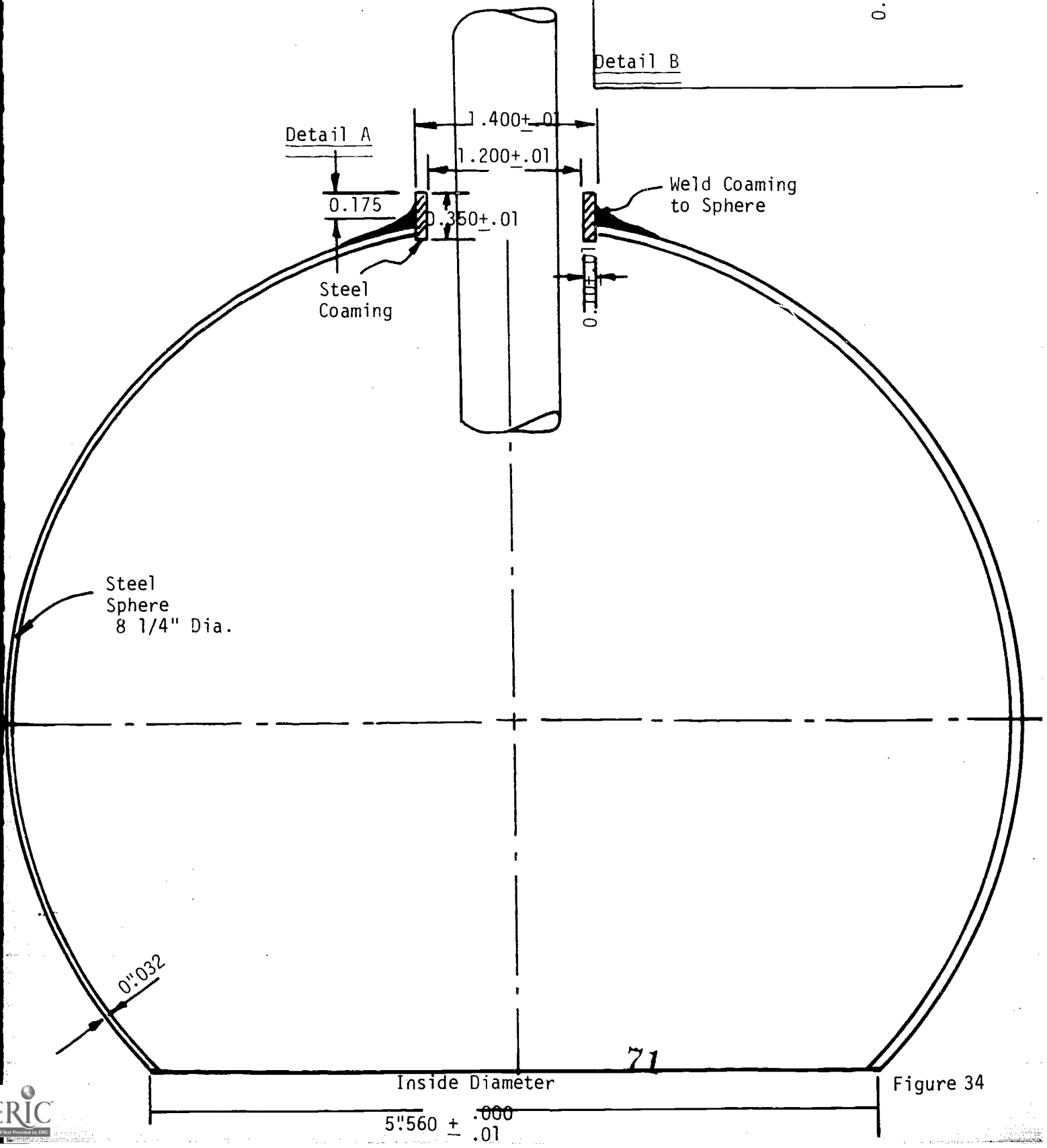

Figure 34

Photo Cell
Aiming Jig

TOP VIEW

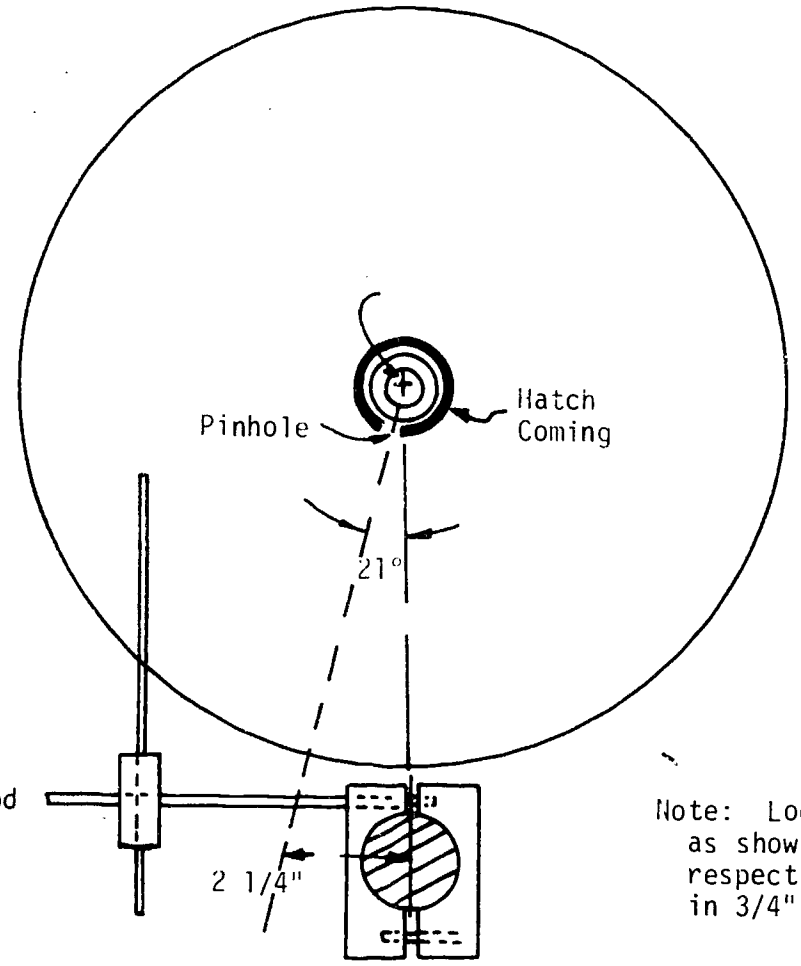

Note: Locate 1/18" rod as shown here with respect to pinhole in 3/4" tube.

SIDE VIEW

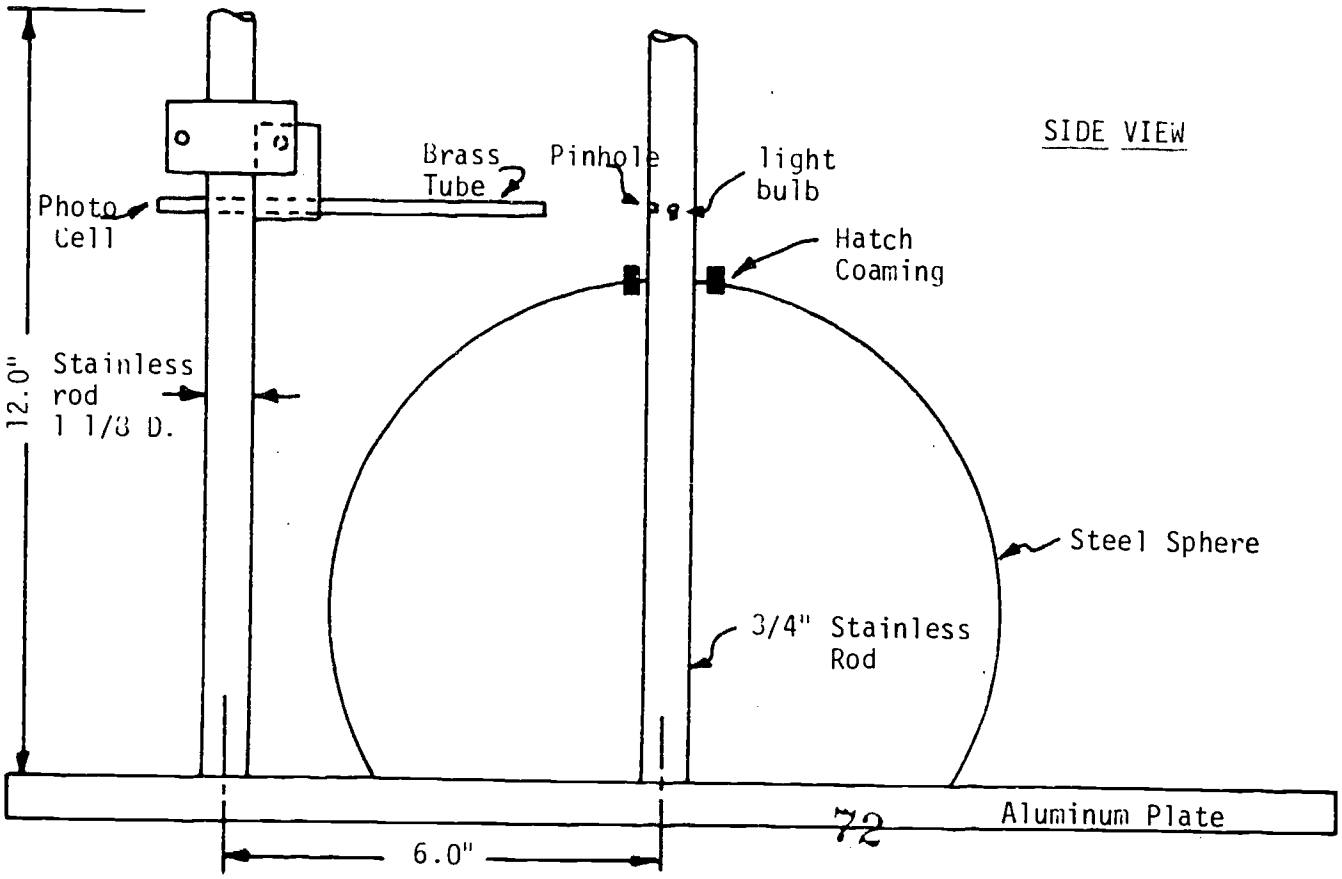

Figure 35

Photo Cell
Aiming Jig

Horizontal Translation
Vertical Rotation

Tolerance: I 0.003"
No. Req.: 1
3 View Sketch

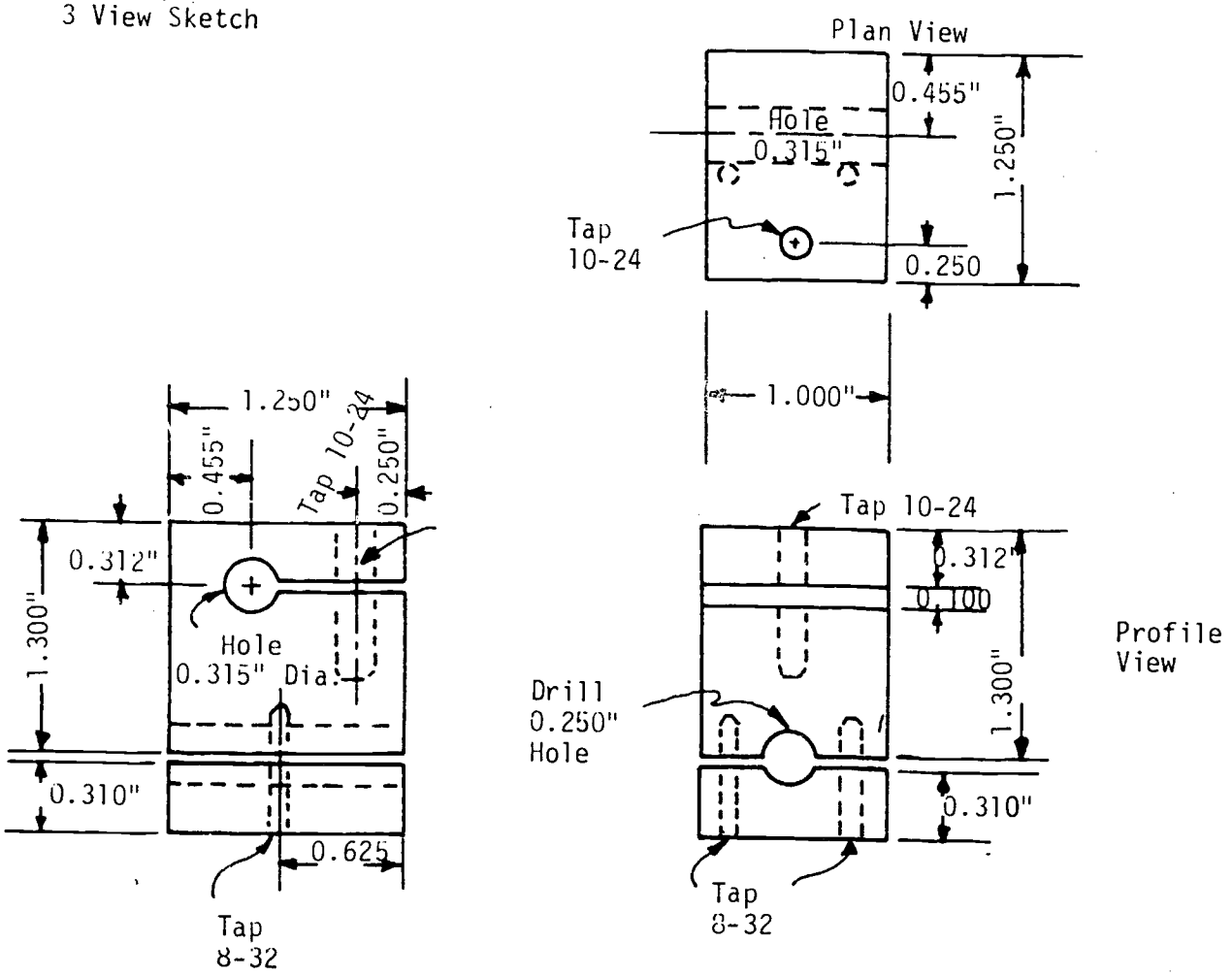

Scale 1" = 1"

Figure 36

Photo Cell
Aiming Jig

Vertical Translation
Horizontal Rotation

Tolerance: ± 0.0003"

. 3 View Sketch

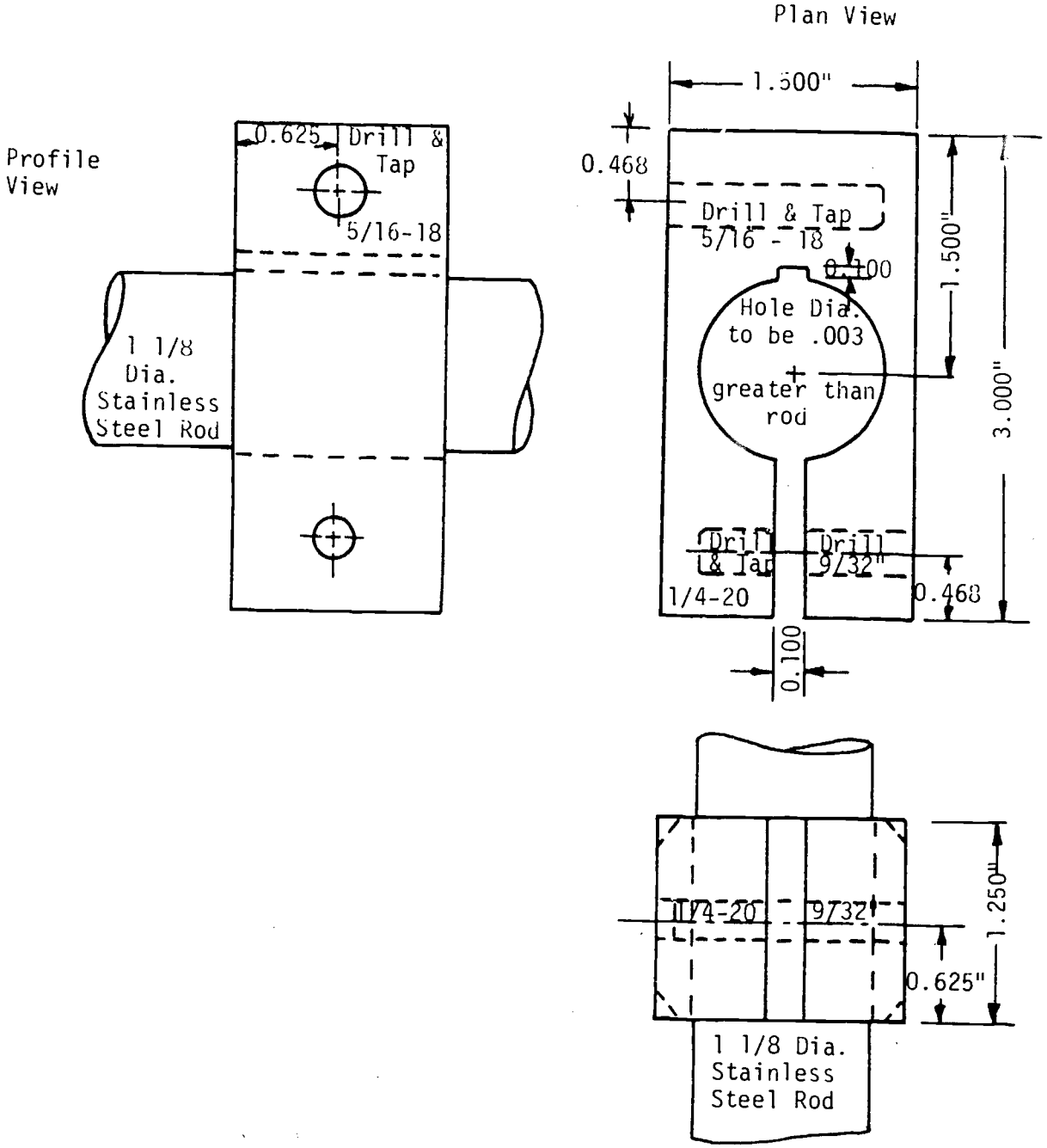

Scale 1" = 1"

Figure 37

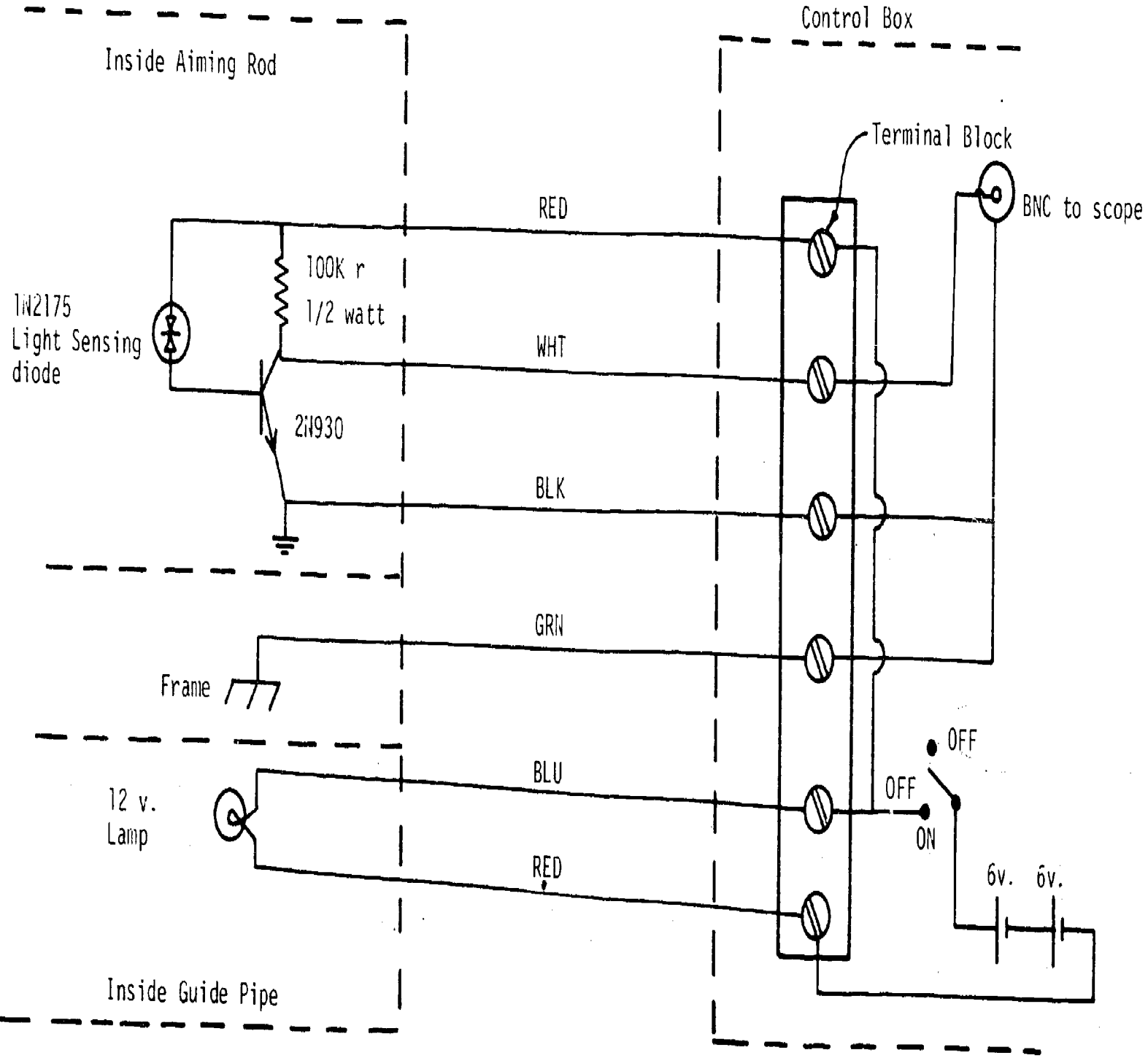
Control Box
Inside Aiming Rod
Terminal Block
BNC to scope
RED
100K r
1/2 watt
1N2175
Light Sensing
diode
WHT
2N930
BLK
GRN
Frame
OFF
BLU
OFF
12 v.
Lamp
ON
RED
6v. 6v.
Inside Guide Pipe

Figure 38

Assembly Drawing

High Pressure Impact Expt.

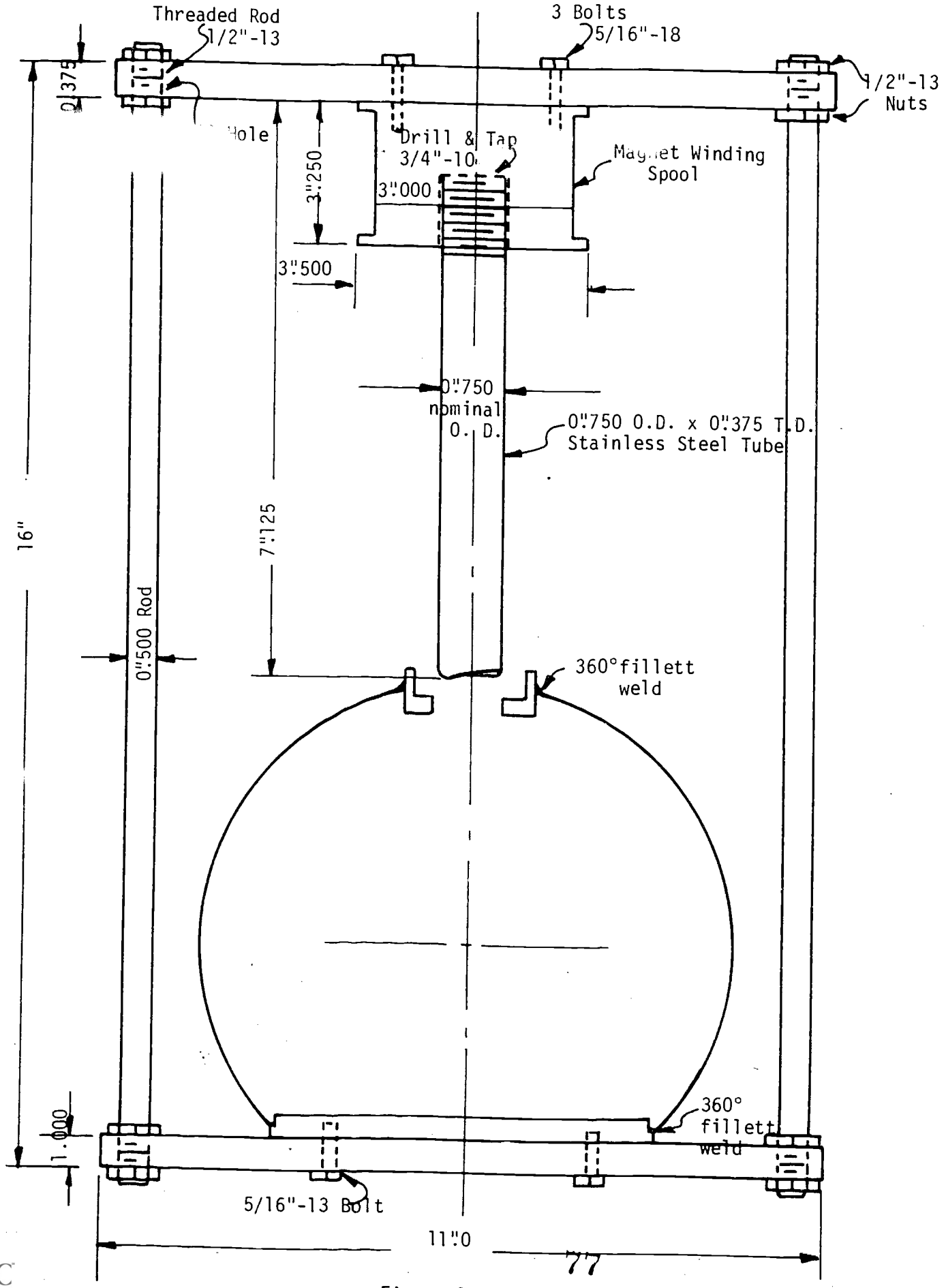

Figure 39

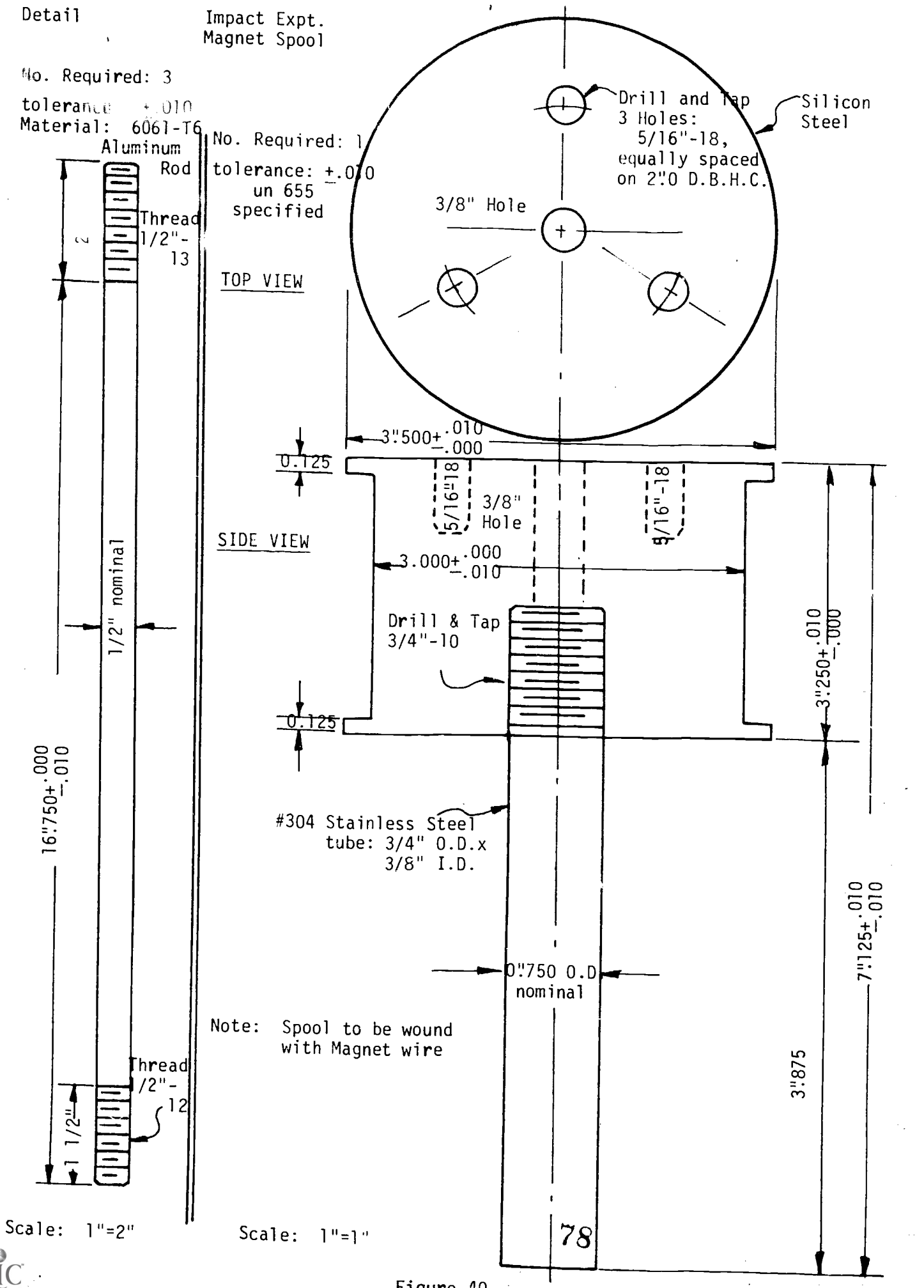
Detail
Impact Expt.
Magnet Spool
No. Required: 3
tolerance: ±.010
Material: 6061-T6
Aluminum Rod
Thread 1/2"-13
2"
1/2" nominal
16".750+.000 -.010
Thread 1/2"-12
1 1/2"
Scale: 1"=2"
No. Required: 1
tolerance: ±.010 un 655 specified
TOP VIEW
Drill and Tap 3 Holes: 5/16"-18, equally spaced on 2".0 D.B.H.C.
Silicon Steel
3/8" Hole
3".500+.010 -.000
0.125
5/16"-18
3/8" Hole
9/16"-18
SIDE VIEW
3.000+.000 -.010
Drill & Tap 3/4"-10
0.125
3".250+.010 -.000
#304 Stainless Steel tube: 3/4" O.D.x 3/8" I.D.
0".750 O.D nominal
Note: Spool to be wound with Magnet wire
3".875
7".125+.010 -.010
Scale: 1"=1"
78

Figure 40

Top End Plate Detail

Impact Expt.

Material: 6061-T6 Aluminum Plate
No. Required: 1
Tolerance: ±0.010 unless specified

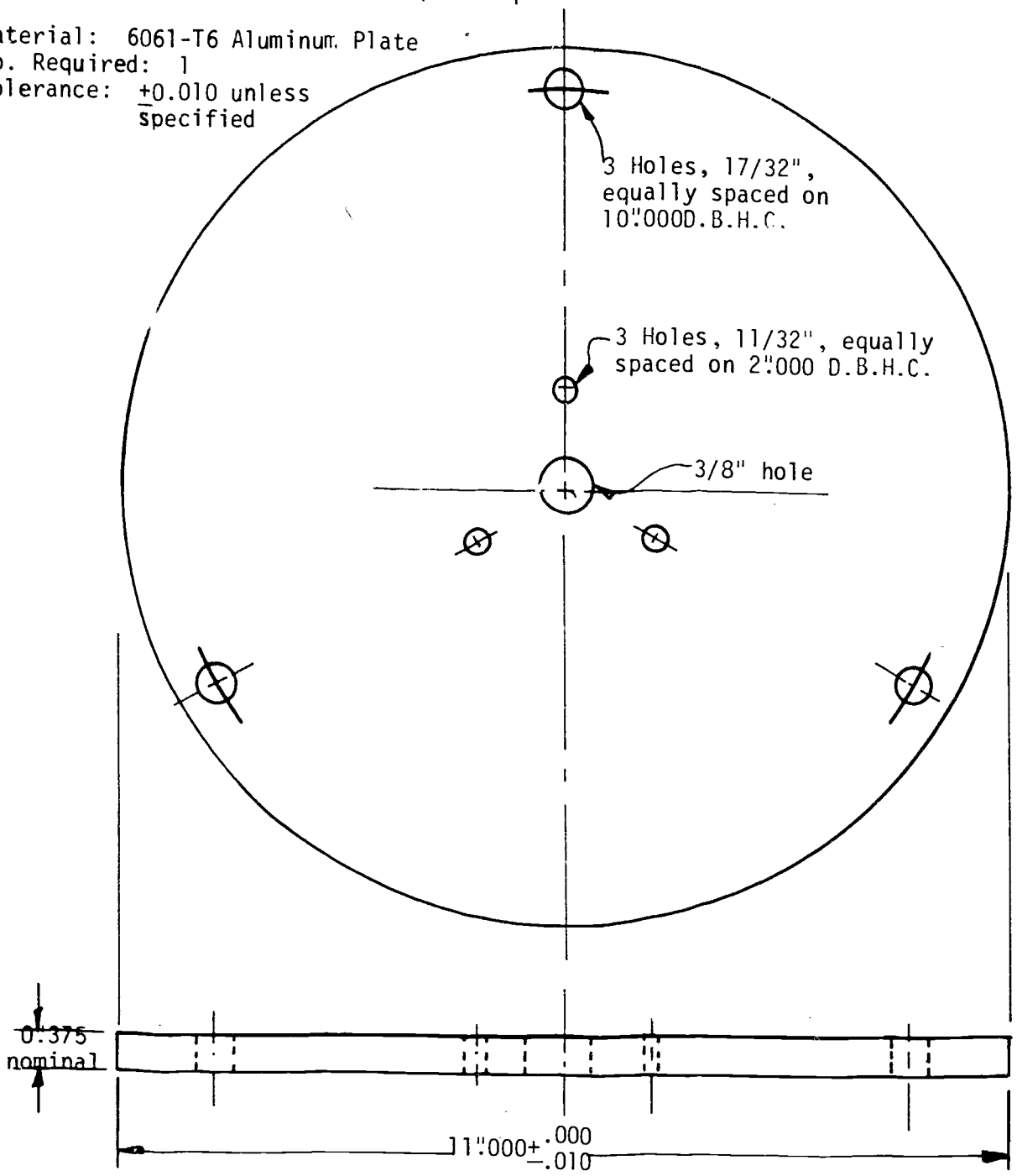

Note: Chamfer edges of holes and plate aprox. 1/32"x1/32"

Scale: 1"=2"

Figure 41

Bottom End

Impact Expt.

Plate Detail

Material: 6061-T6 Aluminum Plate
No. Required: 1
Tolerance: ±0.010 unless specified

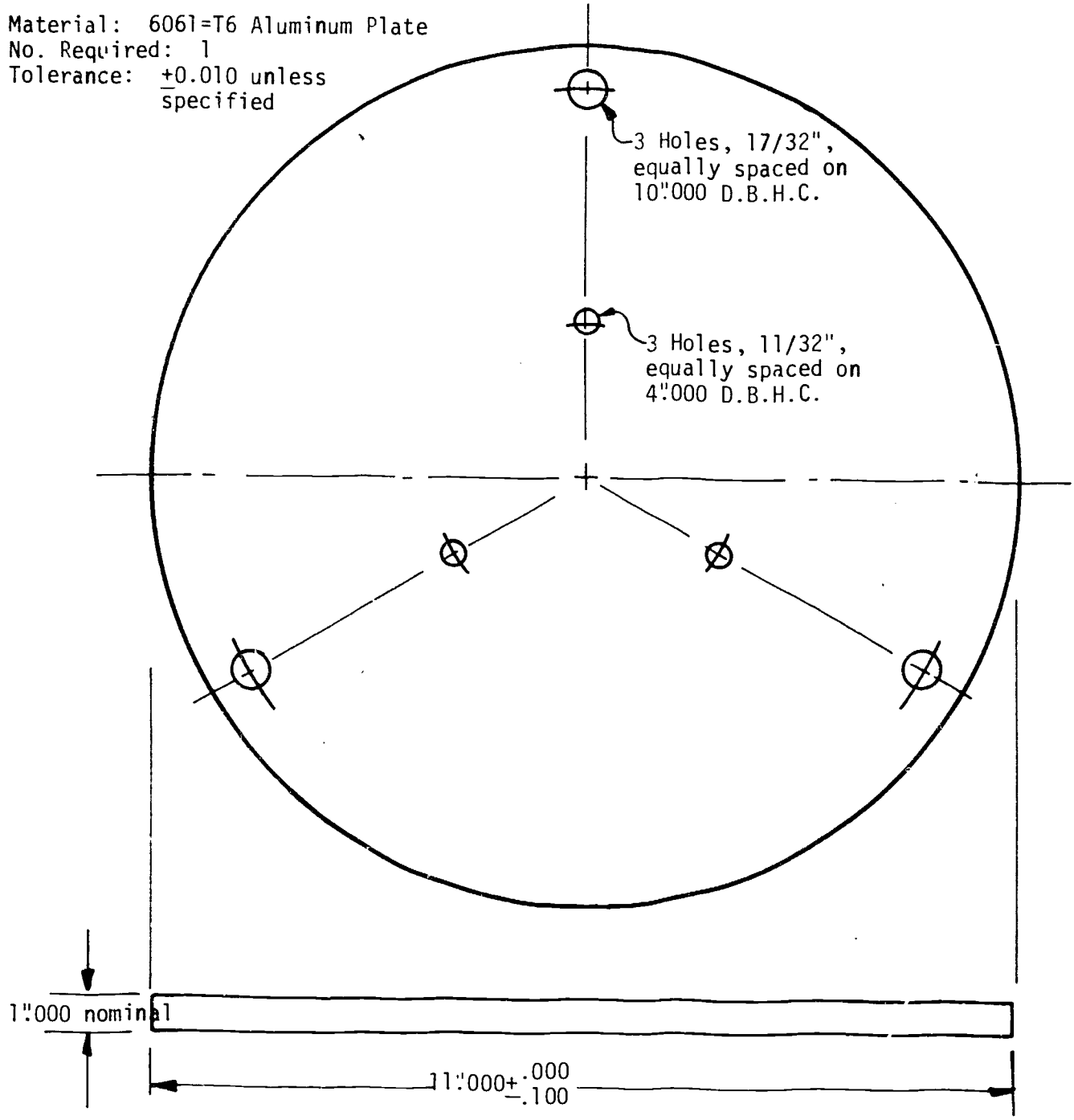

Note: Chamfer edges of holes and plate aprox. 1/32"x1/32"

Scale: 1"=2"

Figure 42

Slide Weight Detail

High Pressure Impact Expt.

Material: Silicon Steel
No. Required: 1
Tolerance: as noted

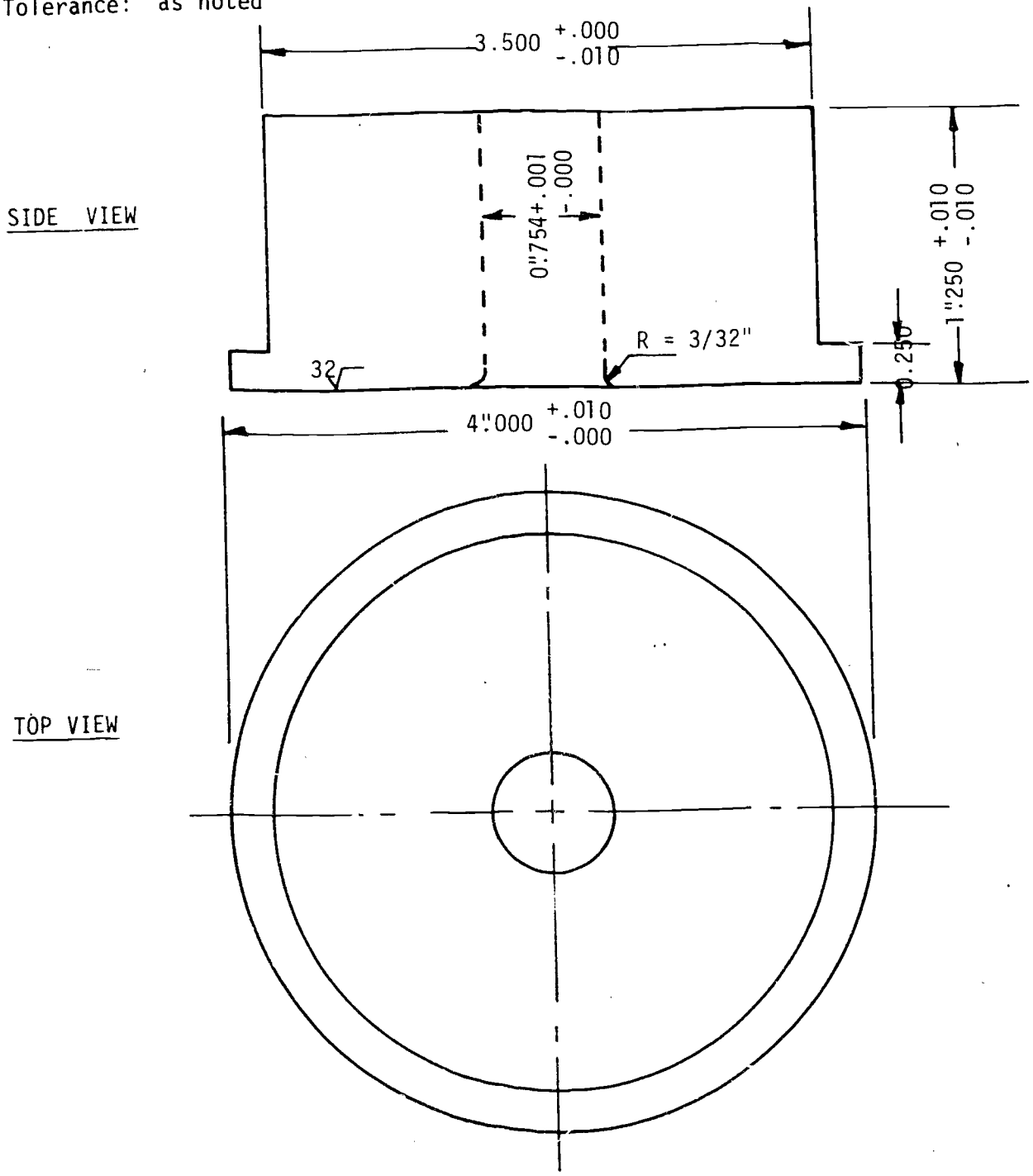

Note: 1) 32√ finish required on bottom surface only

2) Check that slide weight slides freely but with no "slop" along the Stainless Steel tube.

Figure 43

Detail of Test High Pressure
Sphere with Coaming Impact Expt.

Materials: as noted in sketch
No. Required: 1
tolerance: as specified

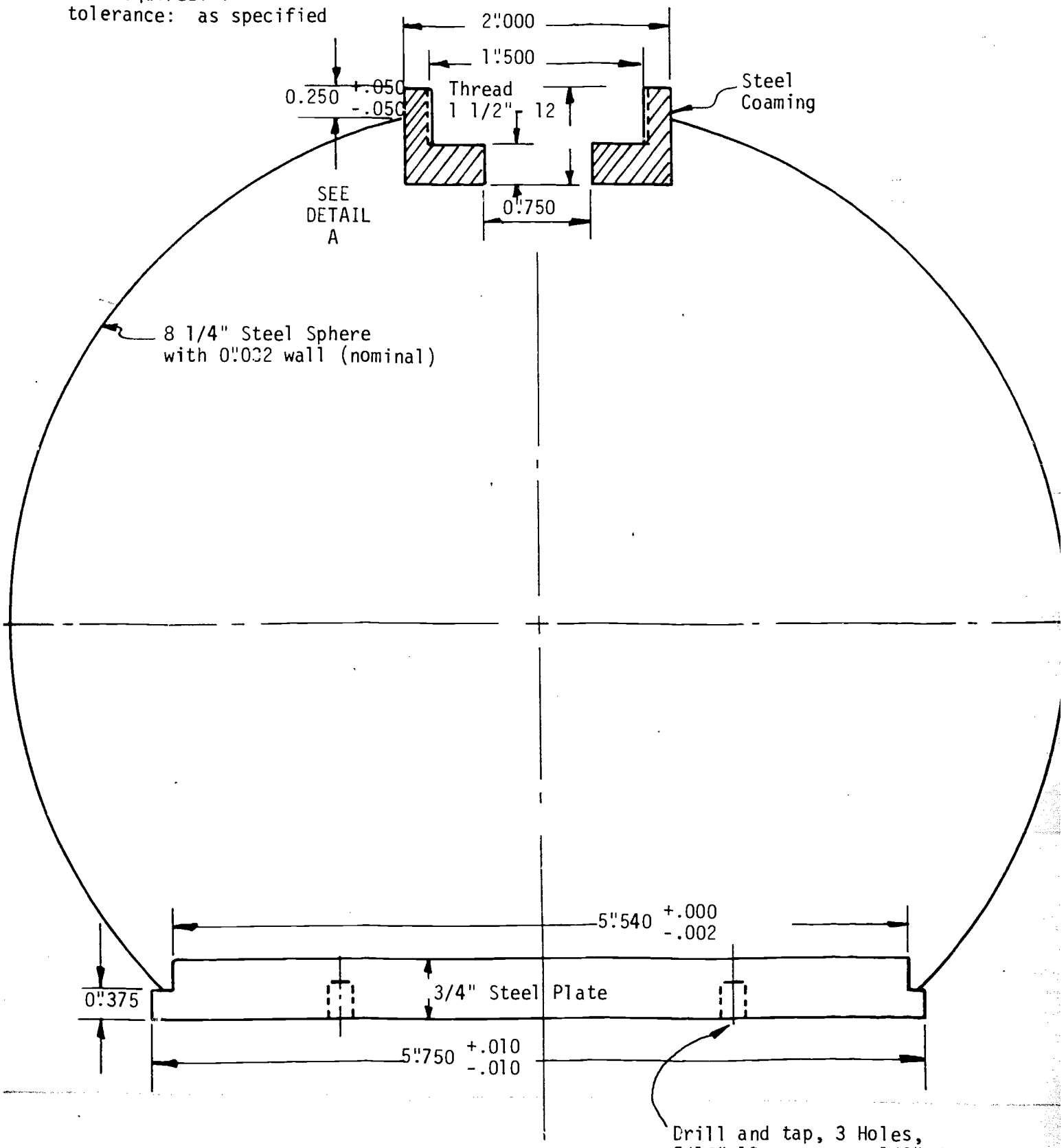

Figure 44

Detail A Impact Expt.

Material: Mild Steel
No. Required: 1

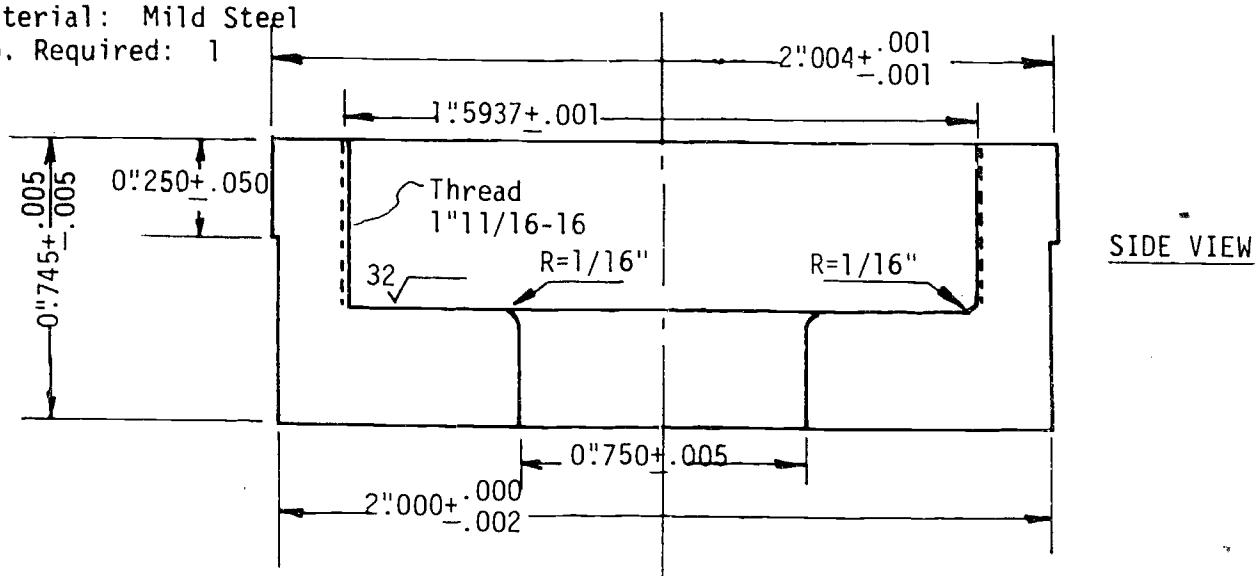

SIDE VIEW

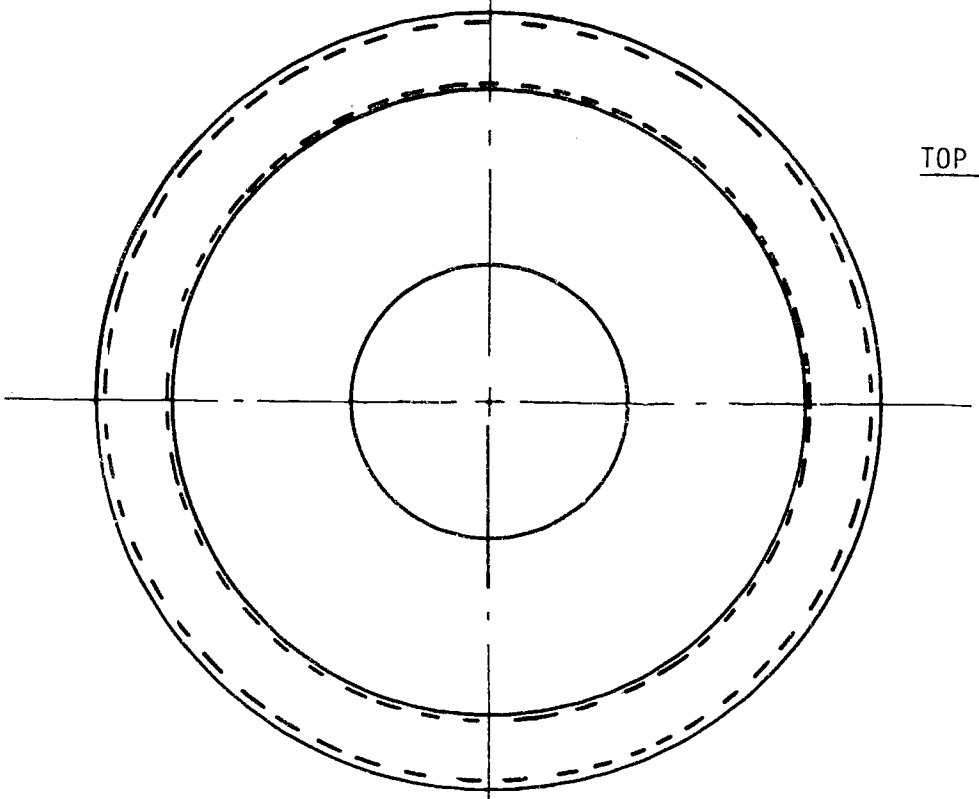

TOP VIEW

Scale: 1"=2"

Assembly Drawing of Seal

Scale: 1"=2"

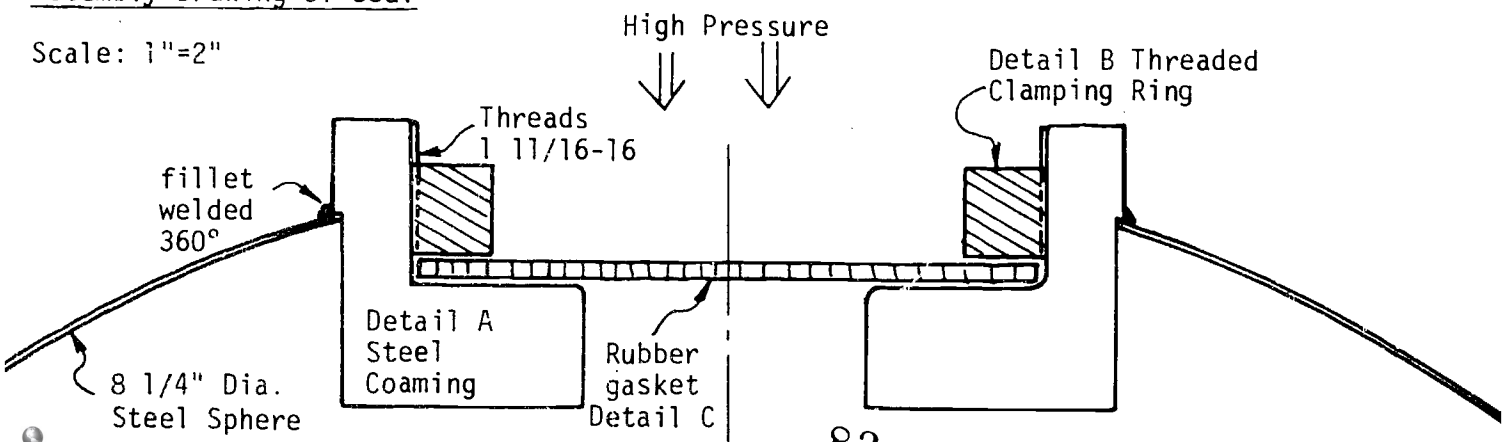

Figure 45

Detail B&C

Material: Mild-Steel
No. Required: 1
Tolerance: As specified

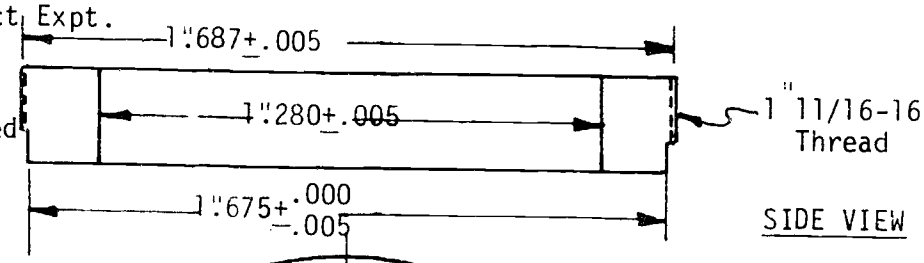

DETAIL B

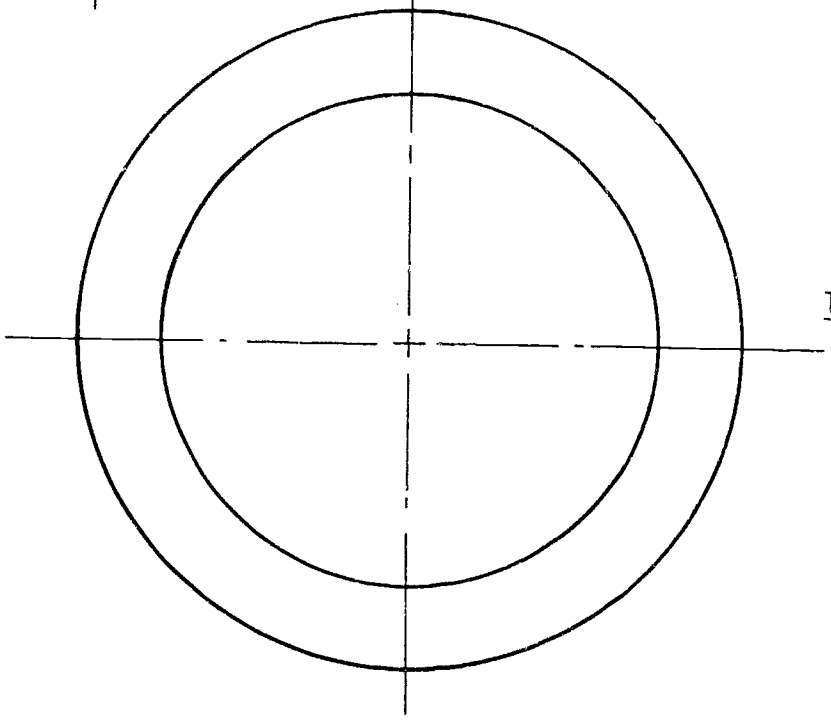

Materials: As Specified
No. Required: 1

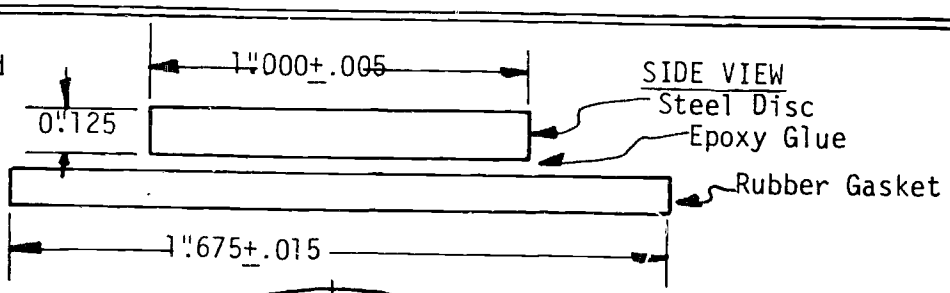

DETAIL C

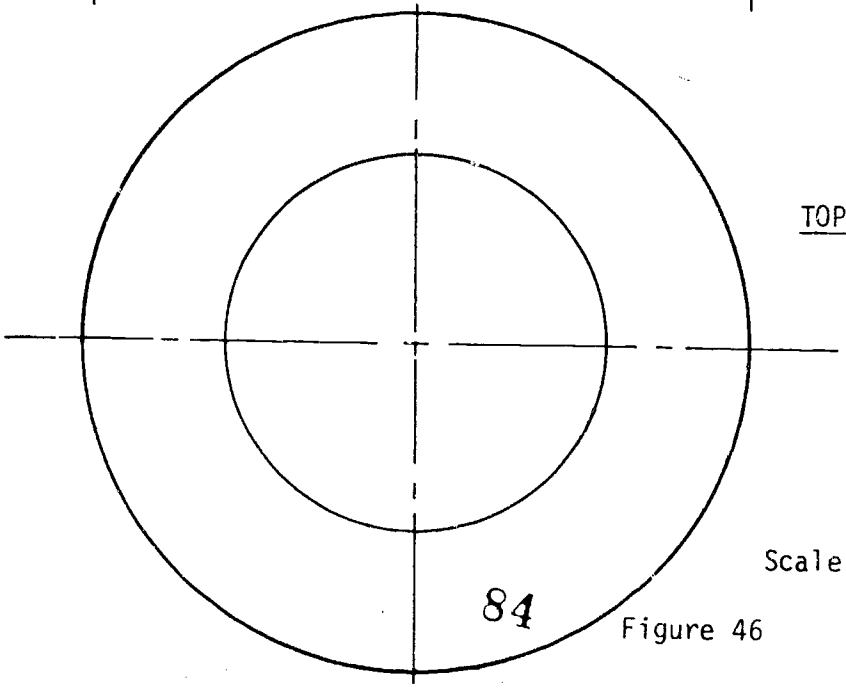

Scale: 1"=2"

Figure 46

THE UMASS. SPECIAL RING MAGNET

Figure 47

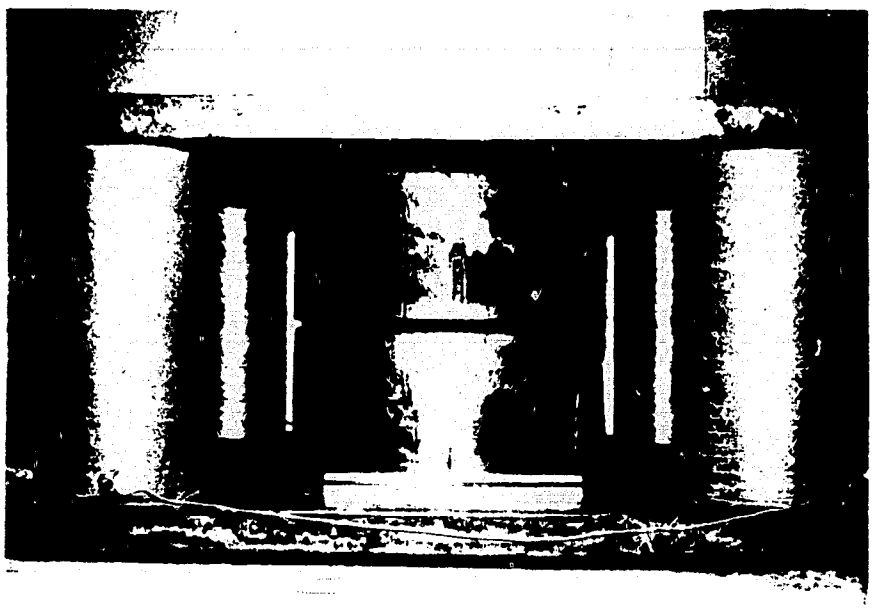

Figure 48

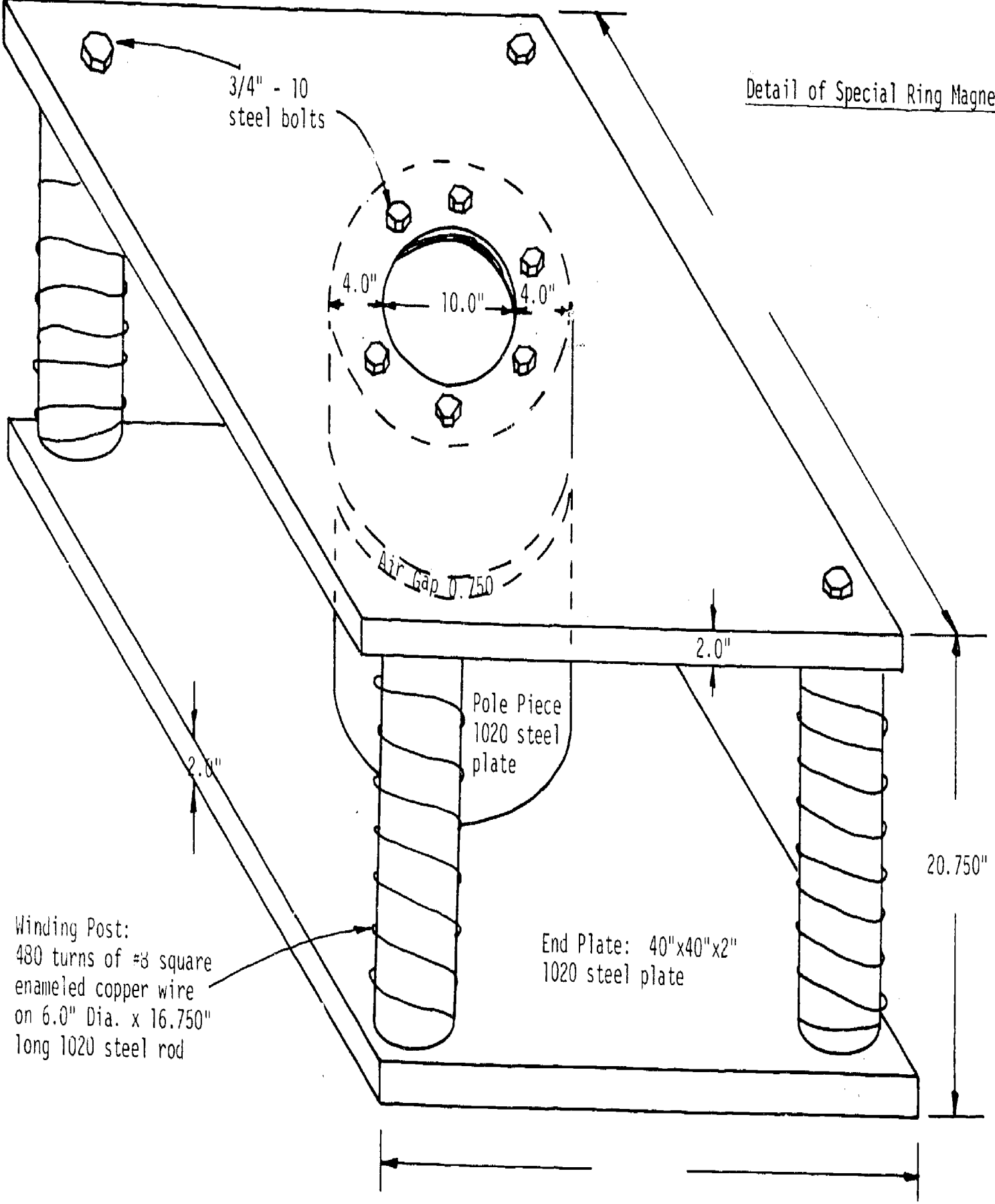
Detail of Special Ring Magnet
3/4" - 10
steel bolts
4.0"
10.0"
4.0"
Air Gap 0.750
2.0"
Pole Piece
1020 steel
plate
2.0"
20.750"
Winding Post:
480 turns of #8 square
enameled copper wire
on 6.0" Dia. x 16.750"
long 1020 steel rod
End Plate: 40"x40"x2"
1020 steel plate

Figure 49

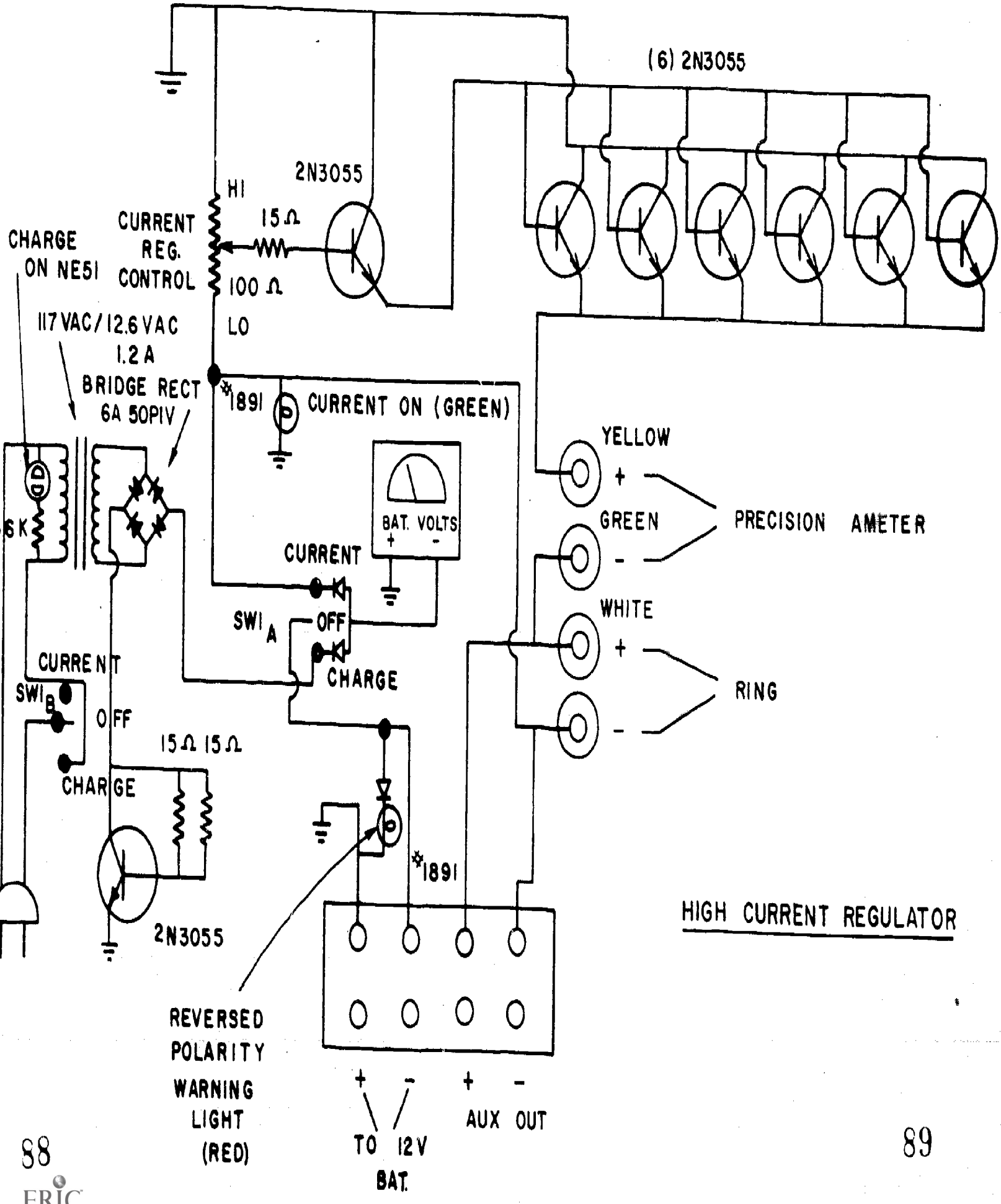
(6) 2N3055
2N3055
HI
15 Ω
CURRENT
REG.
CONTROL
100 Ω
LO
CHARGE
ON NE51
117 VAC / 12.6 VAC
1.2 A
BRIDGE RECT
6A 50PIV
*1891
CURRENT ON (GREEN)
BAT. VOLTS
+ -
CURRENT
SW1 A
OFF
CHARGE
CURRENT
SW1 B
OFF
CHARGE
15 Ω 15 Ω
2N3055
*1891
YELLOW
+
GREEN
-
PRECISION AMETER
WHITE
+
-
RING
HIGH CURRENT REGULATOR
REVERSED
POLARITY
WARNING
LIGHT
(RED)
+ - + -
TO 12V
BAT.
AUX OUT

Figure 50

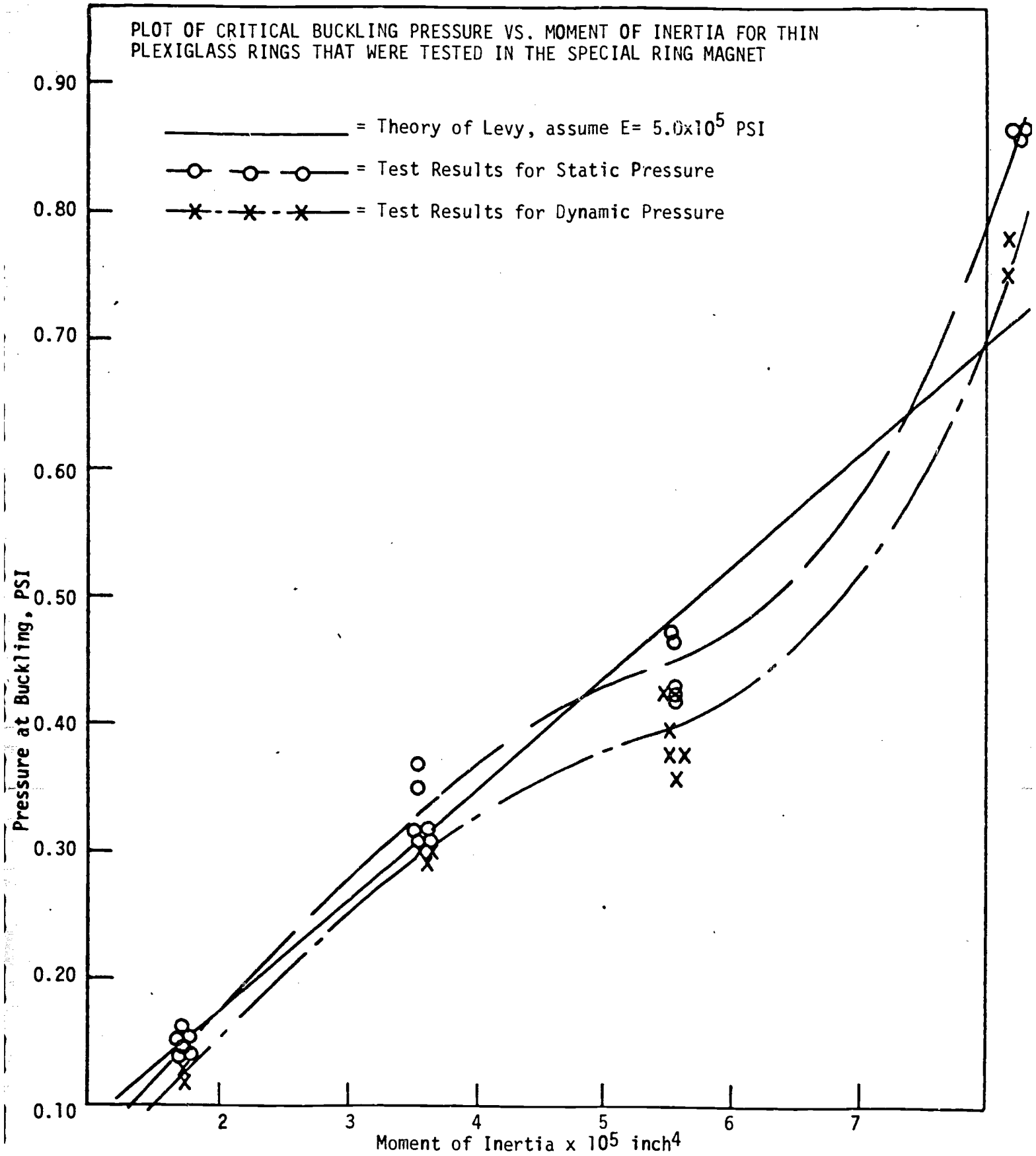
PLOT OF CRITICAL BUCKLING PRESSURE VS. MOMENT OF INERTIA FOR THIN PLEXIGLASS RINGS THAT WERE TESTED IN THE SPECIAL RING MAGNET
= Theory of Levy, assume E= 5.0x10^5 PSI
= Test Results for Static Pressure
= Test Results for Dynamic Pressure
Pressure at Buckling, PSI
0.90
0.80
0.70
0.60
0.50
0.40
0.30
0.20
0.10
2
3
4
5
6
7
Moment of Inertia x 10^5 inch^4

Figure 51

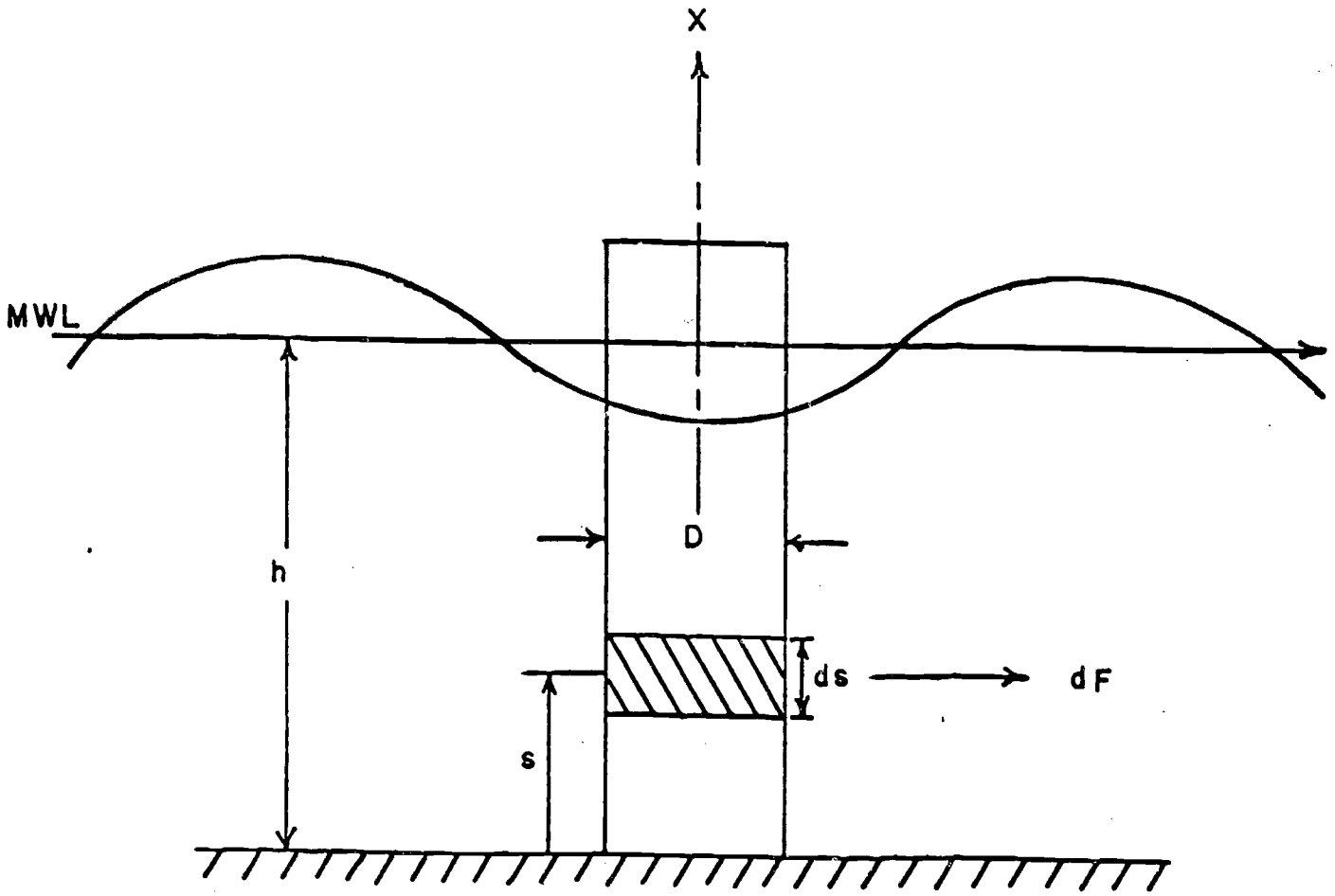

Terminology and symbols used in Morison equations for force and moment on a vertical circular column exposed to progressive water waves.

Figure 52

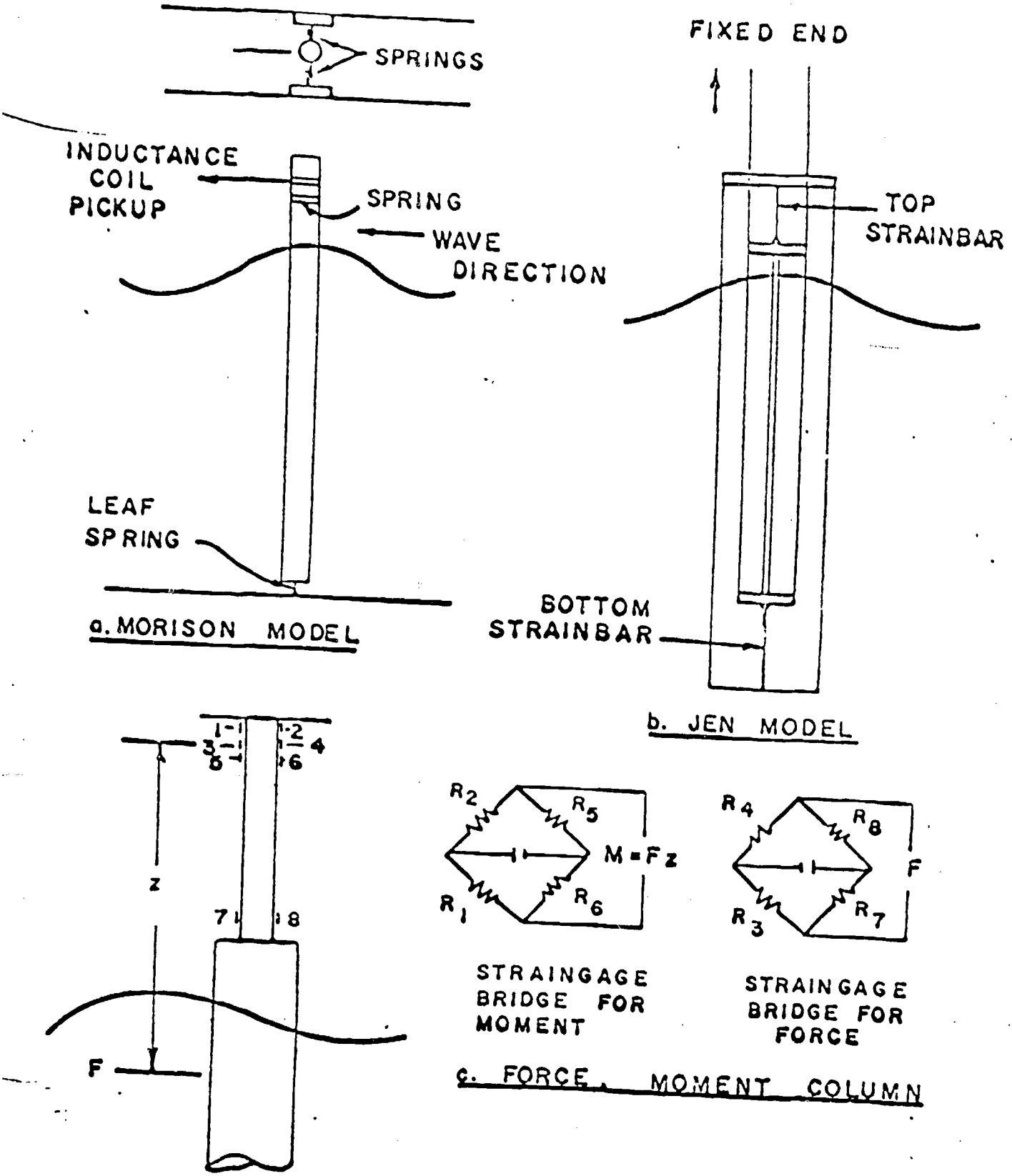

Some experimental arrangements used by other researchers.

Figure 53

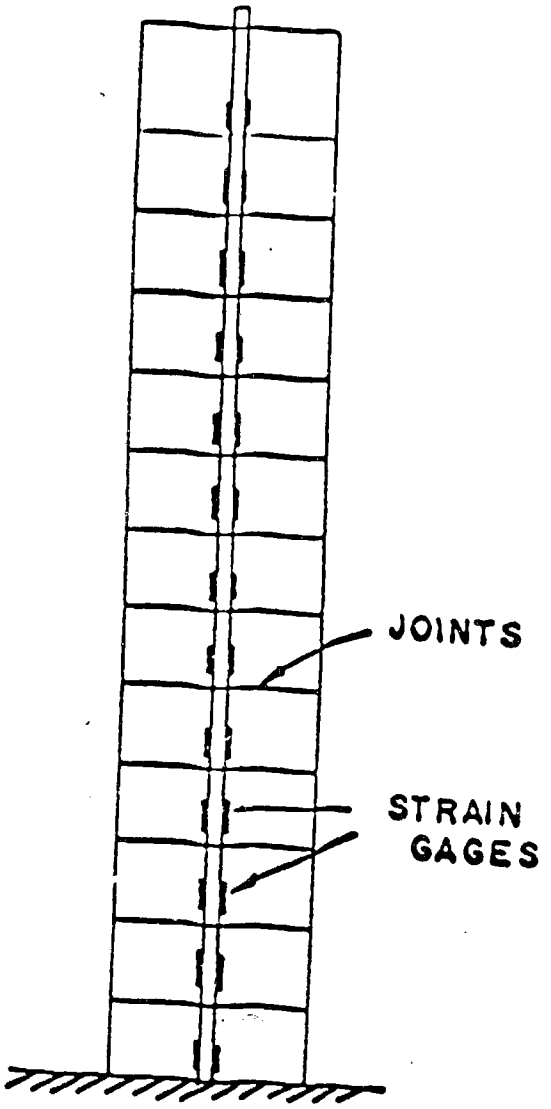

a HAYASHI MODEL

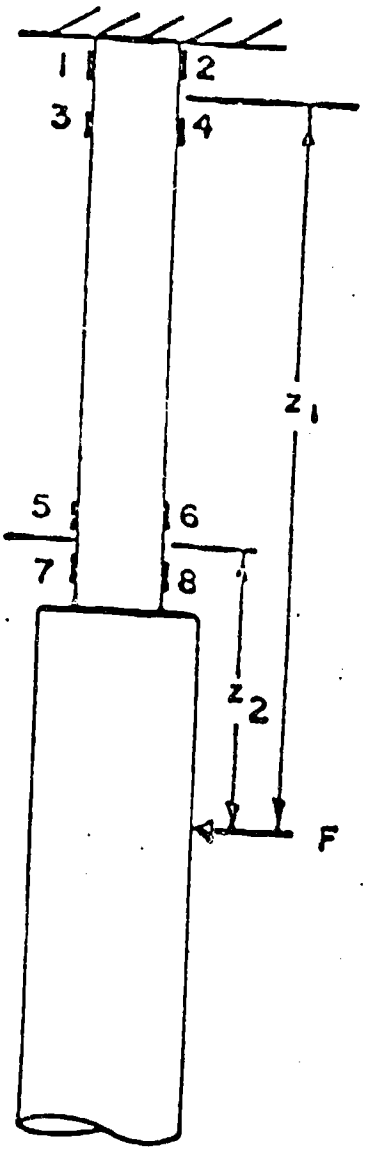

b TWO-MOMENT COLUMN

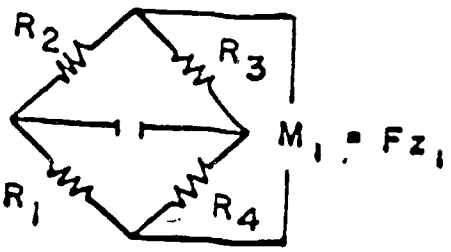

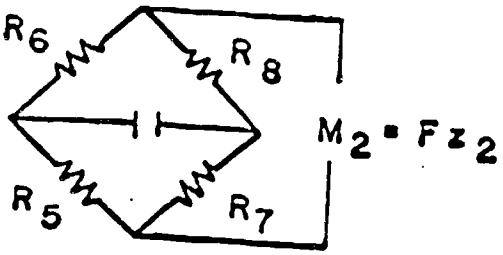

c WIRING FOR TWO MOMENT LOAD CELLS

Some experimental arrangements used by other researchers.

Figure 54

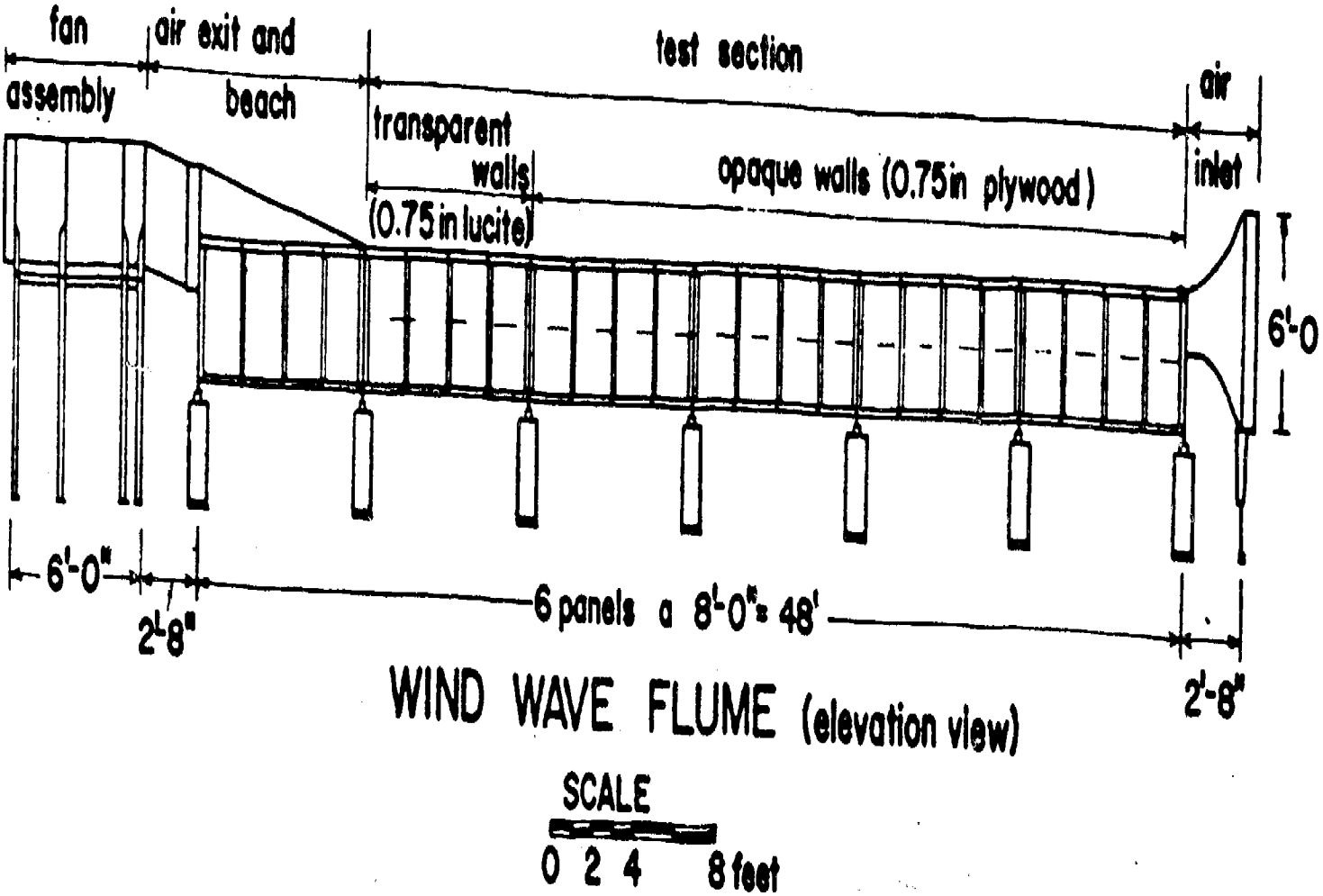

The UMass Wind Wave Research Facility.

Figure 55

Figure 56

The plexiglass model column, with outside diameter of 3.0 in. and 0.125 in. wall thickness, was bolted securely to channel bottom in the lucite seciton of the wave facility.

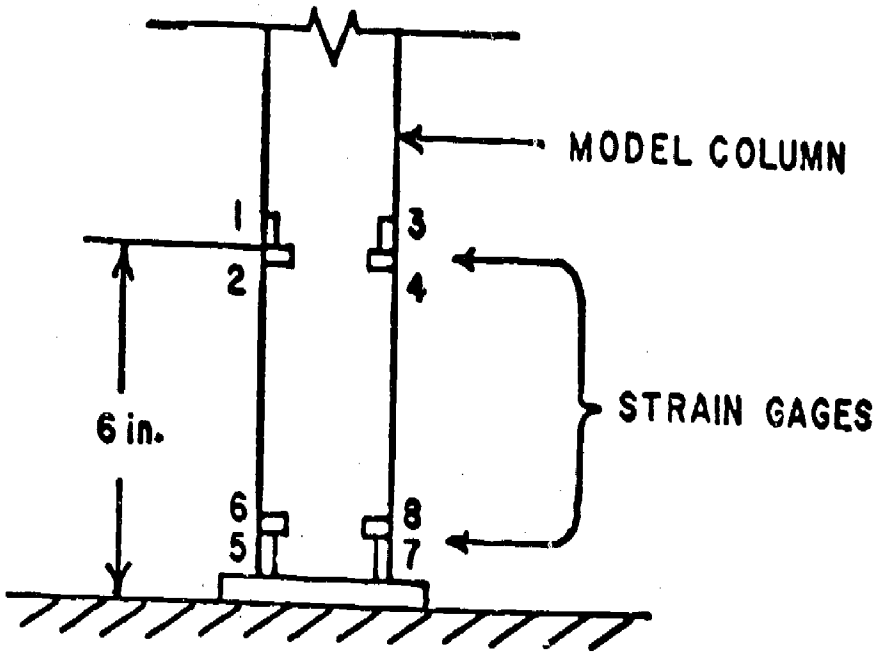

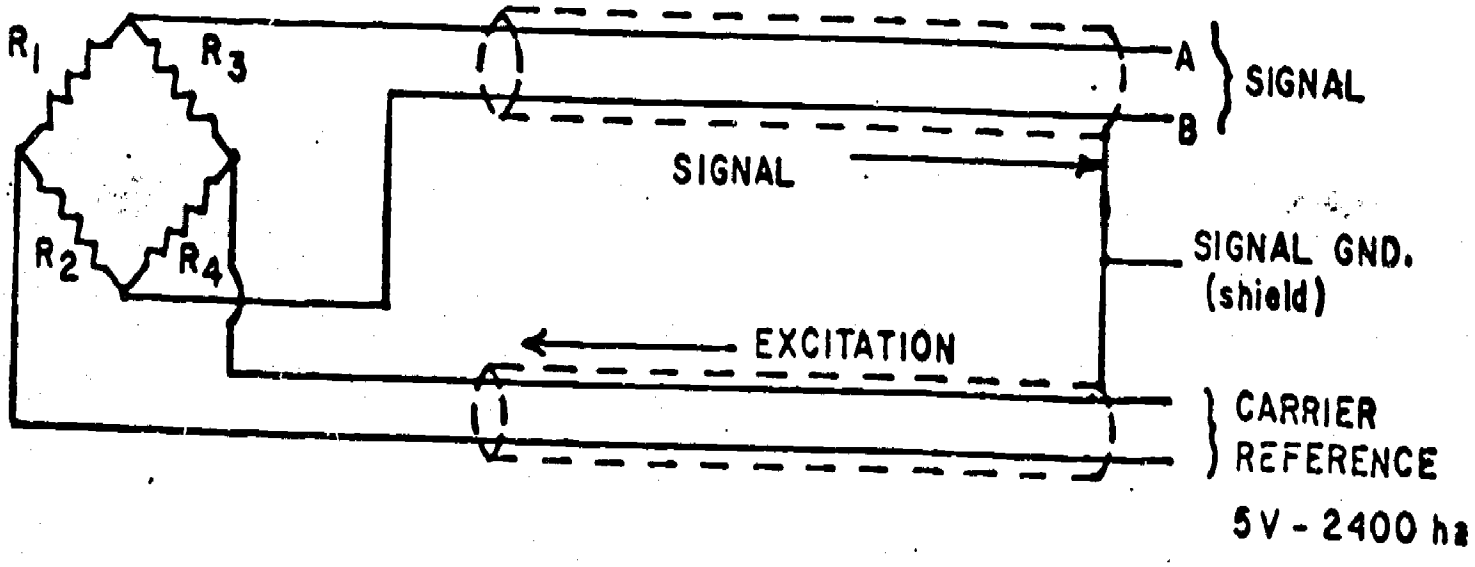

Arrangement of vertical and horizontal strain gages and associated bridge circuitry.

Figure 57

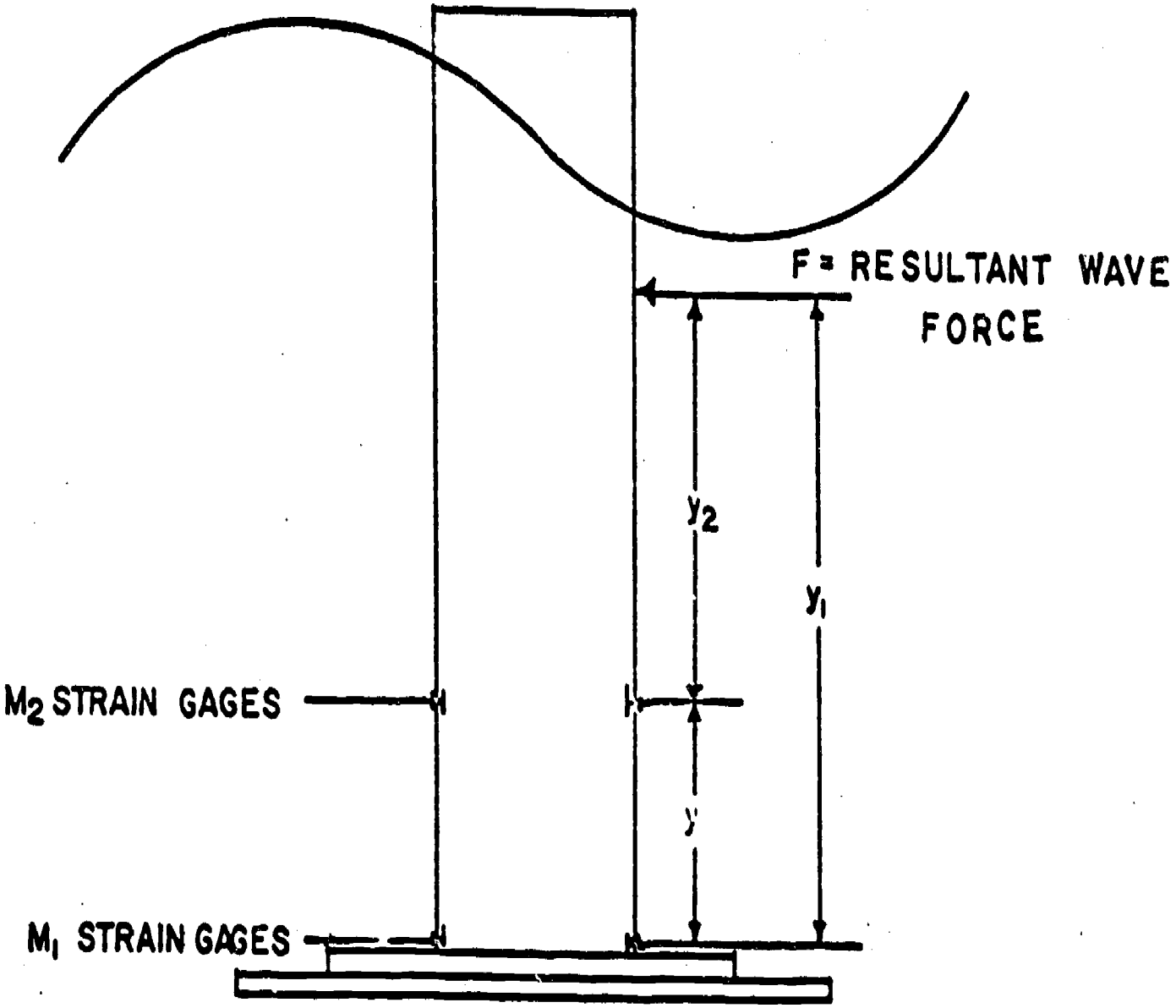

Illustrative sketch of two-moment principle.

Figure 58

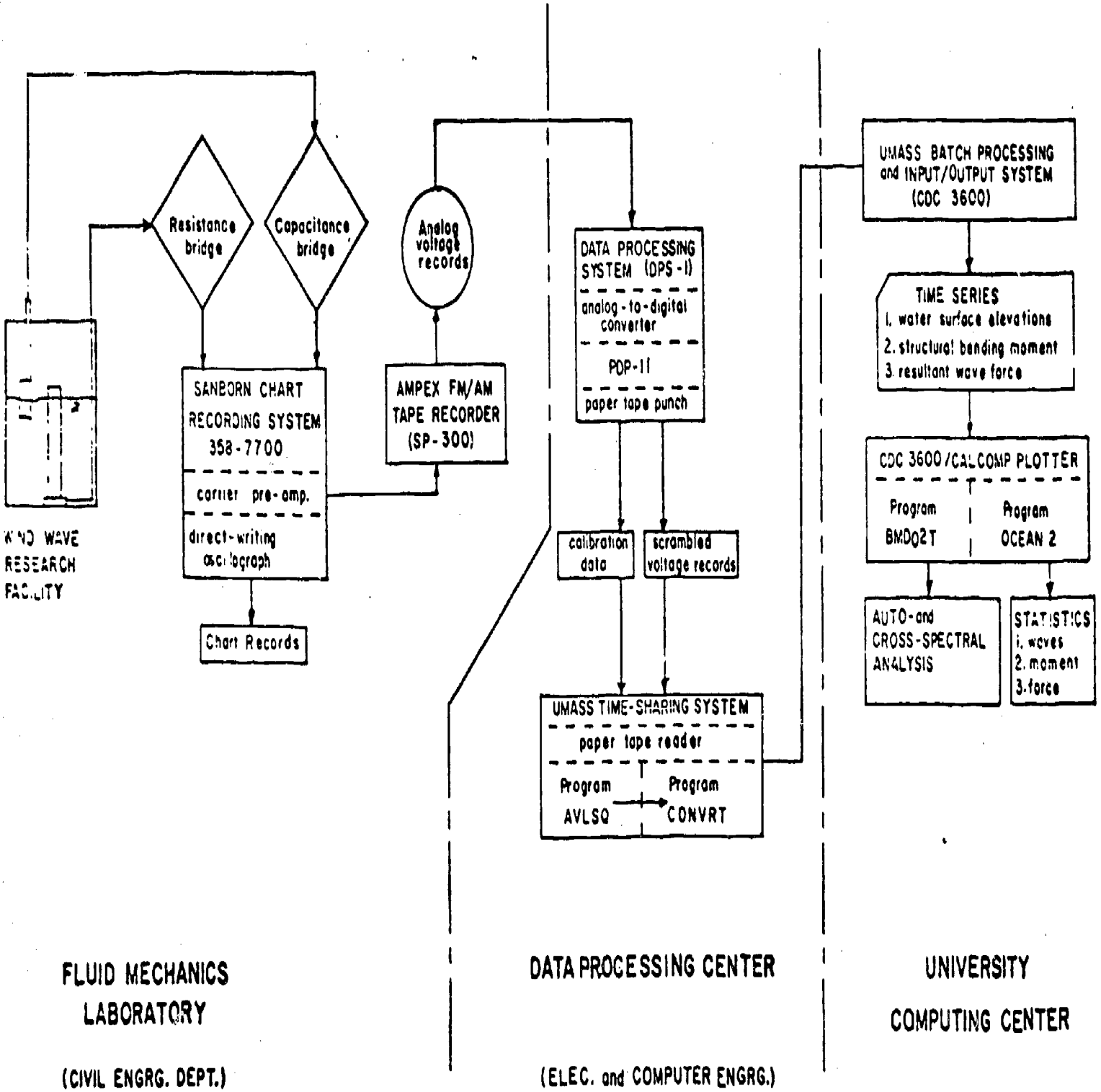

Flow chart of data acquisition and processing procedures.

Figure 59

BIBLIOGRAPHIC DATA SHEET	1. Report No. UMass-1759-1	2.	3. Recipient's Accession No.
4. Title and Subtitle: DEVELOPMENT OF FACILITIES FOR AN OCEAN ENGINEERING LABORATORY.			5. Report Date: July, 1975 (date of issue)
			6.
7. Author(s): W. A. Nash, J. M. Colonell, and R. B. MacPherson			8. Performing Organization Rept. No.
9. Performing Organization Name and Address: University of Massachusetts, Department of Civil Engineering Amherst, Massachusetts 01002			10. Project/Task/Work Unit No. NSF GZ 1759
			11. Contract/Grant No. NSF GZ 1759
12. Sponsoring Organization Name and Address: National Science Foundation, Washington, DC 20550			13. Type of Report & Period Covered: Final Technical Report
			14.

15. Supplementary Notes

16. Abstracts

A collection of seven laboratory facilities and processes dedicated to improving student understanding of the fundamental concepts associated with the structural mechanics of oceanic structures is described. Complete working drawings covering all mechanical and electrical aspects of these systems are presented so that the systems may be reporduced in any instructional laboratory.

17. Key Words and Document Analysis. 17a. Descriptors

SHELLS (Structural forms) 1313
- UF Shell structures
- Thin Shell structures

DEEP OCEAN VEHICLES 1310
- BT Underwater vehicles
- UF Bathyscaphs
- Deep Submersibles

OCEAN WAVES 0803
- BT Water waves
- NT Tsunamis

STRUCTURAL ANALYSIS 1313, 1402
- NT Dynamic Structural analysis
- Stability methods

17b. Identifiers/Open-Ended Terms

OCEANIC STRUCTURAL LABORATORY

17c. COSATI Field/Group: 78-- Ocean Sciences and Engineering
G--Oceanographic Vessels and Platforms

18. Availability Statement	19. Security Class (This Report)	21. No. of Pages
Unlimited distribution	UNCLASSIFIED	29 & 59 Fig.
	20. Security Class (This Page) UNCLASSIFIED	22. Price

FORM NTIS-35 (REV. 3-72)

USCOMM-DC 14952-P72